Politecnico di Torino

Politecnico di Torino

Master's degree in civil engineering
A.Y. 2025/2026
Defense session: July 2026

Advanced laboratory investigation of asphalt mixtures with recycled plastic for sustainable road pavements

Relatori:
Prof. Davide Dalmazzo
Prof. Orazio Baglieri
Prof. Ezio Santagata
Dr. Davide Cimenti

Candidate:
Mohammad Eftekhari

Contents

Abstract

This thesis investigates the mechanical performance of sustainable asphalt mixtures incorporating recycled plastic shreds for different pavement layers. The mixtures considered in this study were developed in previous stages of the Green Roads project; therefore, the present work does not focus on mix design optimization, but rather on the advanced mechanical characterization of the produced mixtures under laboratory-controlled conditions.

The experimental program was carried out using the Asphalt Mixture Performance Tester (AMPT) and complementary analytical procedures. The mechanical response of the mixtures was evaluated through dynamic modulus testing, master curve construction, cyclic fatigue characterization, and low-temperature cracking analysis. Both large and small cylindrical specimens were considered, depending on the specific testing procedure and material availability. Particular attention was given to the viscoelastic stiffness response, damage evolution under repeated loading, and the potential susceptibility of the mixtures to thermal cracking.

Dynamic modulus tests were performed at different temperatures and loading frequencies to characterize the linear viscoelastic behavior of the mixtures. The resulting data were used to construct dynamic modulus master curves and to compare the stiffness response of the tested mixtures over a wide range of reduced frequencies. Master curves were developed using both the standard sigmoidal approach and the 2S2P1D rheological model, allowing the consistency of the fitted viscoelastic response to be evaluated.

Fatigue testing was performed under cyclic direct tension loading using the AMPT. The fatigue data were analyzed within the simplified viscoelastic continuum damage framework. The damage characteristic curve, defined by the relationship between the material integrity parameter C and the accumulated damage variable S, was used to describe the fatigue damage evolution of each mixture. In addition, fatigue-related parameters such as D_R, C_{11}, C_{12}, and S_{app} were considered to support the comparison of fatigue resistance among mixtures.

The low-temperature behavior of the mixtures was also investigated in order to assess their potential susceptibility to thermal cracking. This analysis provided additional information on the cracking response of mixtures containing recycled plastic, complementing the stiffness and fatigue characterization.

The results provide an advanced mechanical characterization of reference and recycled-plastic-modified asphalt mixtures designed for different pavement layers. The findings contribute to a better understanding of how recycled plastic affects the stiffness response, fatigue damage evolution, and low-temperature cracking susceptibility of asphalt mixtures,

and support the use of advanced laboratory methods for evaluating innovative asphalt materials.

Keywords: sustainable asphalt mixtures, recycled plastic, AMPT, dynamic modulus, master curve, 2S2P1D, S-VECD, fatigue, low-temperature cracking, mechanical characterization.

Acknowledgements

I would like to express my sincere gratitude to my supervisors, Prof. Davide Dalmazzo, Prof. Orazio Baglieri, and Prof. Ezio Santagata, for their guidance, support, and valuable feedback throughout the development of this thesis. Their knowledge, experience, and constructive advice played an essential role in shaping this work and improving my understanding of the mechanical characterization of asphalt mixtures.

I am also deeply grateful to Davide Cimenti, PhD student, for his continuous support during the experimental activities. His help, patience, and technical guidance were particularly valuable during specimen preparation, AMPT testing, data analysis, and the interpretation of the experimental results.

I would also like to acknowledge the researchers and students who contributed to the previous stages of this project, especially in the development and mix design of the investigated asphalt mixtures. Their work provided an important foundation for the mechanical characterization carried out in this thesis.

My heartfelt thanks go to my wife, who has always encouraged me and supported me throughout this journey, even during the difficult periods of distance and separation. Her patience, understanding, and constant motivation gave me strength and helped me continue this path with determination.

Finally, I would like to thank my family for their continuous love, encouragement, and support. Their belief in me has always been a source of motivation during my academic journey. I am also grateful to my friends, colleagues, Politecnico di Torino, and the city of Turin for the experiences, memories, and support that accompanied me during this important period of my life.

Introduction

Background and Motivation

Road pavement infrastructures play a fundamental role in modern transportation systems, supporting mobility, economic development, and the movement of goods and people. Among pavement materials, asphalt mixtures are widely used due to their flexibility, durability, and ability to provide adequate performance under traffic and environmental loading conditions. However, the construction and maintenance of asphalt pavements require significant amounts of natural aggregates and bituminous binders, leading to increasing concerns regarding resource consumption, environmental impact, and long-term sustainability.

In recent years, the pavement engineering sector has increasingly moved towards more sustainable solutions, with growing interest in the use of waste and secondary materials in asphalt mixtures. The incorporation of reclaimed asphalt pavement (RAP), waste plastic, and other waste-derived materials represents a promising strategy to reduce the consumption of virgin resources, limit waste disposal, and promote circular economy principles in road construction [1], [2]. In particular, the combined use of RAP and waste plastic has been considered a sustainable paving practice because of its potential environmental and economic benefits [3].

Among these materials, waste plastic has attracted particular attention because of its potential contribution to plastic waste management and its possible influence on the performance of asphalt mixtures. Previous studies have reported that the incorporation of waste plastics in asphalt mixtures may improve rutting resistance, fatigue resistance, moisture resistance, and high-temperature performance. However, challenges related to material compatibility, processing methods, dosage, and low-temperature performance still require careful evaluation [1].

Nevertheless, the use of waste materials in asphalt mixtures cannot be evaluated only from an environmental perspective. Their incorporation may significantly affect the volumetric, rheological, and mechanical behavior of the mixture. Therefore, a performance-based evaluation is necessary to verify whether these mixtures can provide adequate structural response and durability when used in different pavement layers. This aspect is particularly important because each pavement layer is subjected to different stress states, loading conditions, and environmental effects. The overall conceptual framework of the present study, from the constituent materials to the performance-based evaluation, is illustrated in Figure 1.

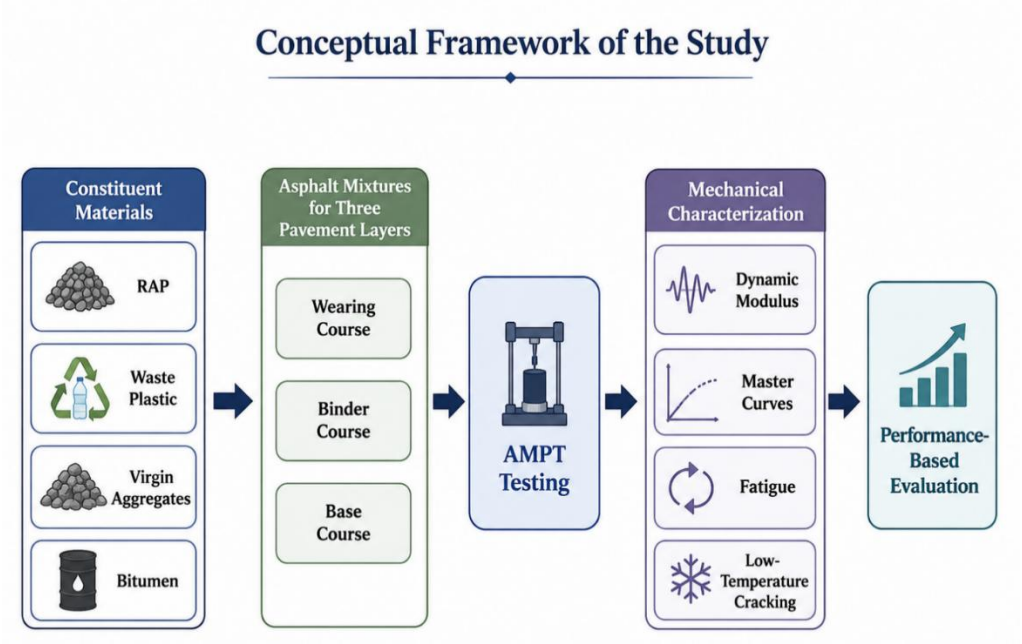

Figure 1 - Conceptual framework of the study, linking constituent materials, pavement layers, AMPT testing, mechanical characterization, and performance-based evaluation.

The present thesis is developed within the framework of the Green Roads project, which aims to investigate sustainable asphalt mixtures incorporating RAP and recycled plastic for road pavement applications. Previous project activities focused on selecting suitable recycled plastic materials, developing mixture formulations and producing asphalt mixtures on a large scale. Building on these phases, this thesis focuses on the advanced laboratory mechanical characterisation of the resulting mixtures.

In the original experimental plan of the project, reference and recycled-plastic-modified mixtures were considered for the three main pavement layers: wearing course, binder course, and base course. This layer-by-layer approach was intended to evaluate the possible effect of recycled plastic within mixtures having different compositions, structural functions, and expected in-service conditions. The mechanical characterization presented in this thesis was therefore designed to provide a performance-based evaluation of the selected mixtures, with particular attention to stiffness response, fatigue damage evolution, and low-temperature cracking susceptibility. Advanced laboratory testing, such as that performed using the Asphalt Mixture Performance Tester (AMPT), provides a useful framework for evaluating the viscoelastic and damage-related behavior of asphalt mixtures. Through dynamic modulus testing, it is possible to characterize the stiffness of the material over a wide range of temperatures and loading frequencies and to construct master curves that describe the time-temperature dependent behavior of the mixture. In addition, fatigue and low-temperature cracking analyses provide further insight into the resistance of the material to damage accumulation and thermally induced cracking.

For these reasons, the mechanical characterization of asphalt mixtures incorporating RAP and waste plastic is essential to assess their suitability for practical pavement applications. The experimental investigation therefore provides a performance-based interpretation of the selected mixtures, supporting the evaluation of recycled-plastic asphalt mixtures within the broader Green Roads project.

Objectives of the Study

The main objective of this thesis is to evaluate the mechanical performance of asphalt mixtures designed for three pavement layers, with particular focus on the effect of waste plastic incorporation. The work forms part of the Green Roads project and builds on previous activities dedicated to selecting materials, formulating mixtures and producing on a plant scale.

The initial experimental framework of the project included the characterization of both reference and recycled-plastic-modified mixtures for the wearing, binder, and base courses. However, during the plant-scale production of the recycled-plastic-modified binder course mixture, technical problems occurred at the asphalt plant, preventing this mixture from being produced and tested within the time frame of the present thesis. Although the modified binder course mixture was produced at a later stage of the project, it could not be included in the experimental campaign reported in this work. Consequently, direct comparison between reference and modified mixtures was possible for the wearing and base courses, whereas the binder course is represented by the reference mixture only.

The experimental investigation aims to determine whether the incorporation of waste plastic affects stiffness, viscoelastic response, fatigue-related behavior, and low-temperature cracking susceptibility of these mixtures.

More specifically, the objectives of this thesis are:

- to characterize the dynamic modulus behavior of the tested asphalt mixtures under different temperature and loading frequency conditions;
- to construct and analyze dynamic modulus master curves in order to describe their viscoelastic response over a wide range of reduced frequencies;
- to compare the mechanical response of reference and recycled-plastic-modified mixtures for the wearing and base courses;
- to evaluate the fatigue-related behavior of selected mixtures under repeated loading conditions;
- to assess the low-temperature cracking susceptibility of the tested mixtures;

- to provide a performance-based mechanical interpretation of the effect of waste plastic on asphalt mixtures designed for different pavement layers.

Through these objectives, the thesis aims to contribute to the validation of waste-plastic asphalt mixtures from a mechanical performance point of view and to support their potential use in pavement applications.

Document outline

This thesis is developed in the following chapters:

Introduction and literature review: this chapter introduces the general background of sustainable asphalt mixtures and the use of reclaimed asphalt pavement (RAP) and waste plastic in pavement engineering. It also provides an overview of the mechanical behavior of asphalt mixtures, with particular attention to dynamic modulus, master curve development, fatigue response, and low-temperature cracking susceptibility. The motivation and objectives of the study are presented by framing the work within the Green Roads project and by highlighting the transition from previous activities on material selection, mixture formulation, and plant-scale production to the performance-based advanced mechanical characterization carried out in this thesis.

Materials and experimental methodology: this chapter describes the materials and mixtures investigated in the experimental program. It presents the materials and the adopted mixture coding system, specimen preparation procedures, volumetric checks, and the laboratory testing methods adopted for mechanical characterization. Particular attention is given to the AMPT testing procedures used to evaluate dynamic modulus, fatigue-related behavior, and low-temperature cracking susceptibility.

Experimental results and discussion: this chapter presents and discusses the results obtained from the laboratory testing program. The mechanical response of the investigated mixtures is analyzed in terms of dynamic modulus, master curves, fatigue behavior, and low-temperature cracking performance. The comparison between reference and recycled-plastic-modified mixtures is carried out on the investigated materials in order to evaluate the effect of waste plastic on their mechanical performance.

Conclusions: this final chapter summarizes the main findings of the thesis and evaluates whether the research objectives have been successfully addressed. It provides concluding remarks on the mechanical performance of asphalt mixtures incorporating waste plastic and RAP, with specific reference to the mixtures actually tested in the experimental campaign. Recommendations for future research are also provided, including further laboratory investigations and possible field validation.

1. Literature Review

1.1. Sustainable Asphalt Mixtures with RAP and Waste Plastic

Asphalt mixtures represent a key component of flexible pavement structures, where their performance depends on the interaction between aggregate skeleton, bituminous binder, air voids, and the applied traffic and environmental conditions. However, their production requires large quantities of virgin aggregates and bituminous binders, increasing the demand for natural resources and raising concerns about the sustainability of pavement construction[4].

Reclaimed asphalt pavement (RAP) is one of the most commonly used recycled materials in asphalt mixtures. RAP is obtained from the milling or removal of existing asphalt layers and contains both aggregates and aged bituminous binder. Its reuse allows part of the virgin aggregates and binder to be replaced, making it a valuable material for more resource-efficient asphalt production. Nevertheless, the aged binder contained in RAP can increase mixture stiffness and may influence cracking and fatigue performance. Therefore, the use of RAP requires careful mechanical evaluation, particularly when it is incorporated into mixtures intended for structural pavement layers [4]. In this context, rejuvenating agents are increasingly used in recycled asphalt mixtures to partially restore the rheological properties of aged binders and to improve the effective use of RAP in asphalt pavement applications [2].

In addition to RAP, waste plastic has attracted increasing attention as a possible additive or modifier in asphalt mixtures. Its incorporation may contribute to plastic waste management while also affecting the mechanical response of asphalt materials [5], [6]. Depending on the type of plastic, dosage, particle size, and incorporation method, waste plastic may modify stiffness, rutting resistance, fatigue behavior, and temperature susceptibility [5]. However, its effect is not universal and must be evaluated experimentally, since compatibility with the bituminous binder, processing conditions, and low-temperature behavior remain important concerns [5], [6].

Waste plastic can be incorporated into asphalt mixtures through different methods, among which the dry process represents the most practical approach for asphalt plant production. In this method, the polymer is added directly to the heated aggregates before the addition of bitumen. This allows the plastic particles to interact with the aggregate skeleton and the bituminous phase during mixing, promoting aggregate coating and possible partial modification of the bituminous phase, without the need to produce a polymer-modified binder separately.

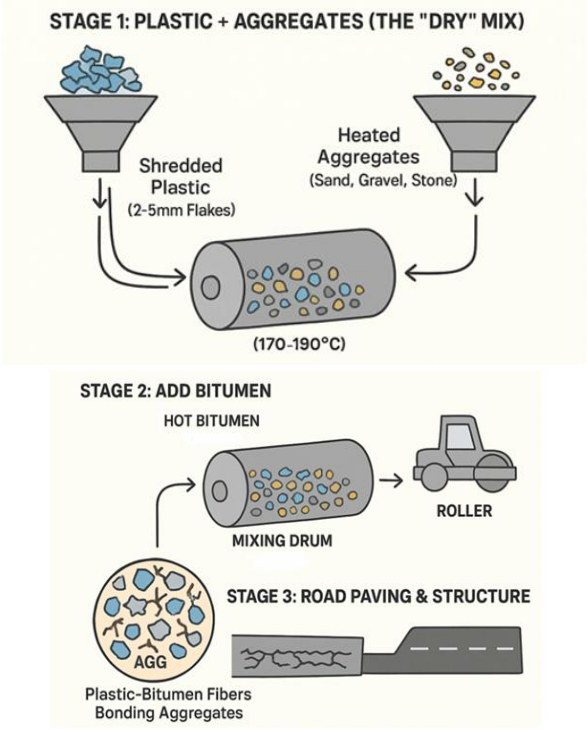

Figure 2 - Schematic representation of the dry process for incorporating recycled plastic into asphalt mixtures, adapted from [6].

In this thesis, RAP and waste plastic are considered within the framework of sustainable asphalt mixture development and, more specifically, within the “Green Roads” project. This project is developed through the collaboration between the Department of Environment, Land and Infrastructure Engineering (DIATI) of Politecnico di Torino and Brillada S.r.l., an asphalt mixture producer located in Borgaro Torinese, Italy. The project aims to develop asphalt mixtures incorporating RAP and waste plastic for industrial-scale application for all the three main pavement layers: wearing course, binder course, and base course. From a technical point of view, the project focuses on defining suitable mixture recipes in terms of aggregate skeleton, added bitumen content, RAP dosage, and waste plastic fraction, while complying with the Italian regulatory framework and ANAS technical specifications. Within the Italian framework, the project is also connected to the Minimum Environmental Criteria, known as Criteri Ambientali Minimi (CAM), which promote the use of recycled materials and the reduction of production and laying temperatures during road construction operations. From an operational point of view, these requirements were reflected in the definition of minimum RAP contents and controlled thermal protocols for mixture production and compaction. In previous phases of the Green Roads project, different RAP contents were adopted depending on the pavement layer: approximately 15% for the wearing course, 25% for the binder course, and 35% RAP for the base course.

The Green Roads project is organized as a multi-stage research program aimed at progressively moving from material selection to laboratory development and, ultimately, field

validation. In the initial stage, attention was devoted to screening different waste plastic materials and identifying suitable mixture formulations through laboratory-scale mix design. The following stage focused on mixtures produced at plant scale, using the outcomes of the laboratory phase as a basis for refining production procedures, assessing mechanical performance through advanced testing, and supporting the transition towards larger-scale production. The final stage of the project is intended to verify the developed solutions against technical requirements and to include broader validation activities, such as environmental assessment and full-scale field applications.

Within this framework, the present thesis is positioned within the advanced mechanical characterization stage of the Green Roads project. While previous activities were mainly devoted to material selection, laboratory mix design, and plant production procedures, this work investigates the response of the selected mixtures through performance-related laboratory testing. Particular attention is given to dynamic modulus characterization, master curve construction, fatigue behavior, and low-temperature cracking susceptibility, which provides a more complete interpretation of mixture behavior beyond conventional volumetric or mix-design indicators.

The scope of this work is centered on the mechanical evaluation of asphalt mixtures designed for the three pavement layers. The experimental framework originally included reference and recycled-plastic-modified mixtures for the wearing, binder, and base courses. However, due to the technical issues encountered during plant-scale production of the recycled-plastic-modified binder course mixture, the experimental campaign reported in this thesis included paired reference and modified mixtures for the wearing and base courses, while the binder course was represented by the reference mixture only.

Because each pavement layer is exposed to different loading and environmental conditions, the mechanical response of the selected mixtures cannot be evaluated only through mixture composition or volumetric properties. Therefore, performance-based laboratory testing is used as the basis for the experimental investigation presented in the following chapters.

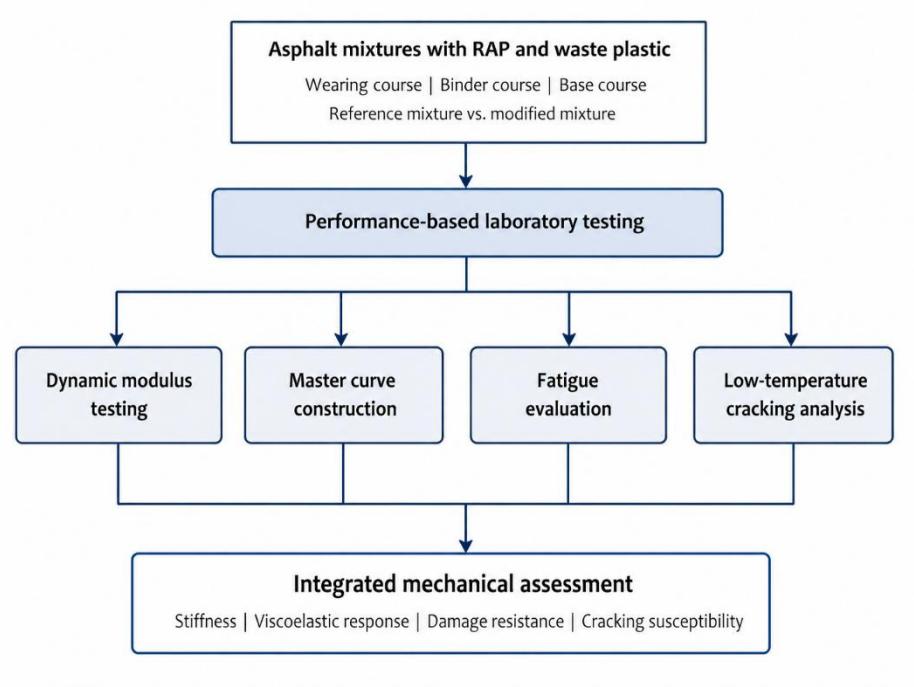

Figure 3 - General performance-based mechanical characterization framework adopted in this thesis.

1.2. Mechanical Behavior of Asphalt Mixtures

Asphalt mixtures are heterogeneous composite materials consisting of mineral aggregates, bituminous binder, air voids, and, in some cases, recycled or waste-derived constituents such as RAP and waste plastic. Their mechanical response is governed by the interaction among these components and is strongly influenced by mixture composition, aggregate structure, binder properties, air void content, temperature, and loading conditions. Unlike purely elastic materials, asphalt mixtures exhibit a viscoelastic response, meaning that their behavior depends on both time and temperature. As a result, the same mixture may behave as a relatively stiff and brittle material at low temperatures or high loading frequencies, while it may exhibit a softer and more viscous response at high temperatures or low loading frequencies [7], [8].

This temperature- and rate-dependent behavior is particularly important in pavement engineering because asphalt layers are continuously subjected to traffic loading and environmental variations. Under moving wheel loads, asphalt mixtures experience repeated stress and strain cycles, which may lead to different distress mechanisms depending on loading and temperature conditions. At high temperatures and slow loading rates, the mixture may be more susceptible to permanent deformation and rutting, while its stiffness and viscoelastic response can be effectively described through dynamic modulus testing and master curve construction [9]. Under repeated intermediate-temperature loading,

progressive damage accumulation may lead to fatigue cracking, which is one of the main structural distresses in flexible pavements and is commonly associated with repeated tensile strains and stiffness degradation [10]. At low temperatures, the increased stiffness of the material may reduce its ability to relax thermally induced stresses, increasing the risk of low-temperature cracking [11].

The mechanical behavior of asphalt mixtures is also affected by the structural role of each pavement layer. Wearing courses are directly exposed to traffic loads, weathering, and surface-related performance requirements, such as skid resistance and durability. Binder courses contribute to load distribution and provide continuity between the surface and the underlying structural layers. Base courses play a major role in supporting the pavement structure and distributing traffic-induced stress to the lower layers. Therefore, mixtures designed for different pavement layers may require different stiffness levels, damage resistance, and temperature-related performance characteristics.

In mixtures containing RAP, the aged binder present in the reclaimed material may contribute to an increase in stiffness and may alter the viscoelastic response of the mixture. This can be beneficial for resistance to deformation, but it may also influence fatigue and cracking performance depending on the amount of RAP, the degree of binder ageing, and the effectiveness of blending between aged and virgin binders. Similarly, the incorporation of waste plastic may affect the internal structure of the mixture by interacting with the bituminous phase, contributing to aggregate coating, or acting as a solid inclusion, depending on plastic type, particle size, melting behavior, and incorporation method. For this reason, the mechanical effects of RAP and waste plastic cannot be assumed a priori and must be evaluated experimentally.

This background provides the basis for interpreting how RAP and waste plastic may influence the mechanical response of mixtures designed for different pavement layers.

1.3. Performance-Based Mechanical Characterization of Asphalt Mixtures

Traditional asphalt mixture evaluation has often relied on volumetric requirements and empirical or semi-empirical mechanical indicators. Although these approaches are useful for mixture design and quality control, they may not fully describe the actual response of asphalt mixtures under the combined effects of traffic loading, temperature variation, ageing, and material heterogeneity. This limitation becomes more relevant when innovative or non-conventional materials, such as RAP and waste plastic, are incorporated into the mixture. In such cases, performance-based mechanical evaluation is necessary to understand how these materials influence stiffness, viscoelastic response, damage accumulation, and cracking susceptibility [12], [13], [14].

Among the different mechanical properties, dynamic modulus is widely used to characterize the linear viscoelastic response of asphalt mixtures. It provides information on material stiffness as a function of temperature and loading frequency and is commonly used as a key input for mechanistic–empirical pavement analysis [12], [14]. Since laboratory tests can only cover a limited range of temperatures and frequencies, dynamic modulus data are commonly shifted to construct master curves, which describe the material response over a wider range of reduced frequencies at a selected reference temperature [12]. In recent performance-related frameworks, dynamic modulus testing is often combined with advanced modelling approaches to interpret the viscoelastic properties of asphalt mixtures more accurately and for supporting further mechanical analyses [12], [13], [14].

Beyond stiffness characterization, the evaluation of fatigue behavior is essential because fatigue cracking represents one of the main distress mechanisms in flexible pavements. Under repeated traffic loading, asphalt mixtures experience progressive damage accumulation, which may lead to stiffness reduction, microcrack development, and eventually macrocrack propagation. Conventional fatigue approaches often rely on empirical relationships, while more advanced methods, such as the Viscoelastic Continuum Damage (VECD) approach, aim to determine intrinsic material properties that are less dependent on specific test conditions [12], [15]. An example of this approach is provided in [12], where fatigue behavior was evaluated using the simplified VECD method and rutting behavior was assessed through a viscoplastic shift model. The results showed that these methods can distinguish differences associated with mixture composition and pavement layer function.

The use of waste plastic or polymeric compounds further increases the need for laboratory evaluation based on mechanical performance indicators. Although the dry incorporation method can be less expensive and more practical than the wet method, it may provide less direct control over binder modification and mixture properties [13]. Previous research has shown that polymeric compounds and waste plastic may increase stiffness and rutting resistance, but their effect on fatigue and cracking resistance is not always consistent. This uncertainty is mainly related to the balance between stiffness increase and damage tolerance. Therefore, mixtures containing waste-plastic-related additives should be evaluated not only in terms of stiffness, but also in terms of fatigue and cracking performance [13].

A similar need exists for RAP-containing mixtures, since the aged binder in RAP can modify both stiffness and fatigue response. The long-term performance of recycled asphalt mixtures depends on several factors, including the amount and source of RAP, the degree of binder ageing, the type of binder or additive used, the production temperature, and the interaction between virgin and aged binders. In this regard, the study reported in [14] showed that warm recycled mixtures containing RAP and polymer-modified bitumen can be assessed through stiffness and fatigue characterization over time, highlighting the importance of monitoring both mechanical properties and ageing-related effects.

Low-temperature cracking is another critical distress mechanism that must be considered when asphalt mixtures become stiff and less able to relax thermally induced stresses. This aspect is particularly relevant for mixtures containing aged binder from RAP or additives that increase stiffness [14]. To address this issue, the reduced testing framework introduced in [16] provides an alternative approach for low-temperature cracking analysis by using AMPT-based dynamic modulus and fatigue data instead of conventional indirect tensile creep compliance and strength tests. The framework is based on a viscoelastic continuum damage model and enables the estimation of low-temperature creep compliance, indirect tensile strength, and critical cracking temperature from mechanical characterization data. This approach is particularly relevant to the present thesis because the low-temperature cracking evaluation is developed from the same dynamic modulus and fatigue characterization framework adopted for the main performance assessment.

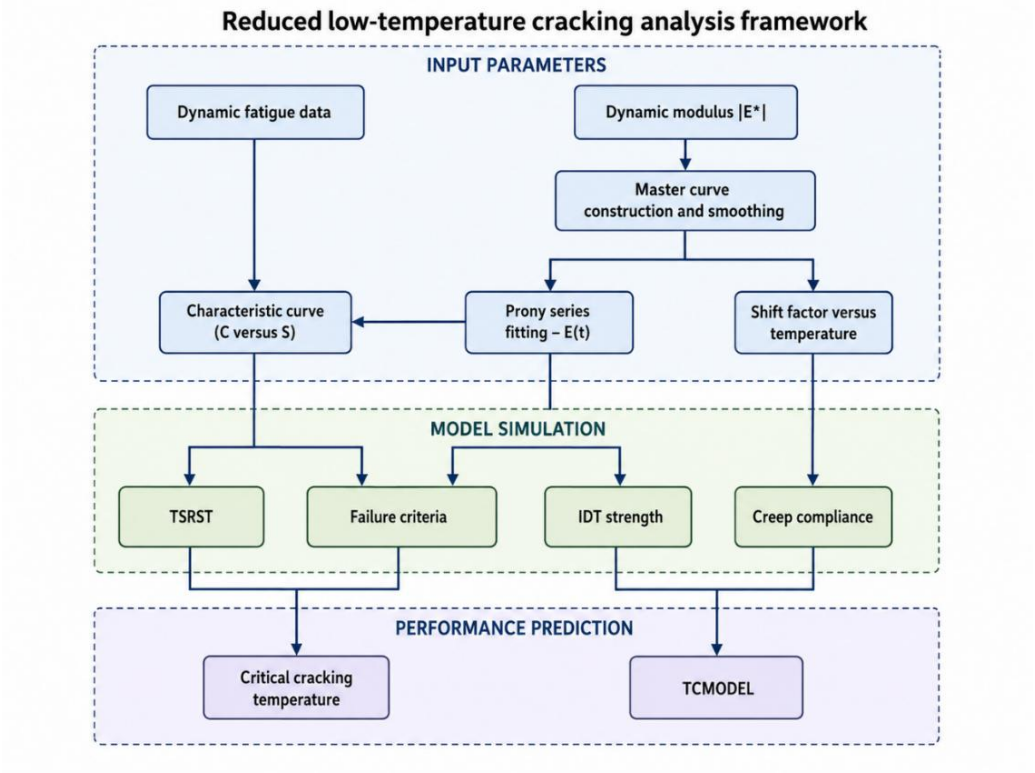

Figure 4 - Reduced testing framework for low-temperature cracking analysis based on AMPT data, adapted from [16]

Accordingly, the present thesis combines dynamic modulus testing, master curve construction, fatigue evaluation, and low-temperature cracking analysis within a single mechanical assessment framework. The detailed experimental procedures and analysis methods are presented in the Materials and Experimental Methodology chapter.

1.4. Research Gap and Aim of the Mechanical Investigation

Previous stages of the Green Roads project mainly focused on mix design and preliminary characterization of innovative asphalt mixtures for wearing, binder, and base courses. These activities addressed mixture composition, volumetric properties, optimum binder content, and basic mechanical indicators, providing an important basis for the development of waste-plastic-modified asphalt mixtures.

However, a specific research gap remains regarding their advanced mechanical response under performance-related loading conditions. In particular, further investigation is required to understand how the incorporation of waste plastic affects stiffness evolution, linear viscoelastic behavior, fatigue resistance, and low-temperature cracking susceptibility. This need is especially relevant because mixtures containing RAP and waste plastic may show different and sometimes competing mechanical effects: RAP may increase stiffness due to the presence of aged binder, while waste plastic may modify the internal structure of the mixture depending on its physical form, thermal behavior, and interaction with the binder and aggregate skeleton [13], [14].

Recent research has shown that performance-based approaches can provide a more reliable interpretation of asphalt mixture behavior than traditional evaluation methods based only on volumetric parameters or basic stiffness indicators. Advanced frameworks based on dynamic modulus testing, master curve construction, and damage-based fatigue analysis allow the intrinsic material response to be assessed over a wider range of loading and temperature conditions [12]. This is especially important for innovative or non-conventional mixtures, for which conventional indicators may not be sufficient to explain the expected field performance.

The main aim of the present thesis is therefore to provide an advanced mechanical characterization of sustainable asphalt mixtures incorporating waste plastic, considering the three main pavement layers: wearing course, binder course, and base course. The original experimental framework included reference and recycled-plastic-modified mixtures for each pavement layer. However, due to technical issues encountered during plant-scale production of the recycled-plastic-modified binder course mixture, the mechanical effect of waste plastic could be assessed directly only for the wearing and base courses. The binder course was therefore represented by the reference mixture, which was used as a mechanical baseline for the intermediate layer.

The experimental investigation focuses on performance-related mechanical properties of the mixtures obtained from the previous phase of the project involving plant-scale production. In particular, the study considers dynamic modulus testing, master curve construction, fatigue characterization, and low-temperature cracking susceptibility. These analyses are selected because they provide complementary information on the behavior of asphalt mixtures under different loading and temperature conditions. Dynamic modulus and master curves describe

the linear viscoelastic stiffness response, fatigue testing provides information on damage accumulation under repeated loading, and low-temperature analysis helps assess the potential susceptibility to thermally induced cracking.

The scope of this thesis is centered on laboratory-based mechanical characterization. The results can support a performance-based interpretation of the tested mixtures and provide useful information for future studies dealing with pavement design, field monitoring, or environmental evaluation.

This thesis aims to contribute to the understanding of how recycled plastic may affect the mechanical behavior of RAP-containing asphalt mixtures designed for different pavement layers. The comparison between reference and modified mixtures provides a basis for evaluating whether the incorporation of recycled plastic is compatible with the mechanical requirements of sustainable asphalt pavements.

2. Materials and Experimental Methodology

This chapter presents the asphalt mixtures investigated in the present thesis and the experimental procedures adopted for their mechanical characterization. Since the mixtures were already developed during previous stages of the Green Roads project, the present chapter does not focus on material selection, mix design optimization and production-scale implementation. The chapter describes the selected mixtures, their main constituents, the adopted mixture coding, specimen preparation procedures, and the testing methods used for the performance-based mechanical evaluation. The chapter is divided into two main parts. First, the investigated materials and mixtures are introduced, including mineral aggregates, reclaimed asphalt pavement, added neat bitumen, and waste plastics. Then, the experimental methodology is presented, with particular attention to volumetric checks, specimen preparation, dynamic modulus testing, master curve construction, fatigue characterization, and low-temperature cracking analysis

2.1. Materials

The materials investigated in this thesis are asphalt mixtures developed within the Green Roads project for the three main pavement layers: wearing course, binder course, and base course. Since the objective of the present work is the advanced mechanical characterization of already designed mixtures, the term “materials” mainly refers to the selected asphalt mixtures rather than to the individual constituents considered separately.

The mixtures considered in this thesis are composed of mineral aggregates, reclaimed asphalt pavement (RAP), added neat bitumen, and recycled plastics when present. The mineral aggregates and RAP form the granular skeleton of the mixtures, while the added neat bitumen provides coating, cohesion, and workability. RAP contributes both aggregate particles and aged binder; therefore, its presence affects not only the sustainability of the mixture but also its volumetric and mechanical response.

The mixtures were designed in previous stages of the Green Roads project in compliance with the Italian framework for sustainable road construction, including the Minimum Environmental Criteria (Criteri Ambientali Minimi, CAM) and the relevant technical requirements for pavement layers. Different RAP contents were adopted according to the function of each layer: approximately 15% RAP for the wearing course, 25% RAP for the binder course, and 35% RAP for the base course. These values were selected to increase the use of recycled materials while maintaining the technical feasibility of production, compaction, and pavement application.

Table 1 summarizes the mixture framework considered in the Green Roads project and the materials actually included in the experimental campaign of this thesis.

Table 1. General composition of the asphalt mixtures considered in this thesis

Pavement layer	Main constituents	RAP	Recycled plastic	Mixtures included in this study
Wearing course	Mineral aggregates, RAP, added neat bitumen, waste plastic when present	15%	0.4%	Reference + modified
Binder course		25%	0.4%	Reference
Base course		35%	0.8%	Reference + modified

The original experimental framework included reference and recycled-plastic-modified mixtures for each pavement layer. However, due to technical issues encountered during plant-scale production of the recycled-plastic-modified binder course mixture, this material was not available within the time frame of the thesis. Therefore, the experimental campaign included paired reference and modified mixtures for the wearing and base courses, while the binder course was represented by the reference mixture only.

The previous mix-design studies provided the basis for the selection of these mixtures: wearing course mixtures were developed to evaluate the feasibility of incorporating waste plastics in surface layers, binder course mixtures were designed to assess the role of recycled plastics in intermediate structural layers, and base course mixtures were optimized to investigate the effect of plastic incorporation on volumetric and mechanical performance.

Waste plastics were introduced in the modified mixtures using the dry method. In this process, the plastic is added directly during mixture production, allowing it to interact with the heated aggregates and the bituminous phase. This method was adopted because it is compatible with conventional asphalt production and allows the use of recycled plastic materials without producing a polymer-modified binder beforehand. However, the behavior of the plastic in the mixture depends on its particle size distribution, thermal response, and interaction with aggregates and bitumen.

Only one waste plastic material, hereafter referred to as plastic M, was considered in this thesis. This material had already been selected during previous stages of the Green Roads project after preliminary empirical evaluations aimed at assessing its suitability for asphalt mixture production. These evaluations included particle size analysis, thermal softening observations, squashing after heating, and interaction tests with pre-heated aggregates. According to the Green Roads project presentations, thermal softening was examined at 200°C, 225°C, and 250°C, while the interaction tests were used to observe possible coating, clustering, and binder-like behavior when recycled plastic M was mixed with hot aggregates.

Figure 5 – Recycled-plastic material M selected for incorporation into the asphalt mixtures.

Plastic M had previously been used in several Green Roads mixture trials and was therefore adopted as the waste plastic material for the mixtures investigated in this thesis. Preliminary observations suggested that M may not behave as a fully homogeneous phase during mixing. Part of the material may soften or partially melt and contribute to aggregate coating, while another fraction may remain as solid particles or polymeric clusters within the mixture. This behavior is relevant for interpreting the mechanical response of the mixtures, since M may act partly as a binder-like phase and partly as a solid inclusion.

Table 2. Waste plastic material considered in the experimental framework

Plastic material	Origin / type	Preliminary selection criteria	Expected behavior during mixing
M	Recycled plastic used in previous Green Roads mixture trials	Particle size, thermal softening, squashing after heating, interaction with hot aggregates	Possible partial softening/melting; possible aggregate coating; possible solid inclusion

In the present thesis, the materials are therefore considered at the mixture scale. The focus is not to repeat the previous mix design process, but to evaluate the mechanical performance of the selected reference and waste-plastic-modified mixtures through dynamic modulus testing, fatigue characterization, and low-temperature cracking analysis. The detailed mixture coding, selected specimens, testing standards, and number of specimens are presented in the following section.

2.2. Experimental methodology

The experimental methodology adopted in this thesis was designed to provide a performance-based mechanical characterization of the selected asphalt mixtures. The experimental program included specimen preparation, volumetric verification, dynamic modulus testing, master curve construction, fatigue characterization, and low-temperature cracking analysis. The tests were performed on mixtures designed for the three pavement layers considered in the Green Roads project: wearing course, binder course, and base course.

The analyzed mixtures were identified through the coding system previously adopted within the Green Roads project. This coding system allows each mixture and specimen to be uniquely identified according to the pavement layer, production method, waste plastic content, added bitumen content, lithic skeleton, thermal protocol, production batch, and sample number. The general structure of the coding system is shown in Figure 6.

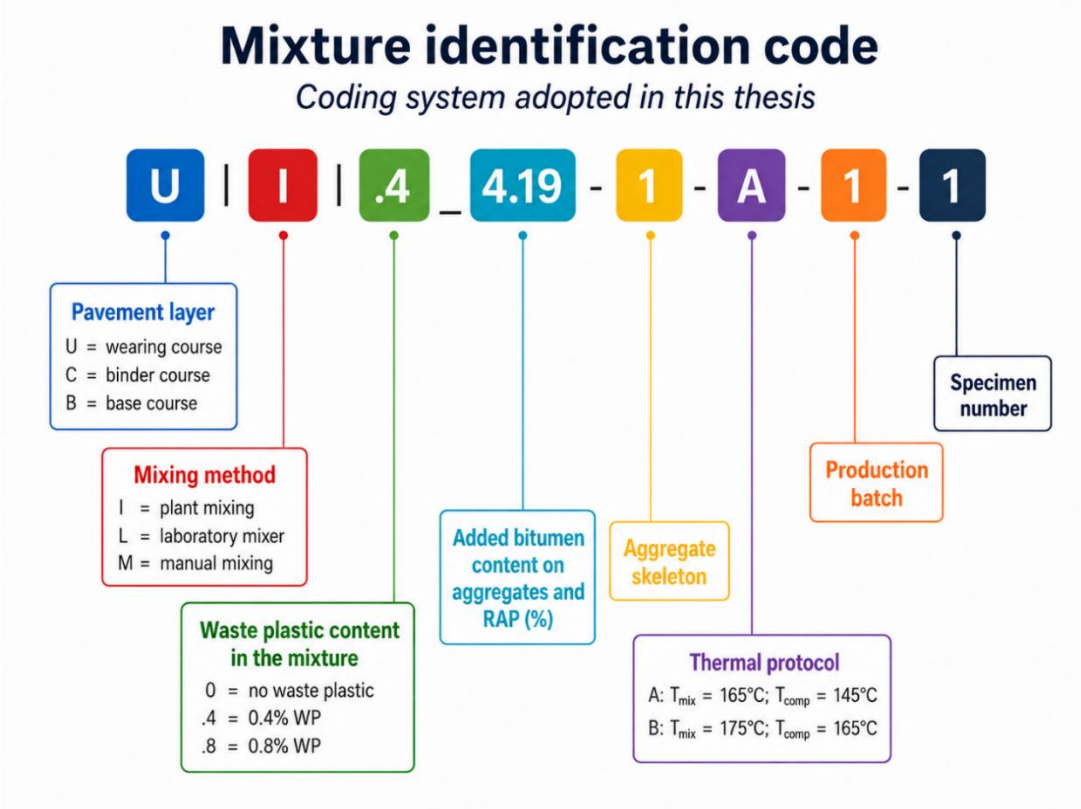

Figure 6 - Mixture coding system adopted for the investigated mixtures

For example, the code UI.4_4.19-1-A-1-1 identifies a wearing course mixture produced by plant mixing, containing 0.4% waste plastic, with 4.19% added bitumen referred to aggregates and RAP, aggregate skeleton 1, thermal protocol A, production batch 1, and specimen number 1.

The testing program was organized according to the type of mechanical information required from each mixture. Dynamic modulus testing was used to characterize the linear viscoelastic stiffness response and to construct master curves. Fatigue testing was adopted to assess damage evolution under repeated loading, while low-temperature cracking analysis was carried out using the AMPT-based dynamic modulus and fatigue framework adopted in this thesis.

The overall experimental workflow is summarized in Figure 7. The procedure starts with the collection of the available plant-produced mixtures, followed by specimen preparation and volumetric checks. The prepared specimens are then tested in the AMPT, and the resulting data are processed to obtain dynamic modulus master curves, fatigue-related parameters, and low-temperature cracking indicators.

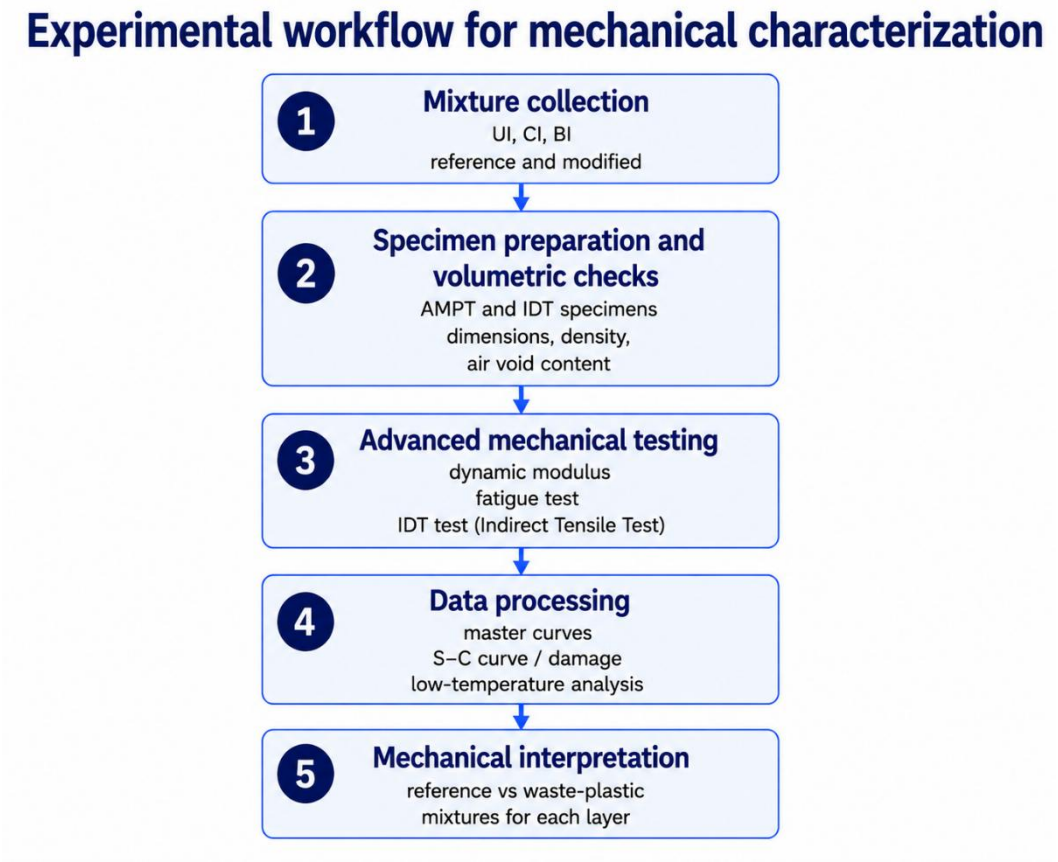

Figure 7 - Experimental workflow adopted for the mechanical characterization of the selected mixtures.

After introducing the mixture identification system and the general experimental workflow, the experimental program is summarized in Table 3. The table links each investigated mixture with the corresponding mechanical tests, reference standards or methodological frameworks, specimen type. The recycled-plastic-modified binder course mixture, although planned within the original Green Roads framework, is not reported in the table because it was not available within the time frame of this thesis and was therefore not tested.

Table 3. Summary of the experimental testing program

Mixture ID	Test performed	Standard	Specimen type (D× H , mm)
UI.4_4.19-1-A-1	Dynamic modulus	AASHTO TP 132	Small cylindrical (38×110)
	Fatigue	AASHTO T 411	Small cylindrical (38×110)
	Low-temperature cracking	AASHTO T 322	Cylindrical ($150 \times 38 - 50$)
UI.0_4.19-1-A-1	Dynamic modulus	AASHTO TP 132	Small cylindrical (38×110)
	Fatigue	AASHTO T 411	Small cylindrical (38×110)
	Low-temperature cracking	AASHTO T 322	Cylindrical ($150 \times 38 - 50$)
CI.0_3.90-1-A-1	Dynamic modulus	AASHTO TP 132	Small cylindrical (38×110)
	Fatigue	AASHTO T 411	Small cylindrical (38×110)
	Low-temperature cracking	AASHTO T 322	Cylindrical ($150 \times 38 - 50$)
BI.8_2.20-0-A-1	Dynamic modulus	AASHTO TP 132	Small cylindrical (38×110)
	Fatigue	AASHTO T 411	Small cylindrical (38×110)
	Low-temperature cracking	AASHTO T 322	Cylindrical ($150 \times 38 - 50$)
BI.0_2.20-0-A-1	Dynamic modulus	AASHTO TP 132	Small cylindrical (38×110)
	Fatigue	AASHTO T 411	Small cylindrical (38×110)
	Low-temperature cracking	AASHTO T 322	Cylindrical ($150 \times 38 - 50$)

2.2.1. Dynamic Modulus

Dynamic modulus testing was performed to characterize the linear viscoelastic stiffness response of the investigated asphalt mixtures. The dynamic modulus, $|E^*|$, represents the relationship between applied cyclic stress and the resulting recoverable cyclic strain under sinusoidal loading. Together with the phase angle, δ, it provides information on the temperature- and frequency-dependent behavior of asphalt mixtures.

Within the experimental program, dynamic modulus testing represents the first step of the performance-based mechanical characterization. The obtained data were used to compare the stiffness response of the investigated reference and waste-plastic-modified mixtures where paired materials were available. In addition, the results were used for the construction of master curves and as input information for the subsequent fatigue and low-temperature cracking analyses.

Dynamic modulus tests were performed only on small cylindrical AMPT specimens following AASHTO TP 132 [17]. The adopted specimen geometry was 38 mm in diameter and 110 mm in height. The use of small specimens was selected because of material availability and

because this geometry allows multiple replicate specimens to be extracted from the same gyratory-compacted parent specimen.

The dynamic modulus testing procedure included three main stages: specimen preparation, definition of test settings, and master curve construction. These stages are described in the following subsections.

2.2.1.1. Specimen preparation

Specimens for dynamic modulus testing were prepared from asphalt mixtures previously produced within the Green Roads project. Therefore, the present work did not include the preparation of the mixtures from individual constituents, but focused on the reheating, compaction, coring, cutting, and volumetric verification of specimens suitable for AMPT testing.

Before compaction, the loose asphalt mixtures were reheated and conditioned until the target compaction temperature of 145°C was reached. The heated material was then compacted using the Superpave Gyratory Compactor (SGC) to produce cylindrical parent specimens with a nominal diameter of 150 mm and a height of approximately 180 mm. These parent specimens were subsequently used for extracting the required AMPT specimens, either large or small, by coring and cutting.

This parent-specimen geometry was selected in accordance with AASHTO R 83 [19], which specifies 150-mm-diameter SGC specimens for the preparation of performance test specimens. The standard indicates a minimum parent-specimen height of 160 mm for compressive tests and 180 mm for tensile or tension tests. In this thesis, 180 mm height was adopted to ensure sufficient material for the preparation workflow. The same standard also defines the final large test specimen as a 100-mm-diameter by 150-mm-tall cylindrical specimen cored and sawed from the SGC specimen [18]

The selection of large or small specimen geometry was primarily governed by the mixture gradation and nominal maximum aggregate size (NMAS). Large specimens provide better representativeness for mixtures with coarser aggregate structures, whereas small specimens are suitable for dense-graded mixtures with a compatible maximum aggregate size. The adopted large-specimen preparation procedure is applicable to dense, gap, and open graded asphalt mixtures with NMAS up to 37.5 mm [18]. In contrast, AASHTO PP 99, Standard Practice for Preparation of Small Cylindrical Performance Test Specimens Using the Superpave Gyratory Compactor (SGC) or Field Cores, covers 38-mm-diameter by 110-mm-height specimens and is intended for dense-graded asphalt mixtures with NMAS up to 19.0 mm [19].

In addition to these applicability limits, the small specimen geometry offers practical advantages when the available material is limited or when a higher number of replicates is required. Since up to four small specimens can be extracted from one gyratory-compacted parent specimen, this geometry allows a more efficient use of material and enables multiple replicate specimens to be obtained from the same compaction condition. Moreover, extracting the cores from the inner portion of the gyratory specimen helps reduce the influence of edge effects and radial air void gradients that may develop during gyratory compaction.

Table 4 - Geometry and applicability of dynamic modulus test specimens

Criterion	Small specimen
Final specimen diameter	38 mm
Final specimen height	110 mm
Parent SGC specimen	150 mm × 180 mm
Main preparation standard	AASHTO PP 99 [19]
Dynamic modulus standard	AASHTO TP 132 [17]
Mixture applicability	Dense-graded mixtures with NMAS up to 19.0 mm

For small-specimen preparation, cylindrical cores with a nominal diameter of 38 mm were extracted from the same type of parent specimens. The coring locations were marked on the SGC specimen and located within the central 100 mm diameter region, allowing up to four small specimens to be obtained from one parent specimen. After coring, both ends of each small core were sawed to achieve the final height of 110 mm and to provide flat and parallel loading surfaces. The main steps of the coring and specimen extraction procedure are illustrated in Figure 8 [19].

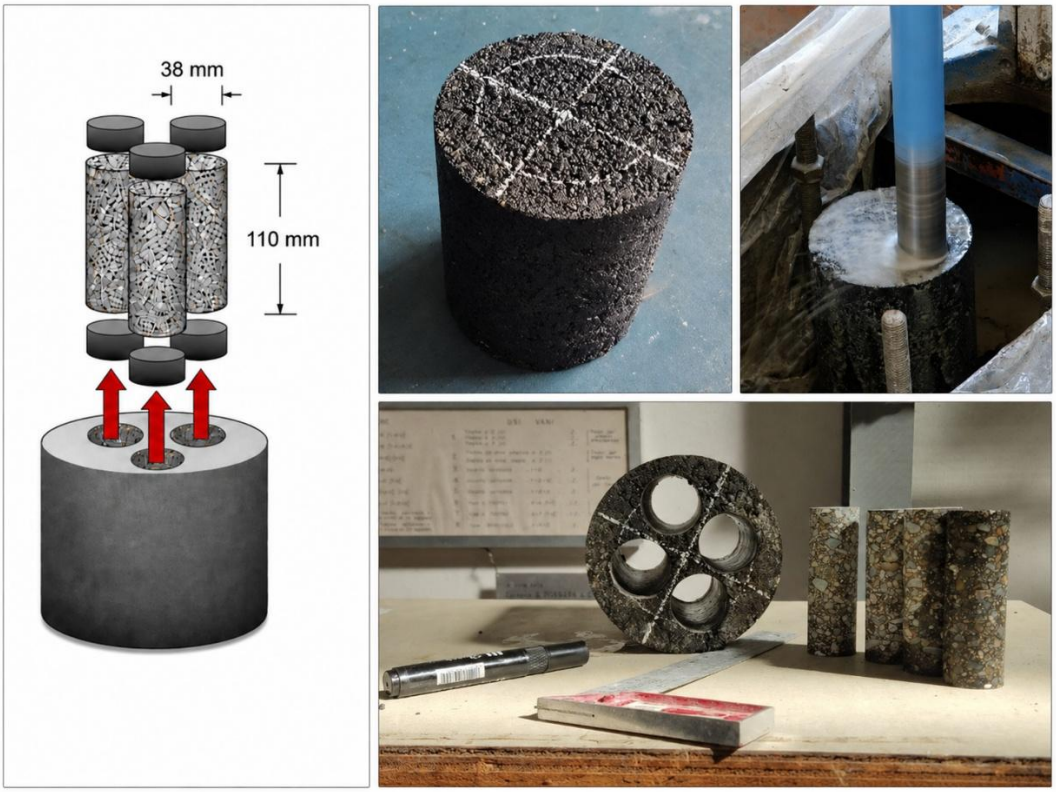

Figure 8 - AMPT specimen preparation procedure: specimen extraction scheme and small-specimen coring process, adapted from Lee et al. (2017); and specimens prepared in the present experimental work.

For both large and small specimens, coring was preferably performed before sawing, and the specimens were extracted from the inner part of the gyratory compacted sample. This procedure was adopted to minimize boundary effects and reduce the influence of radial air void gradients. The quality of coring and cutting was considered essential because specimen geometry, end flatness, and perpendicularity directly affect the reliability of AMPT deformation measurements.

Dimensional tolerances were checked before testing. For large specimens, the required tolerances included an average diameter between 98 and 104 mm, a height between 147.5 and 152.5 mm, a diameter standard deviation not exceeding 0.5 mm, End flatness not exceeding 0.5 mm, and end perpendicularity not exceeding 1.0 mm. For small specimens, the average diameter was required to be between 36 and 40 mm, the height between 107.5 and 112.5 mm, the diameter standard deviation not exceeding 0.5 mm, and both end flatness and end perpendicularity within 0.5 mm. Specimens not satisfying these tolerances were excluded from testing [18], [19].

In addition to dimensional tolerances, the air void content of the prepared specimens was verified before dynamic modulus testing.

The target air void content was selected as 4.0%. This value was adopted because asphalt mixture properties used in mechanistic–empirical pavement analysis are commonly defined at approximately 4% air voids, as reported in the NCHRP 1-37A / MEPDG baseline design inputs for asphalt concrete layers[20]. Therefore, the 4.0% value was used in this thesis as a reference volumetric condition for mechanical characterization, rather than as a new mix-design requirement.

Accordingly, specimens were considered suitable for dynamic modulus testing when their air void content was within 4.0 ± 0.5%, corresponding to an acceptable range between 3.5% and 4.5%. This criterion was adopted to ensure volumetric consistency among replicate specimens and to reduce the influence of air void variability on the measured mechanical response. The selected target and tolerance are also consistent with previous asphalt mixture performance characterization studies, in which specimens cored from 150-mm-diameter by 180-mm-height SGC parent specimens were prepared at a target air void content of 4.0% ± 0.5% [21].

Before dynamic modulus testing, all specimens were checked in terms of bulk density and air void content. The maximum density values used for the air void calculation were taken from the previous Green Roads mixture characterization dataset. These values correspond to the maximum density, ρ_m, reported for each mixture. Therefore, the volumetric verification in this thesis focused on determining the bulk density of the compacted specimens and calculating the corresponding air void content.

For bulk density determination, the European procedure was adopted instead of the AASHTO saturated surface-dry method. AASHTO T 166, *Standard Method of Test for Bulk Specific Gravity (Gmb) of Compacted Hot Mix Asphalt (HMA) Using Saturated Surface-Dry Specimens*, defines the SSD-based procedure for determining the bulk specific gravity of compacted asphalt specimens [22]. However, this procedure refers to measurements performed under a reference water temperature of 25°C. In the present experimental work, the laboratory setup did not allow the water bath and measurement environment to be maintained consistently at this reference temperature. For this reason, the European procedure was selected, since it allows the actual water temperature to be measured and the corresponding density of water to be used in the calculation.

Accordingly, the bulk density was determined according to EN 12697-6, *Bituminous mixtures Test methods Part 6: Determination of bulk density of bituminous specimens* [23]. In this approach, the water temperature was recorded during the test, and the corresponding value of water density was used to calculate the bulk density under the actual laboratory conditions.

The bulk density was calculated as:

$$\rho_b = \frac{M_a}{M_{SSD} - M_w} \times \rho_w(T)$$

where $\rho_b$is the bulk density of the compacted specimen, $M_a$is the dry mass of the specimen in air, M_{SSD} is the saturated surface-dry mass, M_w is the mass of the specimen in water, and $\rho_w(T)$ is the density of water at the measured test temperature.

The air void content was calculated according to EN 12697-8, Bituminous mixtures Test methods Part 8: Determination of void characteristics of bituminous specimens [24].The calculation used the maximum density of the mixture, ρ_m, taken from the previous Green Roads dataset, and the bulk density of the compacted specimen, ρ_b, determined experimentally in this thesis.

The air void content was calculated as:

$$V_a = \frac{\rho_m - \rho_b}{\rho_m} \times 100$$

where $V_a$is the air void content of the compacted specimen, $\rho_m$is the maximum density of the asphalt mixture, and $\rho_b$is the bulk density of the compacted specimen.

Volumetric verification was necessary because air void content directly affects the stiffness response and the repeatability of dynamic modulus results. Specimens with unsuitable geometry or air void content outside the target range of $4.0 \pm 0.5\%$were not used in the mechanical testing program.

Before dynamic modulus testing, gauge points were glued on the lateral surface of each specimen to allow the installation of the specimen-mounted deformation measurement system. For both large and small specimens, the gauge points were attached according to the manufacturer's instructions, and the gauge length was checked before testing. According to the dynamic modulus procedures for both specimens configurations, the gauge length should be 70 ± 1 mm, measured center-to-center between the gauge points [17], [25].

Three vertical LVDTs were then mounted around the specimen, approximately 120° apart, to measure axial deformation during cyclic loading. Correct positioning of the gauge points and LVDTs was necessary to reduce measurement errors, improve deformation uniformity, and ensure reliable calculation of dynamic modulus and phase angle. Figure 9 shows the installation of the gauge points and specimen-mounted LVDTs used for dynamic modulus testing.

Figure 9 - Gauge point installation on AMPT specimens before dynamic modulus testing

2.2.1.2. Test settings

Dynamic modulus tests were conducted using the Asphalt Mixture Performance Tester (AMPT) under unconfined axial cyclic compression loading. During each test, a cyclic compressive load was applied at selected temperatures and loading frequencies, and the resulting axial deformation was measured as a function of time. These measurements were used by the AMPT software to determine the dynamic modulus, $|E^*|$, and the phase angle, δ. In this way, the temperature- and frequency-dependent linear viscoelastic response of the investigated asphalt mixtures was characterized [17], [25]. The experimental setup used for the dynamic modulus test is shown in Figure 10.

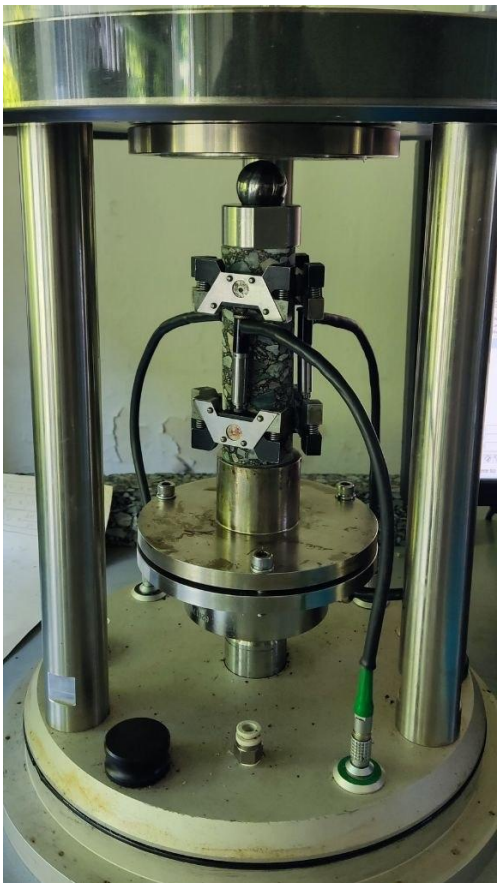

Figure 10 - AMPT setup for dynamic modulus testing of asphalt mixture specimens under unconfined axial cyclic compression loading.

The adopted procedures provided the general framework for specimen preparation, test setup, loading conditions, and data acceptance criteria used in this study [17].

Regarding temperature selection, the recommended test temperatures for small specimens are selected based on the binder performance grade (PG), and the same PG-based framework is also used for master curve construction. Since the mixtures investigated in this thesis were produced with a PG 58-22 binder, 35°C was selected as the high testing temperature, together with 20°C as the intermediate temperature. Although 4°C is included as the recommended low temperature, the available AMPT system could not reliably reach and maintain this temperature under the laboratory conditions of the experimental campaign. An initial low-temperature target of approximately 8.5°C was therefore considered, and a limited number of preliminary tests were conducted at actual temperatures close to 8.4°C. However, reaching and stabilizing the system at this temperature required an excessively long conditioning time. Consequently, the low-temperature set point was subsequently

increased to 10°C for the main experimental campaign. Therefore, the standard testing temperatures adopted for the remaining tests were 10°C, 20°C, and 35°C [17].

Dynamic modulus tests were performed at loading frequencies of 10, 1, and 0.1 Hz for each testing temperature. This frequency range was adopted to characterize the stiffness response of the mixtures under different loading-rate conditions and to provide the experimental basis for master curve construction. The lower frequency of 0.01 Hz was not included, because the experimental program was based only on the small-specimen testing configuration[17].

For each mixture, at least three replicate small specimens were considered. All specimens used for testing had already satisfied the dimensional and volumetric acceptance criteria described in the specimen preparation section. The replicate measurements were used to evaluate the consistency and repeatability of the dynamic modulus and phase angle results before mixture comparison and master curve construction [17].

The adopted dynamic modulus testing conditions are summarized in Table 5.

Table 5. Dynamic modulus test settings adopted in this thesis.

Parameter	Small specimens
Specimen geometry	38 mm × 110 mm
Minimum number of specimens	At least 3 specimens
Loading mode	Unconfined axial cyclic compression
Test temperatures	10°C, 20°C, 35°C
Frequencies	10, 1, 0.1 Hz
Main outputs	$\lvert E^* \rvert$, δ

Before each test, the specimens were conditioned at the selected test temperature. The AMPT testing chamber was allowed to reach the target temperature before specimen installation, and the specimen temperature was required to be within ±0.5°C of the target value before starting the test. The conditioning time was selected according to the test temperature and the small-specimen testing procedure[17].

The testing sequence followed the frequency-sweep approach adopted in the AMPT dynamic modulus procedure. For each specimen, testing started at the lowest temperature and highest frequency. At each temperature, the frequencies were applied in descending order before moving to the next higher temperature. This order was adopted to minimize the risk of damage or excessive permanent deformation during the early stages of testing and to maintain consistency throughout the experimental program [17]

The target strain level was controlled to keep the test within the linear viscoelastic range. For small specimens, the acceptable peak-to-peak strain range was 50–75 με. The applied

load amplitude was automatically adjusted by the AMPT software to maintain the required strain level during the test [17].

The main data quality requirements used for accepting the dynamic modulus results are summarized in Table 6. These parameters were checked by the AMPT software after each test. Tests not satisfying the data quality criteria were repeated when possible.

Table 6. Data quality criteria adopted for dynamic modulus testing [17], [25]

Data quality parameter	Small specimens
Peak-to-peak strain	50–75 με
Load standard error	≤ 8% at 10°C and 20°C; ≤ 12% at 35°C
Deformation standard error	≤ 8% at 10°C and 20°C; ≤ 12% at 35°C
Deformation uniformity	≤ 30%
Phase uniformity	≤ 3°
Deformation drift	In the direction of the applied load, or up to 100% in the opposite direction

The dynamic modulus, $|E^*|$, and phase angle, δ, were obtained automatically from the AMPT software for each temperature–frequency combination. These results were used to evaluate the stiffness response of the tested mixtures and to construct the dynamic modulus master curves described in the following subsection.

In addition to the AMPT data quality indicators, the repeatability of the dynamic modulus results was evaluated. For each mixture and each temperature–frequency combination, the variability among replicate specimens was checked in terms of $|E^*|$ and δ. The repeatability assessment was carried out using the precision framework provided in the corresponding AASHTO procedures before using the data for mixture comparison and master curve construction [17], [18].

Only data satisfying both the quality and repeatability requirements were retained in the final dataset. The accepted data were then used to calculate average dynamic modulus and phase angle values and to construct the corresponding master curves.

A representative example of the repeatability assessment is shown in Figure 11. The figure illustrates how the variability among replicate specimens was checked for both dynamic modulus and phase angle over the tested temperature–frequency combinations. The bars represent the measured range among replicate specimens, while the dashed lines indicate the corresponding repeatability limits.

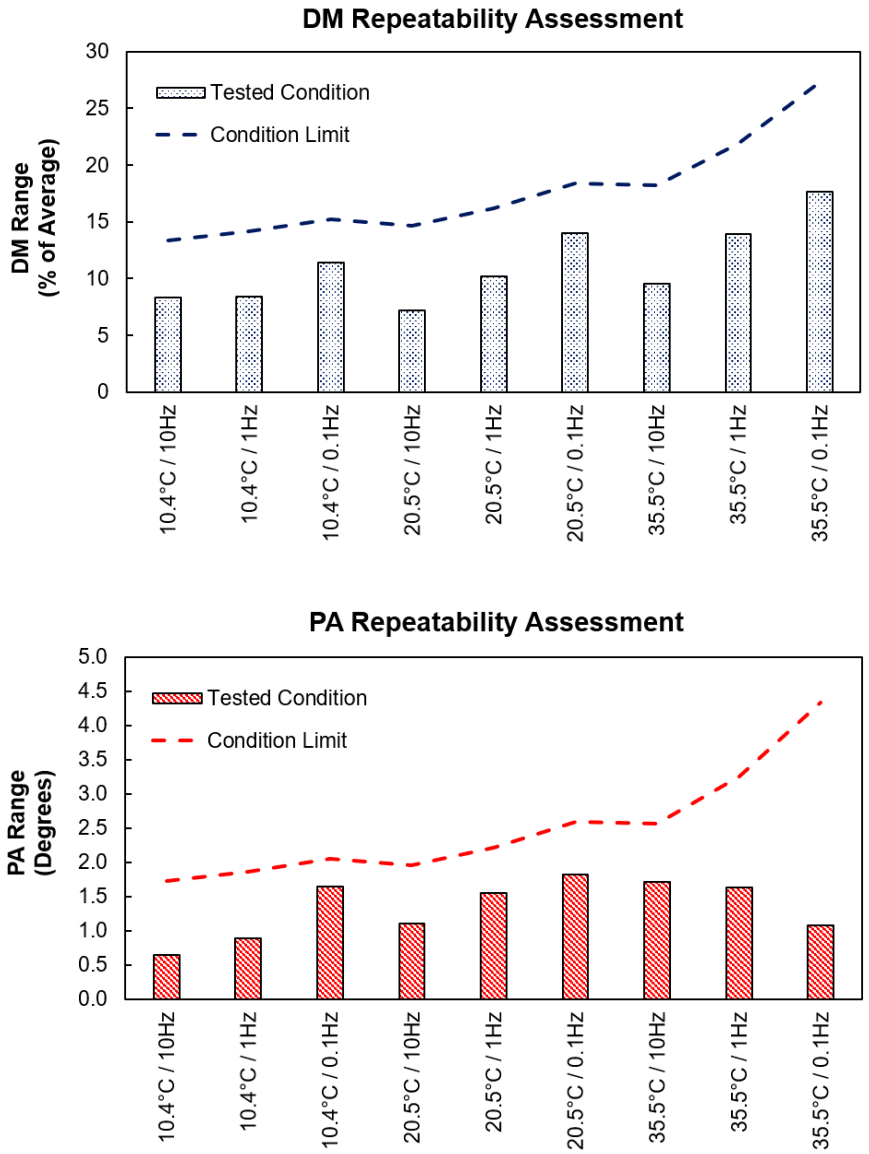

Figure 11 - Example of dynamic modulus and phase angle repeatability assessment based on AASHTO precision limits.

2.2.1.3. Master curves

The dynamic modulus results obtained at different temperatures and loading frequencies were used to construct master curves for the investigated asphalt mixtures. A dynamic modulus master curve provides a continuous representation of the stiffness response of an asphalt mixture over an extended range of loading frequencies at a selected reference temperature. This approach is based on the time–temperature superposition principle, according to which data measured at different temperatures can be shifted along the logarithmic frequency axis to obtain a single continuous curve.

In this thesis, two approaches were used for master curve construction and comparison. The first approach followed the standardized sigmoidal procedure described in AASHTO R 84 [26], while the second approach was based on the 2S2P1D rheological model implemented in FlexMAT. The use of both approaches allowed the stiffness behavior of the mixtures to be evaluated through a standard AMPT-based fitting method and a rheological viscoelastic model consistent with the subsequent fatigue analysis.

The standard [26] procedure describes the testing and analysis steps required to develop dynamic modulus master curves from AMPT data. It is intended for dense- and gap-graded asphalt mixtures with nominal maximum aggregate sizes up to 37.5 mm and provides guidance for selecting suitable test temperatures considering the temperature limitations of the AMPT system.

According to this procedure, dynamic modulus and phase angle data are collected at selected combinations of temperature and loading frequency. The measured data are then shifted to a reference temperature to obtain a continuous function describing the variation of dynamic modulus with frequency and temperature. The master curve is therefore constructed by shifting data from different temperatures along the logarithmic frequency axis.

In the present study, the reference temperature was selected as 21.1°C, corresponding to 70°F. This value was adopted to ensure consistency between the sigmoidal master curves and the master curves obtained from the 2S2P1D-based analysis. Since 70°F is commonly used in FlexMAT for viscoelastic characterization, using the same reference temperature allowed a direct comparison between the two approaches and maintained consistency with the subsequent fatigue analysis.

The first step of the analysis consisted of preparing a dynamic modulus data summary. For each temperature frequency combination, the average dynamic modulus, average phase angle, coefficient of variation of the dynamic modulus, and standard deviation of the phase angle were calculated. These values were used to evaluate the consistency of replicate specimens before fitting the master curve.[26]

The reduced frequency was calculated by shifting the measured loading frequency to the selected reference temperature. In general form, the reduced frequency can be expressed as:

$$\log f_r = \log f + \log a_T$$

where f_r is the reduced frequency at the reference temperature, f is the loading frequency at the test temperature, and a_T is the temperature shift factor [26].

In the sigmoidal procedure, the reduced frequency is calculated using an Arrhenius-type relationship:

$$\log f_r = \log f + \frac{\Delta E_a}{19.14714}\left(\frac{1}{T} - \frac{1}{T_r}\right)$$

where ΔE_a is the activation energy, T is the test temperature in Kelvin, and T_r is the reference temperature in Kelvin. The activation energy is treated as a fitting parameter during the optimization process[26].

The shift factor at each temperature can therefore be expressed as:

$$\log a_T = \frac{\Delta E_a}{19.14714}\left(\frac{1}{T} - \frac{1}{T_r}\right)$$

where a_T represents the horizontal shift required to move the data measured at temperature T to the reference temperature[26].

The dynamic modulus master curve was fitted using the sigmoidal model:

$$\log | E^* | = \delta + \frac{Max - \delta}{1 + e^{\beta + \gamma \log f_r}}$$

where $| E^* |$ is the dynamic modulus, f_r is the reduced frequency, Max is the limiting maximum modulus, and δ, β, and γ are fitting parameters.

The limiting maximum modulus is estimated from mixture volumetric properties using the Hirsch model. The main volumetric parameters required for this calculation are the voids in mineral aggregate, VMA, and the voids filled with asphalt, VFA. After estimating the limiting maximum modulus and selecting the reference temperature, the remaining fitting parameters are determined through numerical optimization.

The optimization was carried out by minimizing the sum of squared errors between the logarithm of the measured dynamic modulus values and the logarithm of the values

predicted by the sigmoidal model. The fitting parameters determined during this process were δ, β, γ, and ΔE_a. The fitted curve was then used to describe the variation of dynamic modulus as a function of reduced frequency[26].

The quality of the fitted master curve was evaluated using the goodness-of-fit indicators S_e, S_y, S_e/S_y, and R^2. The fitted curve was considered acceptable when:

$$\frac{S_e}{S_y} < 0.05 \text{ and } R^2 > 0.99$$

These criteria were used to verify whether the fitted master curve provided an adequate representation of the measured dynamic modulus data[26].

The standard sigmoidal analysis followed in this thesis can therefore be summarized as follows: dynamic modulus and phase angle data were first obtained from AMPT testing; replicate results were summarized at each temperature–frequency combination; the reference temperature was selected as 21.1°C; reduced frequencies and shift factors were calculated; the sigmoidal master curve was fitted using numerical optimization; and the goodness of fit was finally checked using $S_e/S_y$and $R^2[26]$. The main steps followed for dynamic modulus master curve construction, from AMPT data processing to goodness-of-fit evaluation, are summarized in Figure 12.

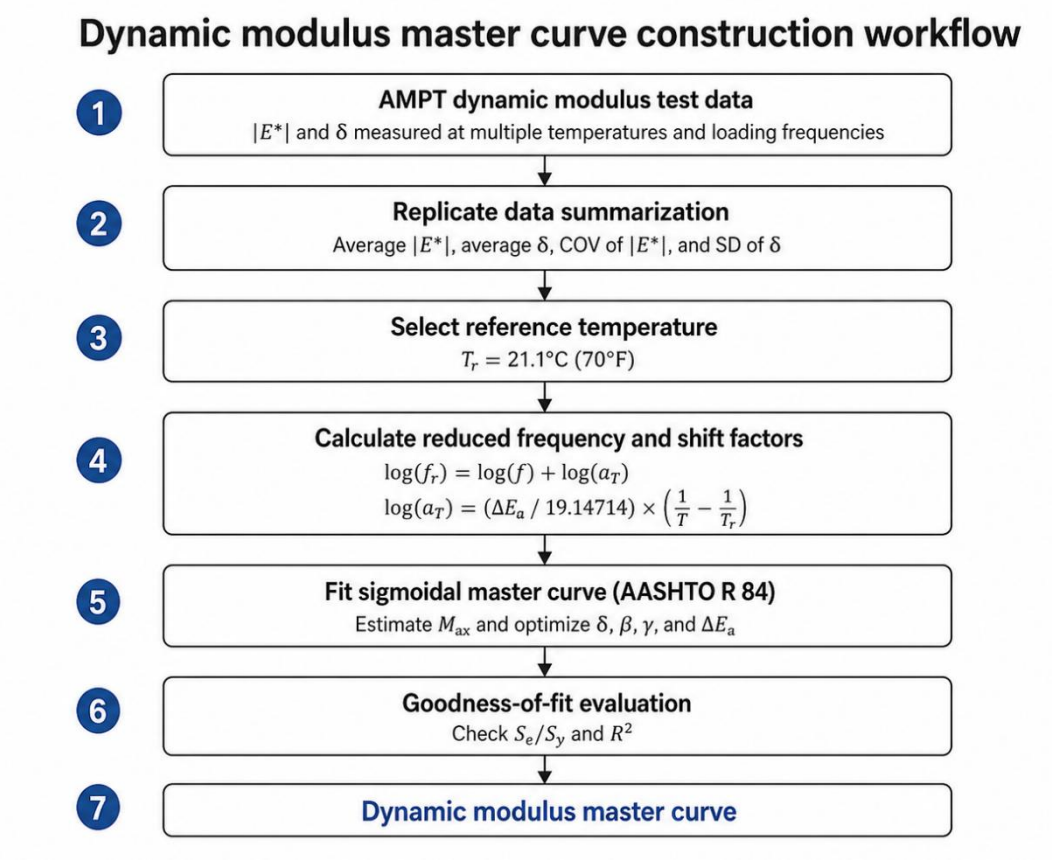

Figure 12 - Workflow adopted for dynamic modulus master curve construction based on time–temperature superposition.

The same dynamic modulus data were also analyzed using the 2S2P1D-based approach. This model was originally proposed by Olard and Di Benedetto (2003) and has been adopted in recent VECD-based asphalt mixture studies for fitting the storage modulus master curve. In this approach, the model is fitted to the storage modulus:

$$E_1 = | E^* | \cos \delta$$

because E_1 is required for the subsequent fatigue analysis within the VECD framework.

The 2S2P1D model is a linear viscoelastic rheological model used to describe the complex modulus behavior of asphalt binders and asphalt mixtures. Its name refers to its mechanical representation, which consists of two springs, two parabolic elements, and one dashpot. The springs represent the elastic limits of the material response, the parabolic elements describe the delayed viscoelastic behavior, and the dashpot accounts for viscous flow at very low

reduced frequencies. A schematic representation of the 2S2P1D rheological model is shown in Figure 13.

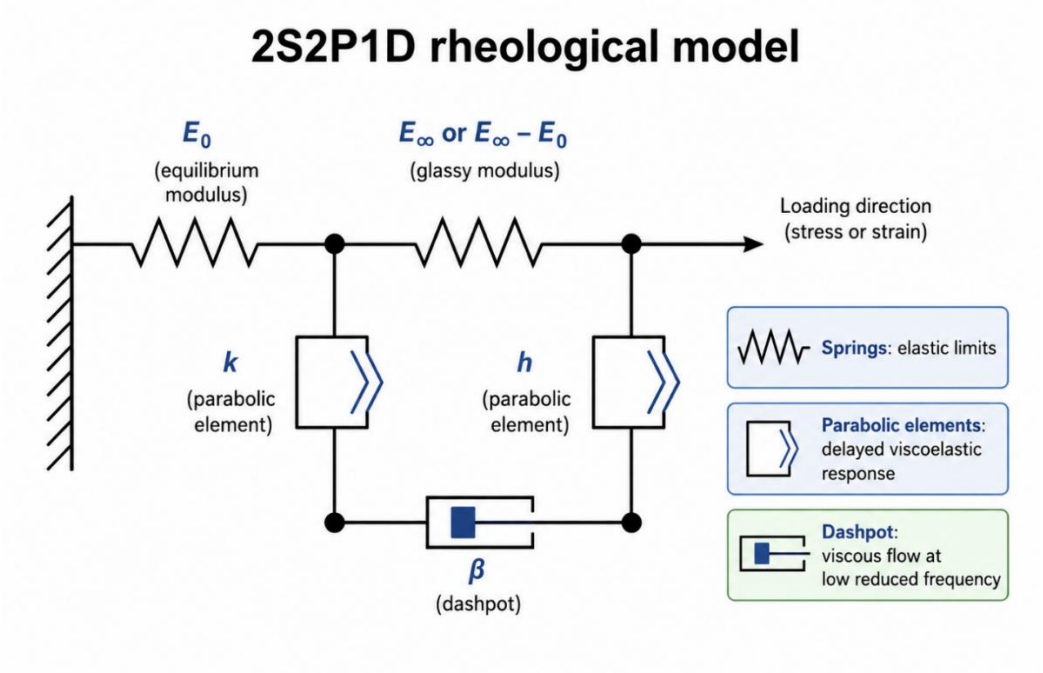

Figure 13 - Schematic representation of the 2S2P1D rheological model used for asphalt mixture viscoelastic characterization.

The storage modulus formulation can be written as:

$$E_1(i\omega\tau) = E_{1,0} + \frac{E_{1,\infty} - E_{1,0}}{1 + \delta(i\omega\tau)^{-k} + (i\omega\tau)^{-h} + (i\omega\beta\tau)^{-1}}$$

where $E_1$is the storage modulus, $E_{1,0}$is the storage modulus when $\omega \to 0$, $E_{1,\infty}$is the storage modulus when $\omega \to \infty$, $\omega$is the angular frequency, $\tau$is the characteristic time, $k$and $h$are parameters related to the two parabolic elements, $\delta$is a proportional constant between the parabolic elements, and $\beta$is associated with the Newtonian viscosity of the dashpot [12].

The angular frequency is defined as:

$$\omega = 2\pi f$$

where $f$is the loading frequency.

The characteristic time is temperature-dependent and can be expressed as:

$$\tau(T) = a_T(T)\tau_0$$

where $a_T(T)$is the shift factor at temperature T, and $\tau_0$is the characteristic time at the reference temperature. Therefore, this approach also uses the time–temperature superposition principle to describe the temperature-dependent viscoelastic response of asphalt mixtures.

At very low reduced frequencies, corresponding to high temperature or slow loading, the viscous component becomes more influential, and the modulus approaches the equilibrium modulus $E_{1,0}$. At very high reduced frequencies, corresponding to low temperature or fast loading, the material response becomes stiffer and approaches the glassy modulus $E_{1,\infty}$. The parabolic elements control the transition between these two limits and describe the shape of the viscoelastic response in the intermediate frequency range.

The parameters $k$and $h$control the slopes of the curve in the viscoelastic transition zone and are generally constrained between 0 and 1, with $k < h$. The parameter δ_p controls the relative contribution of the parabolic elements, while βcontrols the influence of the dashpot at low frequencies. Because of this structure, the 2S2P1D model provides a more physically interpretable representation of the viscoelastic response than a purely empirical curve-fitting equation.

The 2S2P1D model parameters were calibrated using the storage modulus, $E' =\mid E^* \mid \cos\delta$, calculated from the measured dynamic modulus and phase angle. Although the fitting procedure was performed in terms of E', the 2S2P1D model defines the complete complex modulus response. After calibration, the corresponding dynamic modulus magnitude was calculated from the storage and loss modulus components as:

$$\mid E^* \mid = \sqrt{(E')^2 + (E'')^2}$$

where $E''$is the loss modulus predicted by the 2S2P1D model. The resulting $\mid E^* \mid$values were used to construct the 2S2P1D dynamic modulus master curves and to compare them with the measured dynamic modulus data and the sigmoidal predictions.

The comparison between the two approaches was performed by plotting the predicted dynamic modulus magnitude, $\mid E^* \mid$, as a function of reduced frequency at the same reference temperature of 21.1°C. The sigmoidal approach represents the master curve using a fitted mathematical function, while the 2S2P1D-based approach represents the same viscoelastic response using a rheological model. Using the same reference temperature was essential because a different reference temperature would shift the position of the master curve along the frequency axis and would make a direct comparison less meaningful.

The two approaches were used for complementary purposes rather than as competing methods. The sigmoidal procedure provided a standardized AMPT-based framework for master curve construction, including data summarization, shift-factor calculation, curve fitting, and goodness-of-fit evaluation. The 2S2P1D-based analysis provided a rheological viscoelastic representation of the same data and supplied the input required for the subsequent fatigue characterization. Therefore, the comparison between the two approaches was used to verify the consistency of the fitted master curves and to support the interpretation of the mixture stiffness response.

Agreement between the two fitted master curves indicates that the measured dynamic modulus data are consistent and that the stiffness response is well represented by both approaches. Differences between the two models may occur especially at the very low and very high reduced-frequency ranges, where fewer experimental data are available and model extrapolation has a stronger influence. For this reason, the comparison was mainly used to evaluate the general trend of the master curves and the consistency of the viscoelastic characterization, rather than to select one model as superior to the other.

Taken together, the master curve analysis allowed the dynamic modulus response of each mixture to be represented over an extended frequency range. This continuous stiffness representation was used to compare the reference and waste-plastic-modified mixtures and to provide input information for the subsequent fatigue and low-temperature cracking analyses.

2.2.2. Fatigue test

Fatigue testing was performed to evaluate the damage resistance of the investigated asphalt mixtures under repeated cyclic loading. In asphalt pavements, fatigue cracking is one of the main distress mechanisms and is mainly associated with the progressive accumulation of micro-damage caused by traffic-induced tensile strains. Therefore, fatigue characterization was used to assess the ability of each mixture to tolerate repeated loading before reaching failure.

In this thesis, the fatigue response was analyzed within the simplified viscoelastic continuum damage framework. This approach describes fatigue behavior through material-related damage properties rather than only through empirical fatigue relationships. The analysis is based on the relationship between the material integrity parameter, C, and the accumulated damage variable, S. This relationship is referred to as the damage characteristic curve, or C-S curve.

Fatigue tests were carried out using the Asphalt Mixture Performance Tester (AMPT) on small cylindrical specimens, following AASHTO T 411 [27]. The fatigue analysis was linked to the dynamic modulus characterization presented in the previous section, since the

viscoelastic properties derived from the dynamic modulus master curve were required for the calculation of the damage parameters and the construction of the C-S relationship.

The fatigue testing procedure included three main stages: specimen preparation, definition of the test settings, and determination of the damage parameters $S$and C. These stages are described in the following subsections.

2.2.2.1. Specimen preparation

Fatigue specimens were prepared using the same general coring, cutting, and volumetric verification procedure described for dynamic modulus testing. Therefore, the description of mixture reheating, parent specimen compaction, dimensional checks, and bulk density determination is not repeated in detail in this section. The main additional preparation step for fatigue testing was the bonding of the specimens to the loading platens, which was required because the cyclic fatigue test was performed in direct tension.

Fatigue tests were performed only on small cylindrical AMPT specimens. The adopted specimen geometry was 38 mm in diameter and 110 mm in height, in accordance with the small-specimen configuration specified for AMPT cyclic fatigue testing[27]. The number of specimens tested for each mixture is reported in the experimental program summary in Table 3.

Before fatigue testing, the prepared specimens were checked in terms of air void content using the same volumetric procedure described in Section 2.2.1.1. The target air void content was 4.0 ± 0.5%, corresponding to an acceptable range of 3.5% to 4.5%. Specimens outside this range were not considered suitable for testing.

Gauge points were then attached to the lateral surface of each specimen to allow the installation of the on-specimen axial deformation measurement system. Axial deformation was measured over a gauge length of 70 ± 1 mm, using three deformation sensors placed approximately 120° apart around the specimen. This arrangement was used to monitor the axial strain response during cyclic loading and to check the reliability of the measured deformation [27].

After the gauge points were positioned, the top and bottom loading platens were glued to the specimen using epoxy adhesive. This step was essential for transferring the cyclic tensile load from the AMPT actuator to the asphalt specimen. Before bonding, the platen surfaces were cleaned and prepared to improve adhesion and reduce the risk of debonding during the fatigue test. The specimens were carefully centered between the platens, and the adhesive layer was allowed to cure before testing. The standards require the loading platens to be bonded to the top and bottom of the specimen in order to ensure proper load transfer during direct tension cyclic fatigue testing [27], [28].

Figure 14 shows the preparation of the fatigue specimens, including gauge point installation and bonding of the specimen to the loading platens.

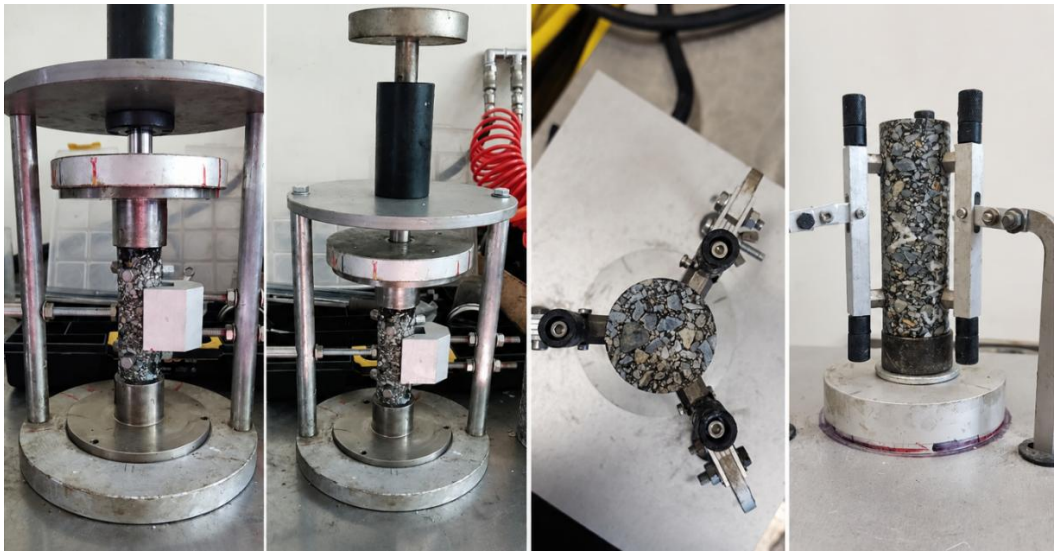

Figure 14- Preparation of AMPT fatigue specimens with gauge points and bonded loading platens.

2.2.2.2. Test settings

Fatigue tests were performed in the AMPT under direct tension cyclic loading. The test was conducted in actuator displacement control mode, in which a repeated axial tensile displacement was applied to the specimen until failure. During the test, the applied load and the on-specimen axial strain response were recorded and used for the subsequent fatigue damage analysis. The experimental setup used for the cyclic direct tension fatigue test is shown in Figure 15.

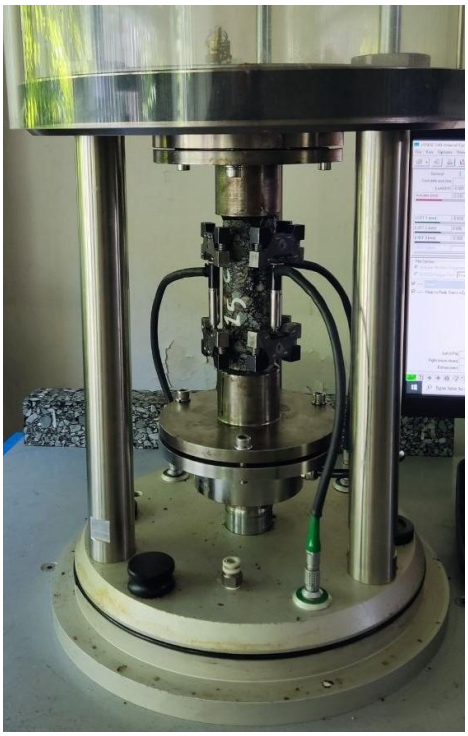

Figure 15 - AMPT setup used for cyclic direct tension fatigue testing of asphalt mixture specimens

All fatigue tests were performed at $21°C$ and 10 Hz. The test temperature was selected according to the AMPT cyclic fatigue testing framework, in which the fatigue temperature is defined based on the binder performance grade and is limited to a maximum of $21°C$ for conventional mixtures. The same temperature and loading frequency were adopted for all mixtures to ensure a consistent comparison between the reference and waste-plastic-modified mixtures[27].

Before each cyclic fatigue test, a fingerprint dynamic modulus test was carried out on the same specimen. This preliminary step was used to check the stiffness consistency of the fatigue specimen and to identify possible specimen-to-specimen variability before damage testing. The fingerprint test was performed at $21°C$ and 10 Hz, using axial tension–compression loading within the linear viscoelastic range. The target peak-to-peak on-specimen strain was maintained between 50 and 75 $\mu\varepsilon$[27].

During the fingerprint test, the AMPT software adjusted the load amplitude during the initial cycles and then applied the selected load level for 50 cycles. The quality of the fingerprint response was evaluated using the acceptance indicators summarized in Table 7. Specimens that did not satisfy the required limits were excluded from the fatigue analysis [27].

Table 7. Cyclic fatigue test: data quality statistic requirements for fingerprint test.[27], [28]

Indicator	Limit
Standard error of the applied stress	≤ 10%
Average standard error of the measured strains	≤ 10%
Uniformity coefficient of the measured strains	≤ 35%
Uniformity coefficient of the phase angle measurements	≤ 3°

The fingerprint modulus was also compared with the corresponding modulus obtained from the dynamic modulus master curve. This comparison was expressed through the dynamic modulus ratio, DMR, defined as:

$$DMR = \frac{|\ E^*\ |_{\text{fingerprint}}}{|\ E^*\ |_{\text{LVE}}}$$

where $|\ E^*\ |_{\text{fingerprint}}$ is the dynamic modulus measured during the fingerprint test, and $|\ E^*\ |_{\text{LVE}}$ is the linear viscoelastic dynamic modulus obtained from the master curve at the same temperature and frequency. A value of DMR close to 1 indicates that the fatigue specimen has a stiffness response consistent with the reference master curve. In this thesis, values between 0.85 and 1.15 were considered acceptable[27].

After the fingerprint test, the specimen was allowed to rest for at least 5 min before starting the cyclic fatigue test. The fatigue test was then performed at 10 Hz under direct tension using actuator displacement control. The strain level was selected manually for each specimen in order to obtain a number of cycles to failure within the acceptable range of 2,000 to 80,000 cycles. The selected strain level therefore depended on the stiffness and expected fatigue resistance of each mixture[27].

In addition to the number of cycles to failure, the failure location was also checked after testing. Only specimens showing middle failure, in which the macrocrack developed within the instrumented gauge area, were considered suitable for fatigue analysis. Specimens showing end failure were excluded because the crack developed outside the deformation measurement zone and could therefore lead to a non-representative damage characteristic curve. Examples of acceptable middle failure and unacceptable end failure are shown in Figure 16[27].

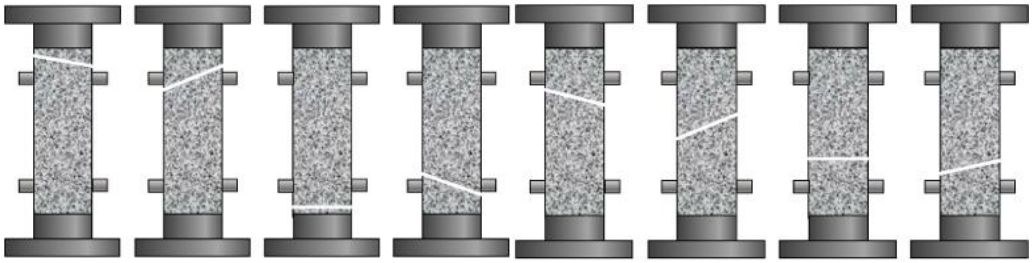

Figure 16 - Cyclic fatigue test: examples of (a) end failure and (b) middle failure, adapted from AASHTO T 411 [27].

According to the AMPT cyclic fatigue procedures, the fatigue characterization of each mixture requires at least three valid tests. A valid test is defined as a test satisfying the fingerprint acceptance criterion, the required range of cycles to failure, and the middle-failure requirement. These conditions must be satisfied before the fatigue data are used for determining the damage characteristic curve and the failure criterion [27].

2.2.2.3. Determination of S and C

The fatigue data obtained from the AMPT cyclic fatigue tests were analyzed within the simplified viscoelastic continuum damage, S-VECD, framework. This approach combines the linear viscoelastic properties obtained from dynamic modulus testing with the stress–strain response measured during cyclic fatigue loading. The main output of the analysis is the relationship between the material integrity parameter, C, and the accumulated damage variable, S, commonly referred to as the damage characteristic curve or C-S curve.

In the AMPT cyclic fatigue procedures, the damage variable $S$is defined as an internal state variable that quantifies microstructural changes in the asphalt mixture, while Crepresents the pseudo secant modulus in the stress–pseudostrain space. The C-S curve describes the relationship between the structural integrity of the material and the amount of accumulated damage. Therefore, as fatigue loading progresses, Sincreases and C decreases, representing the gradual loss of material integrity caused by cyclic loading [27].

The calculation of S and C requires the viscoelastic properties of the mixture. For this reason, the storage modulus master curve and the time–temperature shift factors obtained from the dynamic modulus analysis were used as input information. The measured stress and on-specimen strain histories from the cyclic fatigue test were converted into pseudostrain-based quantities, allowing the damage evolution to be separated from the linear viscoelastic response. In this way, the damage characteristic curve can be treated as a material-related property rather than as a result dependent only on the specific test condition.

The damage characteristic curve was fitted using the following power-law relationship:

$$C = 1 - C_{11}S^{C_{12}}$$

where C is the pseudo stiffness or material integrity parameter, S is the accumulated damage variable, and $C_{11}$and $C_{12}$are fitting coefficients. The coefficient C_{11}mainly controls the magnitude of the integrity reduction, while C_{12}controls the curvature of the damage characteristic curve. This formulation is commonly used in S-VECD-based asphalt mixture studies and allows the fatigue damage evolution of each mixture to be represented by a fitted C-S curve [12].

For each mixture, only valid fatigue tests were used to determine the representative C-S curve. A test was considered valid when the acceptance criteria described in Section 2.2.2.2 were satisfied, including an acceptable dynamic modulus ratio, a number of cycles to failure within the required range, and middle failure within the instrumented gauge area. The resulting C-S curves from replicate specimens were then checked for consistency before fitting the final curve for each mixture.

The number of cycles to failure, N_f, was determined according to the AMPT cyclic fatigue procedure. It corresponds to the cycle at which the product of the peak-to-peak stress and the number of cycles reaches a maximum value after a stable increase during cyclic loading. This criterion provides a consistent definition of failure for the S-VECD analysis and avoids the need to identify failure directly from phase angle measurements [12].

In addition to the damage characteristic curve, the cumulative loss of material integrity was calculated during cyclic loading. At each cycle, the reduction in pseudo stiffness is expressed as $1 - C$. The cumulative value up to failure is therefore obtained by summing the reduction in integrity over the loading history:

$$Cum(1 - C)$$

This quantity represents the accumulated loss of material integrity up to the failure cycle. The pseudo energy-based fatigue failure criterion, D_R, was then calculated as the ratio between the cumulative loss of integrity and the number of cycles to failure:

$$D_R = \frac{\int_0^{N_f}(1 - C)\, dN}{N_f}$$

For cycle-by-cycle experimental data, the same relationship can be written in discrete form as:

$$D_R = \frac{\mathrm{Cum}(1-C)}{N_f}$$

where $\mathrm{Cum}(1-C)$ is the cumulative summation of the pseudo stiffness reduction up to failure and $N_f$is the number of cycles to failure. Graphically, D_R can be interpreted as the slope of the relationship between $\mathrm{Cum}(1-C)$ and N_f. A higher D_R value indicates that the mixture can tolerate a larger average reduction in integrity before failure and is therefore associated with higher fatigue toughness[13], [27], [28].

For each valid specimen, D_R was calculated individually. The representative D_R value of each mixture was then obtained by averaging the values from the valid replicate specimens. The AMPT cyclic fatigue procedures require the reporting of the fingerprint dynamic modulus, the DMR value, the D_R value for each specimen, and, at the mixture level, the damage characteristic curve coefficients $C_{11}$and C_{12}, the parameter α, and the average D_R [27], [28].

The apparent damage capacity index, S_{app}, was considered as a fatigue cracking index for comparing the fatigue performance of the investigated asphalt mixtures. This index was developed within the S-VECD framework to account for the combined effects of mixture stiffness and fatigue toughness on cracking resistance. Unlike D_R, which mainly represents failure criterion related to the material toughness, S_{app}also incorporates the influence of the linear viscoelastic dynamic modulus. Therefore, it provides a broader indicator for evaluating and comparing the fatigue resistance of asphalt mixtures under a given climatic condition.

The S_{app}index is calculated at a reference temperature associated with the climatic PG condition of the project location. Higher S_{app}values generally indicate greater apparent damage capacity and, consequently, better fatigue cracking resistance. Therefore, in this thesis, $S_{\mathrm{app}}$was used to rank and compare the investigated mixtures in terms of their apparent fatigue damage capacity [12], [29].

The apparent damage capacity index is expressed as:

$$S_{\mathrm{app}} = 1000\left(\frac{\alpha}{2}-1\right) a_{T(S_{\mathrm{app}})}^{\frac{1}{\alpha+1}} \left(\frac{D_R}{C_{11}}\right)^{\frac{1}{C_{12}}} \frac{1}{|E^*|_{\mathrm{LVE},S_{\mathrm{app}}}^{\alpha/4}}$$

where $a_T$is the time–temperature shift factor corresponding to the S_{app}reference temperature, $D_R$is the fatigue failure criterion, $C_{11}$and $C_{12}$are the fitting coefficients of the damage characteristic curve, $\alpha$is the damage evolution rate parameter, and $|E^*|_{\mathrm{LVE},S_{\mathrm{app}}}$is

the linear viscoelastic dynamic modulus calculated at the S_{app} reference temperature and at the corresponding reduced frequency.

Since S_{app} incorporates stiffness, damage characteristic parameters, and fatigue toughness, it was used as a synthetic index to compare the fatigue resistance of the mixtures. However, the interpretation of S_{app} was carried out together with D_R and the fitted C-S curves, because these parameters describe different aspects of the fatigue response [14], [29].

In addition to providing a comparative fatigue indicator, S_{app} can also be used as an index-based criterion for mixture design, mixture acceptance, and quality assurance. Recommended threshold values have been proposed for different traffic categories expressed in million equivalent single-axle loads (MESALs). These limits were developed using a database of 105 asphalt mixtures and were supported by information from State highway agencies, accelerated pavement testing facilities, field test sections, and pavement performance simulations. Therefore, the proposed thresholds provide a practical basis for classifying asphalt mixtures according to their expected fatigue cracking resistance under different traffic levels.[29]

The recommended S_{app} limits indicate that mixtures subjected to higher traffic levels require greater apparent damage capacity. For traffic levels below 10 MESALs, a minimum S_{app} value of 8 is recommended. For traffic between 10 and 30 MESALs, the recommended limit increases to 24. For heavy traffic levels greater than 30 MESALs, S_{app} should exceed 30, while very slow and extremely heavy traffic conditions require a higher threshold of 36. These thresholds can be used as reference values for interpreting the fatigue performance of the mixtures investigated in this thesis.[29].

Table 8. Recommended S_{app} threshold values for different traffic levels [29].

Traffic (MESALs)	S_{app} Limits	Tier	Designation
Less than 10	S_{app}>8	Standard	S
Between 10 and 30	S_{app}>24	Heavy	H
Greater than 30	S_{app}>30	Very heavy	V
Greater than 30 and slow traffic	S_{app}>36	Extremely heavy	E

Accordingly, the S_{app} values obtained in this study were compared with these recommended limits to provide an additional interpretation of the fatigue performance of the mixtures considered in the fatigue analysis.

In this thesis, the fatigue analysis was carried out using the FlexMAT framework. The software was used to process the AMPT cyclic fatigue data, calculate $S$and C, fit the damage characteristic curve, and determine the fatigue-related parameters. However, the interpretation of the results was based on the S-VECD parameters themselves, namely the C-S curve, C_{11}, C_{12}, D_R, $\mathrm{Cum}(1-C)$, and S_{app}, rather than on the software output alone.

The parameters obtained from this analysis were used to compare the fatigue response of the tested mixtures. The C-S curve was used to describe damage evolution, $D_R$was used as an indicator of fatigue toughness, and $S_{\mathrm{app}}$was used as a synthetic index combining stiffness, damage tolerance, and toughness. These results are presented and discussed in the following chapter.

2.2.3. Low thermal cracking Susceptibility Analysis

Low-temperature cracking is a major distress mechanism in asphalt pavements exposed to cold climatic conditions. During cooling, restrained thermal contraction generates tensile stresses within the asphalt layer. Cracking may occur when these thermally induced stresses reach or exceed the tensile resistance of the asphalt mixture. Accordingly, the low-temperature cracking susceptibility of the investigated mixtures was evaluated by comparing the calculated thermal stress with their indirect tensile strength.

The adopted methodology was inspired by the reduced viscoelastic continuum damage framework proposed by Medeiros et al. In its original form, this framework uses dynamic modulus and fatigue data obtained from AMPT testing to estimate the low-temperature tensile response and the critical cracking temperature of asphalt mixtures. This approach was proposed to reduce the need for conventional low-temperature IDT creep compliance and strength testing by combining viscoelastic material properties with fatigue-derived damage characteristics.

In the present study, the procedure consisted of two stages. First, the low-temperature IDT strength was estimated analytically using the dynamic modulus master curve and the S-VECD damage relationship. This step was performed to follow the logic of the reduced AMPT-based framework and to obtain a preliminary prediction of the tensile strength. Second, direct IDT tests were performed to assess the consistency of the analytical prediction and to provide the experimentally measured tensile-strength threshold used in the final thermal cracking analysis.

2.2.3.1. Analytical Prediction of IDT Strength

The dynamic modulus master curve was used to obtain the relaxation modulus, $E(t)$, while the S-VECD fatigue analysis provided the damage characteristic relationship, $C(S)$. These properties were combined within a pseudostrain framework to estimate the tensile stress response under a simulated low-temperature IDT loading condition.

Pseudostrain was used to separate the linear viscoelastic response from the material damage response and was calculated as:

$$\varepsilon^R(t) = \frac{1}{E_R}\int_0^t E(t-\tau)\frac{d\varepsilon(\tau)}{d\tau}d\tau$$

where $\varepsilon^R(t)$is the pseudostrain, $E(t-\tau)$is the relaxation modulus, $\varepsilon(\tau)$is the applied strain history, and $E_R$is the reference modulus. The relaxation modulus used in this calculation was derived in FlexMAT from the dynamic modulus master curve.

The reduction in material integrity caused by damage accumulation was represented by the S-VECD damage characteristic relationship:

$$C(S) = 1 - C_{11}S^{C_{12}}$$

where $S$is the damage variable, and $C_{11}$and $C_{12}$are fitting coefficients obtained from the fatigue damage characteristic curve.

By treating $C(S)$as a normalized integrity function, the tensile stress response was estimated in the stress–pseudostrain space as:

$$\sigma(t) = C(S)E_R\varepsilon^R(t)$$

The IDT loading condition was simulated at a target temperature of approximately $-10°C$using a constant tensile strain rate of:

$$\dot{\varepsilon} = 4.0 \times 10^{-4}\ s^{-1}$$

This strain rate was selected according to the reference methodology, in which a representative tensile strain rate was adopted for the IDT strength calculation. A numerical loading window of 3 s was used to ensure that the peak calculated stress was captured. This duration was not assumed to represent a fixed experimental failure time for all mixtures. The analytically estimated IDT strength was defined as the maximum value of the calculated stress response:

$$\sigma_{\mathrm{IDT,estimated}} = \max[\sigma(t)]$$

The analytical result was considered a preliminary prediction because the spreadsheet implementation did not reproduce the complete incremental damage-evolution algorithm of the original VECD procedure.

2.2.3.2. Direct IDT Testing

Direct IDT strength tests were subsequently performed to provide an experimental tensile-strength reference for the low-temperature cracking analysis. The tests were carried out according to the main requirements of AASHTO T 322 [30]. For each mixture, at least three replicate disc specimens were considered in order to obtain a representative tensile strength value. The specimens had a nominal diameter of 150 mm and a thickness within the 38–50 mm range specified by the standard.

Before testing, the specimens were conditioned at the target temperature. The IDT strength tests were performed under a low-temperature condition of $-10 \pm 0.5^{\circ}C$. After the target temperature was reached, the specimens were kept at the test temperature for the required conditioning period before loading.

The specimens were then loaded along the vertical diametral plane up to failure. The loading rate was set to $12.5\ \mathrm{mm/min}$, corresponding to the vertical ram movement rate specified in AASHTO T 322 [30]for the tensile strength test.

The indirect tensile strength was calculated from the measured peak load as:

$$\sigma_{\mathrm{IDT,measured}} = \frac{2P_{\max}}{\pi D h}$$

where $P_{\max}$is the maximum applied load, $D$is the specimen diameter, and $h$is the specimen thickness. The peak load was expressed in newtons and the specimen dimensions in millimetres, resulting in a tensile strength expressed in MPa.

Figure 17- Indirect tensile strength test setup and typical diametral fracture of an asphalt mixture specimen after testing.

The measured IDT strength was compared with the analytical prediction to assess its consistency. However, because the analytical implementation adopted in this thesis represents a simplified version of the original framework, the experimentally measured tensile strength was used as the final tensile-resistance threshold in the critical-temperature calculation. The final value used in the analysis was obtained as the average tensile strength of the valid replicate specimens.

2.2.3.3. Thermal Stress Calculation

Thermally induced stress was calculated by retaining the linear viscoelastic component of the reference framework. This was necessary because the stress generated during cooling depends not only on the instantaneous stiffness of the mixture, but also on its ability to relax stress over time.

Under transient temperature conditions, real time was converted into reduced time using the temperature shift factor:

$$d\xi = \frac{dt}{a_T}$$

where $d\xi$is the reduced-time increment, $dt$is the real-time increment, and $a_T$is the temperature shift factor obtained from the dynamic modulus master curve.

The temperature dependence of the shift factor was represented by a second-order polynomial relationship:

$$\log_{10}(a_T) = A(T - T_{\mathrm{ref}})^2 + B(T - T_{\mathrm{ref}}) + C$$

where T is the temperature, T_{ref} is the master-curve reference temperature, and A, B, and C are fitting coefficients. A reference temperature of:

$$T_{\mathrm{ref}} = 21.1°C$$

was used consistently throughout the calculations.

The thermal strain increment associated with each temperature change was calculated as:

$$d\varepsilon_T = \alpha_T dT$$

where α_T is the coefficient of thermal contraction and dT is the temperature increment.

A constant cooling rate of: $10°C/h$

was adopted in accordance with the TSRST-based thermal stress calculation used in the reference methodology. The cooling history was discretized into small temperature increments, and the corresponding real-time and reduced-time increments were determined for each step.

The thermally induced stress was calculated through the linear viscoelastic convolution of the relaxation modulus with the thermal strain history:

$$\sigma_T(t) = \int_0^t E[\xi(t) - \xi(\tau)] \frac{d\varepsilon_T(\tau)}{d\tau} d\tau$$

where $\sigma_T(t)$ is the thermally induced stress and $E[\xi(t) - \xi(\tau)]$ is the relaxation modulus evaluated at the corresponding reduced-time difference.

In the spreadsheet implementation, the FlexMAT-derived relaxation modulus was interpolated on a log–log scale. A contribution matrix was then constructed so that the stress at each temperature step was obtained by summing the remaining contributions of all previous thermal strain increments.

2.2.3.4. Determination of the Critical Cracking Temperature

The critical cracking temperature was defined as the temperature at which the calculated thermal stress reached the experimentally measured IDT strength:

$$\sigma_T(T_{\text{crit}}) = \sigma_{\text{IDT,measured}}$$

The intersection was determined by linear interpolation between the two adjacent temperature steps surrounding the crossing point. This is consistent with the reference framework, in which the critical cracking temperature is identified as the point where the calculated thermally induced stress reaches the tensile strength threshold.

A lower and more negative critical temperature indicates better low-temperature cracking resistance, as the mixture can tolerate colder conditions before the thermally induced stress reaches its tensile strength. Conversely, a higher critical temperature indicates greater susceptibility to thermal cracking.

Therefore, although an AMPT- and VECD-based analytical prediction of IDT strength was initially performed, the final low-temperature cracking assessment was based on the calculated viscoelastic thermal stress and the experimentally measured IDT strength. The resulting critical temperatures were used as comparative indicators of the low-temperature performance of the investigated mixtures.

3. Results and discussion

This chapter presents and discusses the mechanical characterization results obtained for the investigated asphalt mixtures. The results are organized into dynamic modulus results, cyclic fatigue results, low-temperature cracking susceptibility analysis. The discussion is developed by considering both the pavement layer and the mixture composition, in order to interpret the mechanical response of the tested materials within a consistent performance-based framework.

The comparison between reference and recycled-plastic-modified mixtures is carried out for the wearing and base courses, where both mixture types were available. The binder course reference mixture is included as a mechanical baseline for the intermediate layer, but it is not used for a direct assessment of the effect of recycled plastic because the corresponding modified mixture was not available within the experimental campaign.

Before interpretation, the validity and consistency of the experimental data were checked within each testing framework. Dynamic modulus data were evaluated in terms of repeatability and suitability for master curve construction; fatigue results were screened according to the validity criteria required for S-VECD analysis; and low-temperature cracking results were interpreted by considering the consistency of the IDT strength values, thermal stress curves, and critical cracking temperatures.

Overall, the chapter aims to evaluate how the incorporation of recycled plastic affects stiffness response, viscoelastic behavior, fatigue damage evolution, and low-temperature cracking susceptibility, while also highlighting the differences associated with the structural function of the investigated pavement layers.

3.1. Dynamic Modulus Results

3.1.1. Effect of Temperature and Loading Frequency

After verifying the validity and repeatability of the dynamic modulus data, the influence of temperature and loading frequency on the stiffness response of the mixtures was examined. The complete dynamic modulus and phase angle results for all tested conditions are reported in Appendix A. Therefore, the discussion in this section focuses on the main trends observed in the accepted experimental data.

For all mixtures, the dynamic modulus, $|E^*|$, increased as the loading frequency increased at a given temperature. This trend reflects the viscoelastic nature of asphalt mixtures: under

faster loading, the material has less time to relax and consequently exhibits a stiffer response. In contrast, lower modulus values were generally measured at lower frequencies, where the longer loading time allowed a greater viscous contribution.

Temperature had a clear influence on the measured stiffness. At the same loading frequency, higher $|E^*|$ values were obtained at lower temperatures, whereas the modulus decreased as temperature increased. This behavior is mainly related to the temperature-dependent response of the bituminous binder. At low temperatures, the binder becomes stiffer and the mixture response is more elastic; at higher temperatures, binder softening leads to a more compliant response.

The phase angle, δ, was also considered to support the interpretation of viscoelastic behavior. Lower phase angle values indicate a response closer to elastic behavior, while higher values reflect a stronger viscous component. Therefore, the phase angle results were used together with the dynamic modulus values to describe the combined effect of temperature and loading rate.

Table 9. Representative dynamic modulus and phase angle results for one specimen

Specimen ID	Temperature (°C)	Frequency (Hz)	$\|E^*\|$ (MPa)	δ (°)
UI.0_4.19-1-A-1-5	10	10	17343	9.57
	10	1	13294	12.39
	10	0.1	9534	16.61
	20	10	11459	17
	20	1	7511	22.76
	20	0.1	4387	28.79
	35	10	4566	27.36
	35	1	2166	32.56
	35	0.1	918	33.78

As shown in Table 9, the selected specimen shows the expected increase in dynamic modulus with increasing loading frequency and decreasing temperature. The phase angle values were also used to support the interpretation of the viscoelastic response of the mixture.

The comparison between reference and recycled-plastic-modified mixtures was carried out separately for each pavement layer. This choice was necessary because mixtures belonging to different layers have different gradations, binder contents, and material compositions, which directly affect their stiffness response. As a result, the effect of recycled plastic was interpreted within each mixture family rather than through direct comparison among all pavement layers.

The observed temperature–frequency trends confirmed the expected dependence of asphalt mixture stiffness on temperature and loading frequency. These data provided the basis for the construction of the dynamic modulus master curves, which are presented in the following section.

For clarity and readability, only representative results and average values are reported in the main text. The complete specimen-by-specimen dynamic modulus and phase angle results for all mixtures, temperatures, and loading frequencies are provided in Appendix A.

3.1.2. Dynamic Modulus Master Curves

The accepted dynamic modulus results were used to construct the 2S2P1D master curves presented in Figures 18 to 20. As described in Section 2.2.1.3, this model was adopted to represent the linear viscoelastic response of the investigated mixtures. The following discussion compares the stiffness characteristics of the reference and waste-plastic-modified mixtures within each pavement layer.

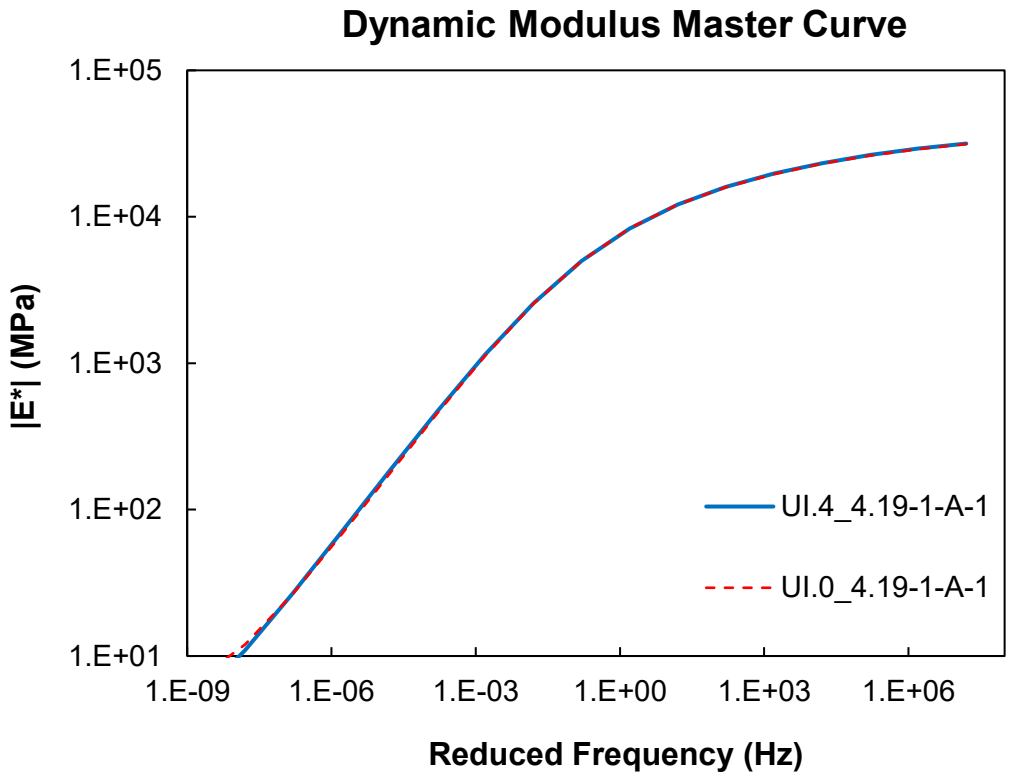

Figure 18 - Comparison of fitted dynamic modulus master curves for the wearing course mixtures

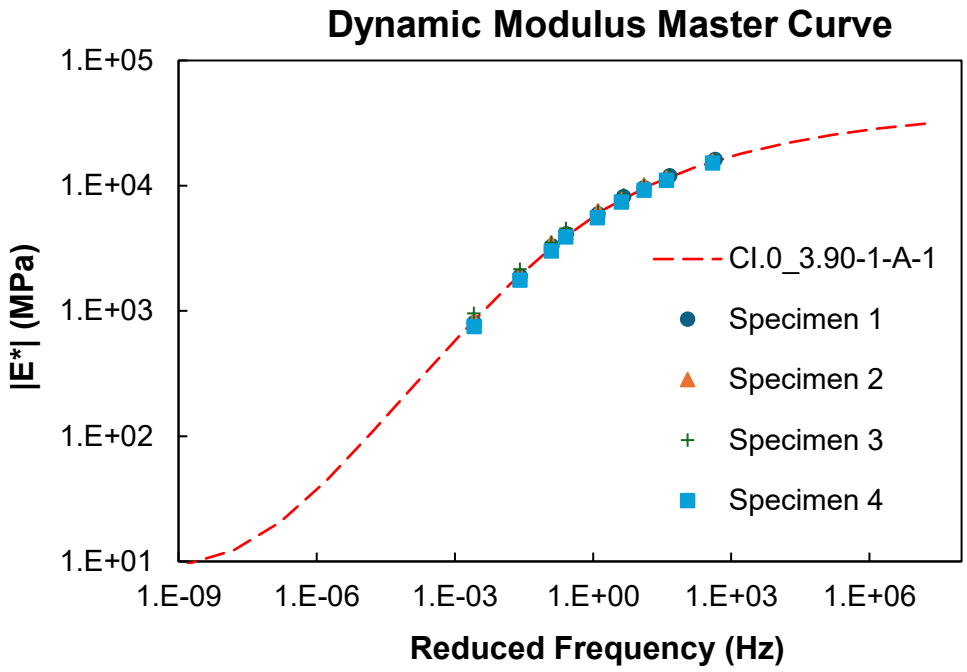

Figure 19 - Fitted dynamic modulus master curve for the binder course reference mixture

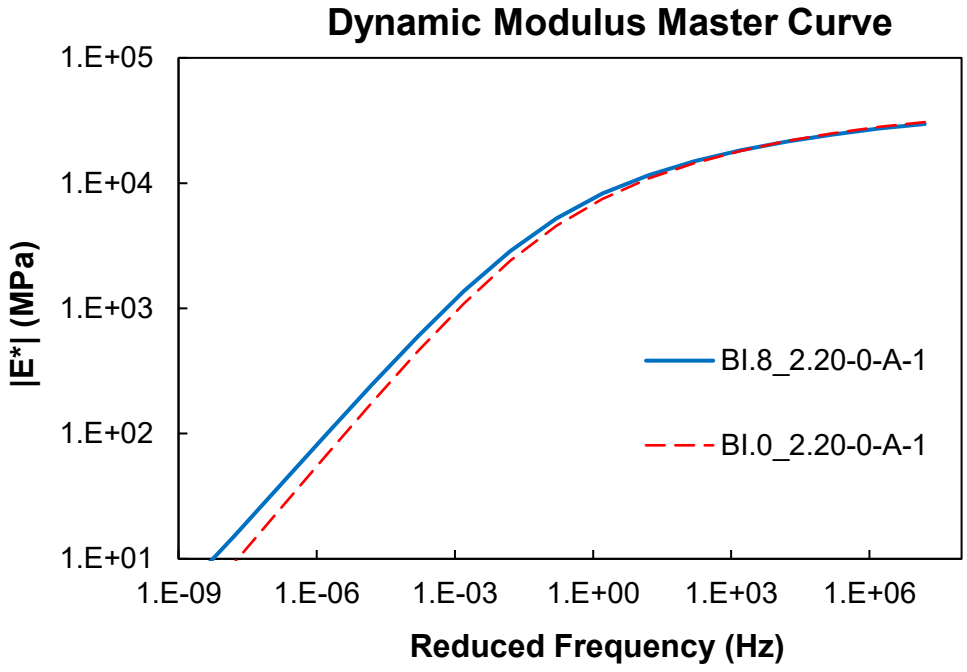

Figure 20 - Comparison of fitted dynamic modulus master curves for the base course mixtures

Figure 18 compares the dynamic modulus master curves of the wearing course mixtures, UI.4 and UI.0. For both mixtures, the modulus increased progressively with reduced frequency, which is consistent with the frequency-dependent response of asphalt materials. The curves remained close over most of the investigated range, showing that the two mixtures had broadly comparable stiffness characteristics. Nevertheless, UI.4 exhibited slightly higher modulus values in part of the frequency domain. This difference points to a moderate stiffening effect associated with waste plastic, while the general frequency dependence of the wearing course mixture remained essentially unchanged.

Figure 19 presents the master curve of the binder course reference mixture, CI.0. A smooth and continuous increase in modulus was observed across the reduced-frequency range, reflecting a consistent viscoelastic response. Because no waste-plastic-modified binder course mixture was included in the experimental campaign, CI.0 represents only the reference behavior of the intermediate pavement layer. Consequently, no conclusion regarding the influence of waste plastic could be drawn for this layer.

Figure 20 compares the base course mixtures, BI.8 and BI.0. BI.8 exhibited higher modulus values than BI.0 over most of the reduced-frequency range. The separation between the curves was greater than that observed for the wearing course mixtures, which indicates a stronger stiffening effect in the base course. Despite this difference in magnitude, the curves followed similar trends, implying that waste plastic primarily increased the modulus without substantially altering its dependence on reduced frequency.

Taken together, the master curves showed a consistent viscoelastic response for all investigated mixtures. Waste-plastic modification increased the stiffness of both the wearing and base course mixtures, although the effect was more evident in the base course. The resulting master curves were subsequently used as the principal viscoelastic input for the fatigue and low-temperature cracking analyses.

Although the sigmoidal and 2S2P1D models were both fitted to the accepted dynamic modulus data, the subsequent analyses were based on the 2S2P1D model. The sigmoidal model was considered as the standard AMPT-based reference approach for master curve construction, in accordance with AASHTO R 84 [26], and was used to verify the consistency of the fitted response. The corresponding sigmoidal fits and their comparison with the 2S2P1D predictions are provided in Appendix A. The 2S2P1D model was retained for the main discussion and the subsequent mechanical analyses because it provides a rheological representation of the linear viscoelastic response and allows the derivation of the time-domain viscoelastic properties required for the fatigue and low-temperature cracking analyses. Therefore, the 2S2P1D master curves were adopted as the principal viscoelastic input in the remainder of this study.

3.2. Fatigue Results

3.2.1. Damage Characteristic Curves

The representative damage characteristic curves obtained from the accepted fatigue tests are presented in Figures 21 to 23. Fatigue damage evolution was evaluated through the fitted relationship between the material integrity parameter, (C), and the accumulated damage variable, (S). As damage develops under cyclic loading, the progressive reduction in (C) reflects the loss of material integrity. The discussion in this section focuses on the representative fitted curves, whereas the complete specimen-level (C)-(S) data and the corresponding fitting results are provided in Appendix A.

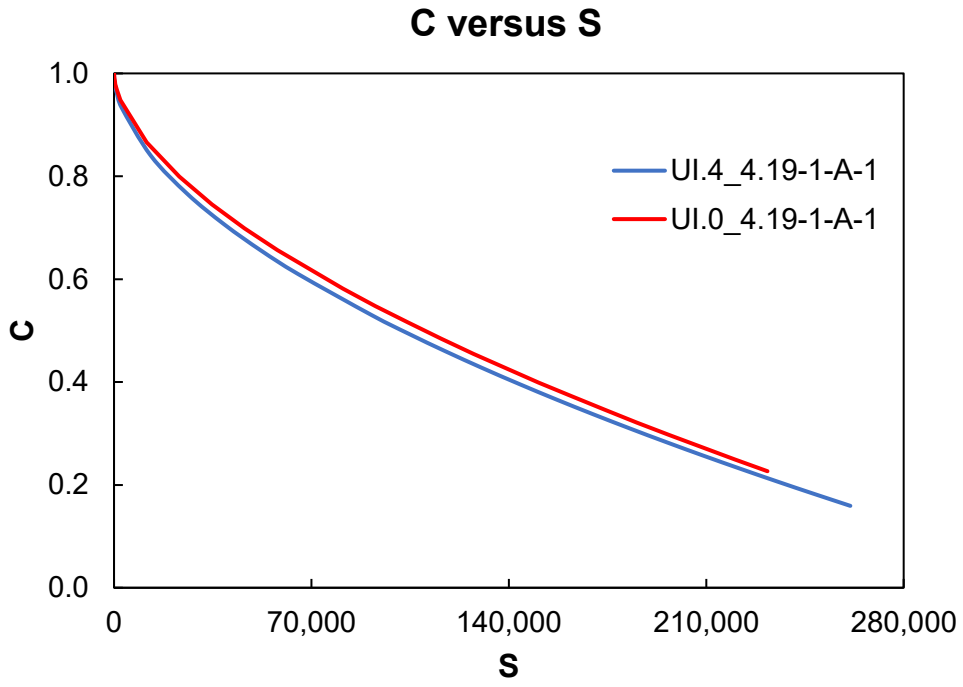

Figure 21 - Representative fitted C-S curves for the wearing course mixtures.

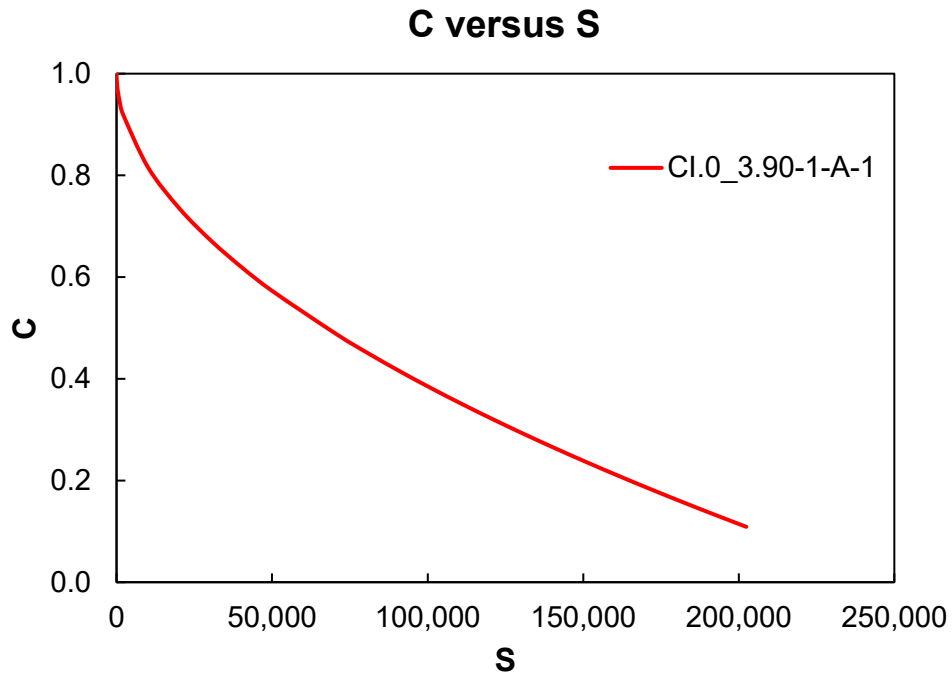

Figure 22 - Representative fitted C-S curve for the binder course reference mixture.

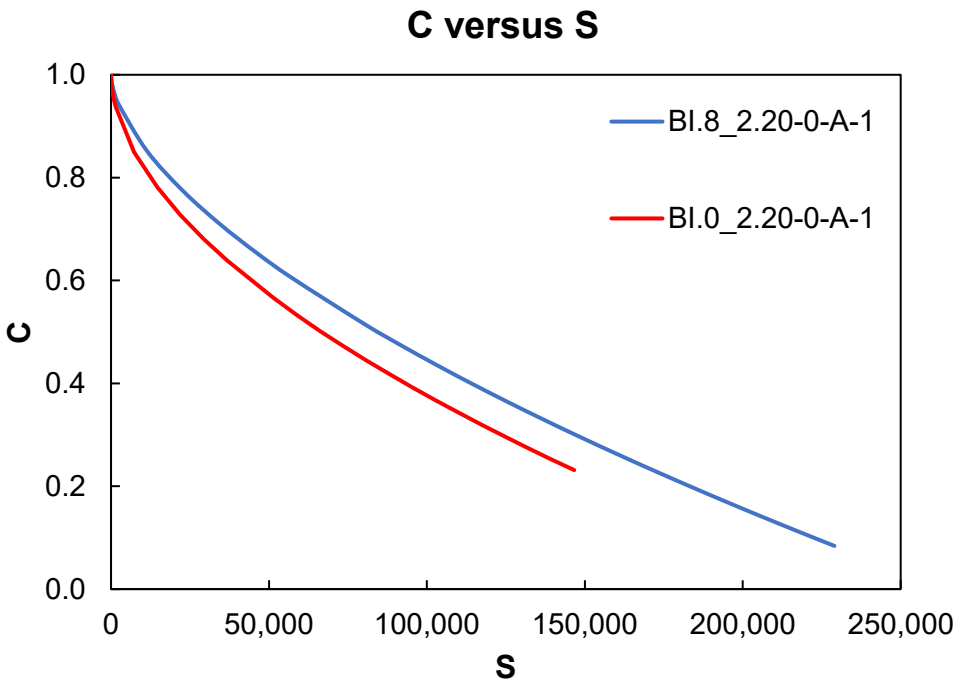

Figure 23 - Representative fitted C-S curves for the base course mixtures.

Figure 21 shows the comparison between the representative (C)-(S) curves of the wearing course mixtures, UI.4 and UI.0. The curves are closely aligned over most of their common damage range, indicating that the two mixtures experienced broadly comparable patterns of

fatigue damage evolution. Nevertheless, small differences can be identified. UI.0 generally maintains marginally higher (C) values at equivalent (S) levels, whereas UI.4 reaches a somewhat larger accumulated damage level before approaching the lower integrity range. These observations indicate that the incorporation of waste plastic did not markedly change the overall shape of the damage characteristic relationship in the wearing course, although minor differences in the progression and extent of damage were observed.

The fatigue damage profile of the binder course reference mixture, CI.0, is illustrated in Figure 22. Its fitted curve exhibits a smooth and continuous loss of material integrity throughout the investigated (S) range, without irregular variations in the damage progression. Because a corresponding plastic-modified binder course mixture was not included in the experimental program, CI.0 is considered only as a representative reference response for this pavement layer. Consequently, no conclusion regarding the effect of waste plastic can be drawn for the binder course.

A clearer distinction is observed between the base course mixtures BI.8 and BI.0, as shown in Figure 23. At comparable accumulated damage levels, BI.8 consistently retains higher (C) values than BI.0, reflecting a more gradual reduction in material integrity. The plastic-modified mixture also develops a greater accumulated damage level before reaching the low-(C) region. Within the adopted fatigue characterization framework, this response points to a more favorable damage evolution for BI.8 than for the reference base mixture.

The representative (C)-(S) curves therefore provide an effective qualitative description of how fatigue damage develops in the investigated mixtures. They were not, however, considered sufficient on their own for ranking fatigue performance. The comparisons were complemented by the fatigue indicators presented in the following section, particularly D_R and S_{app} , which offer a more direct and quantitative basis for evaluating the reference and waste-plastic-modified mixtures within each pavement layer.

The fitted parameters of the representative damage characteristic curves are summarized in Table 10. The representative C–S relationships were obtained from the accepted fatigue tests for each mixture and were subsequently used in the calculation of the fatigue-related parameters.

Table 10. Fitting parameters of the representative damage characteristic curves.

Mixture	Number of accepted fatigue tests	Final fitted C_{11}	Final fitted C_{12}
UI.4_4.19-1-A-1	4	8.39×10^{-4}	5.54×10^{-1}
UI.0_4.19-1-A-1	5	5.58×10^{-4}	5.86×10^{-1}
CI.0_3.90-1-A-1	3	1.44×10^{-3}	5.26×10^{-1}
BI.8_2.20-0-A-1	3	5.11×10^{-4}	6.07×10^{-1}
BI.0_2.20-0-A-1	3	1.17×10^{-3}	5.45×10^{-1}

3.2.2. Fatigue Failure Parameters: D_R and S_{app}

Figures 24 to 28 present the relationship between the cumulative loss of integrity, $\mathrm{Cum}(1 - C)$, and the number of cycles to failure, N_f, for the accepted fatigue tests. As described in Section 2.2.2.3, the fatigue failure parameter D_R was calculated at the specimen level and then averaged for each mixture. The resulting mixture-level average D_R values are reported in Table 11 together with the corresponding S_{app} values.

The plotted points provide a visual representation of the accumulated loss of material integrity at failure for the accepted fatigue tests. Higher values of $\mathrm{Cum}(1 - C)$ indicate that the specimen reached failure after accumulating a greater loss of integrity. Therefore, these plots support the interpretation of the D_R values, while the quantitative comparison among mixtures is based on the average indicators.

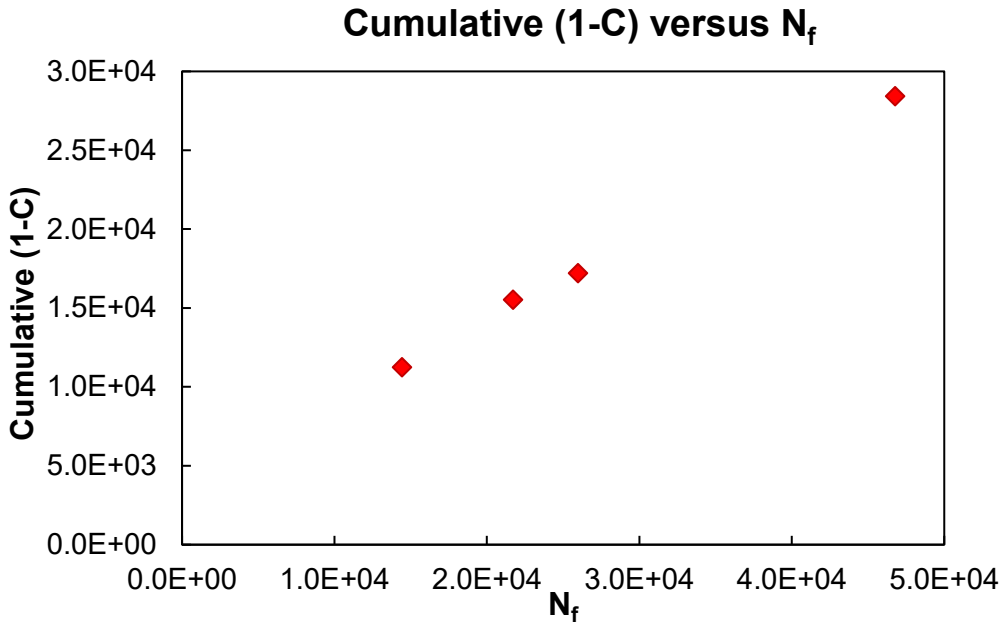

Figure 24 - Relationship between cumulative loss of integrity, $Cum(1-C)$, and number of cycles to failure, N_f for mixture UI.4_4.19-1-A-1.

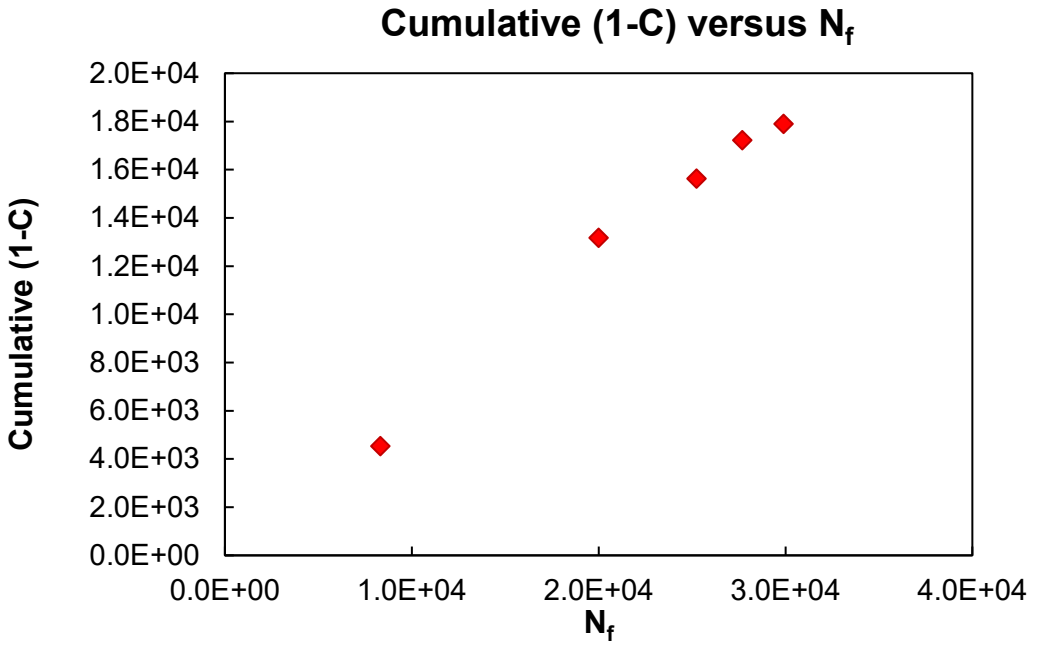

Figure 25 - Relationship between cumulative loss of integrity, $Cum(1-C)$, and number of cycles to failure, N_f for mixture UI.0_4.19-1-A-1.

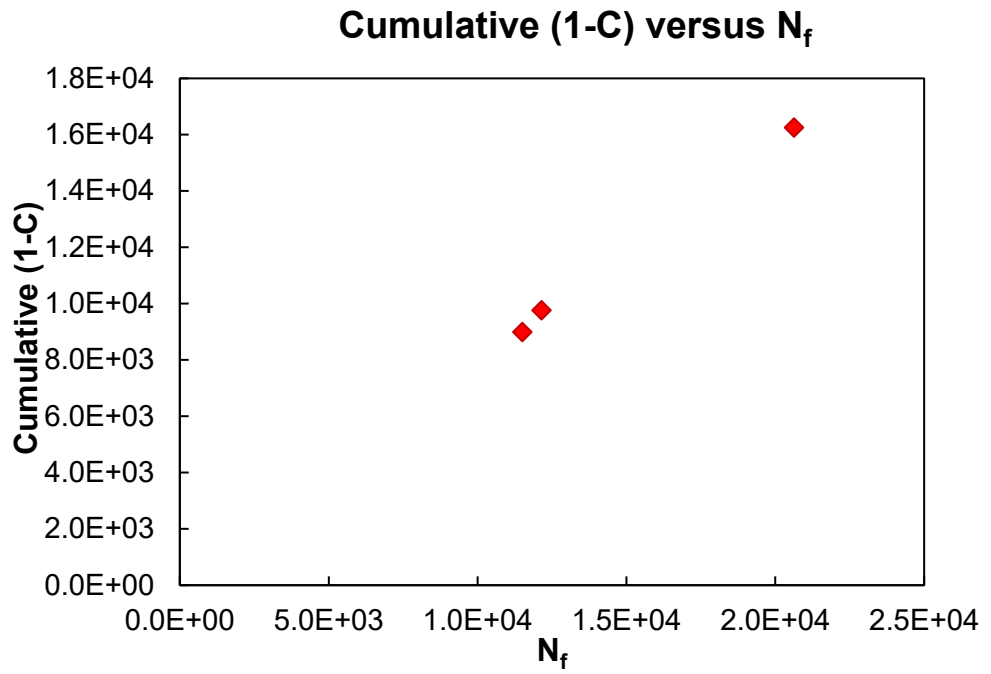

Figure 26- Relationship between cumulative loss of integrity, $Cum(1-C)$, and number of cycles to failure, N_f for mixture CI.0_3.90-1-A-1.

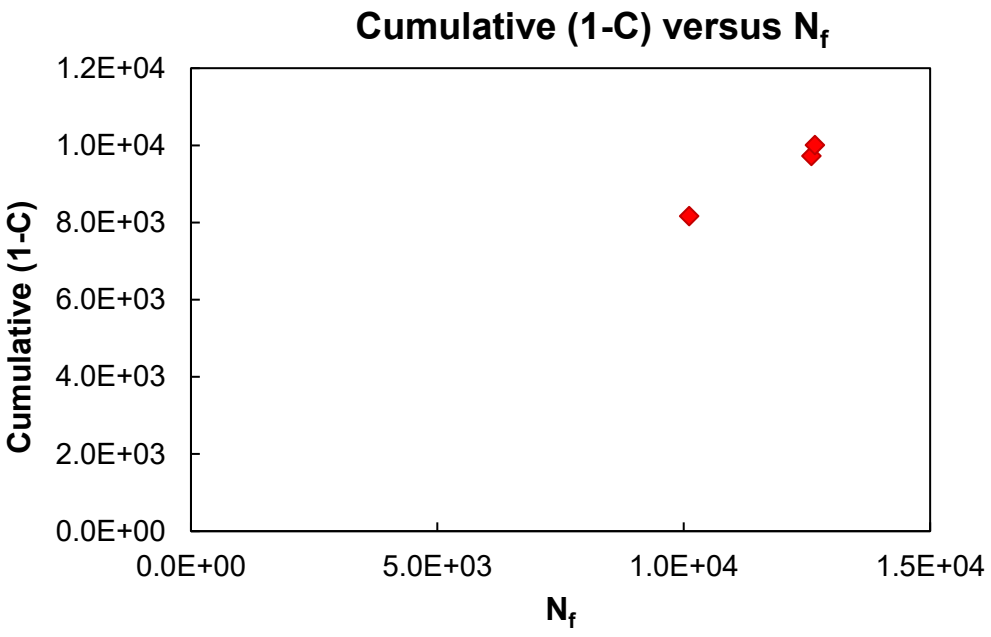

Figure 27 - Relationship between cumulative loss of integrity, Cum(1−C), and number of cycles to failure, N_f for mixture BI.8_2.20-0-A-1.

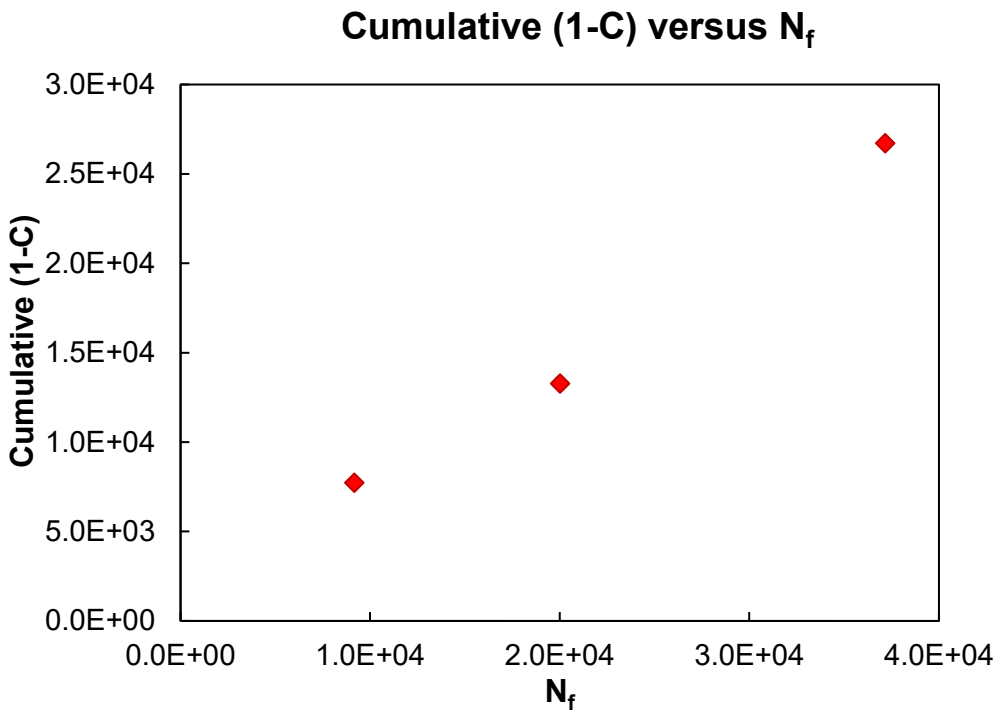

Figure 28 - Relationship between cumulative loss of integrity, Cum(1−C), and number of cycles to failure, N_f for mixture BI.0_2.20-0-A-1.

The corresponding S_{app} values were calculated under the Turin reference condition and are reported together with D_R in Table 11.

Table 11. Average D_R and corresponding S_{app} values of the investigated mixtures calculated from accepted cyclic fatigue tests.

MIX ID	D_R	S_{app}
UI.4_4.19-1-A-1	0.69	22.15
UI.0_4.19-1-A-1	0.61	17.67
CI.0_3.90-1-A-1	0.79	21.64
BI.8_2.20-0-A-1	0.79	24.46
BI.0_2.20-0-A-1	0.72	18.10

The comparison of fatigue performance was mainly carried out within each pavement layer. For the wearing course, UI.4 showed higher values of both D_R and S_{app}than UI.0. This indicates that the waste-plastic-modified wearing mixture had a greater apparent fatigue damage capacity under the adopted evaluation framework.

For the base course, BI.8 also showed higher $D_R$and S_{app}values than BI.0. This result supports the interpretation that the incorporation of waste plastic improved the apparent fatigue damage capacity of the base course mixture. The detailed specimen-level fatigue summaries used to calculate the average values reported in Table 11 are provided in Appendix A.

Considering all mixtures together, BI.8 showed the highest S_{app}value, followed by UI.4 and CI.0, while UI.0 and BI.0 showed lower values. However, this overall comparison was used only to identify general trends. The main interpretation remains the layer-by-layer comparison, because mixtures designed for different pavement layers differ in gradation, RAP content, binder content, stiffness level, and structural function.

3.3. Low-Temperature Cracking Susceptibility Results

The low-temperature cracking results presented in this section are summarized in terms of measured IDT tensile strength, calculated thermal stress evolution, and critical cracking temperature. The detailed IDT test results and the complete thermal stress calculation outputs for each mixture are reported in Appendix A.

Figures 29 to 31 compare the calculated thermal stress with the measured IDT tensile-strength threshold for the investigated mixtures. In the comparative figures, the blue solid and red dashed curves represent the thermally induced stresses of the waste-plastic-modified and reference mixtures, respectively, while the green solid and orange dashed horizontal lines represent their corresponding IDT strengths measured at $-10 \pm 0.5°\mathrm{C}$. Since IDT strength was measured at a single temperature, it was plotted as a constant threshold to identify its intersection with the corresponding thermal stress curve. This intersection was taken as the critical cracking temperature. A lower critical temperature indicates a more favorable low-temperature cracking response.

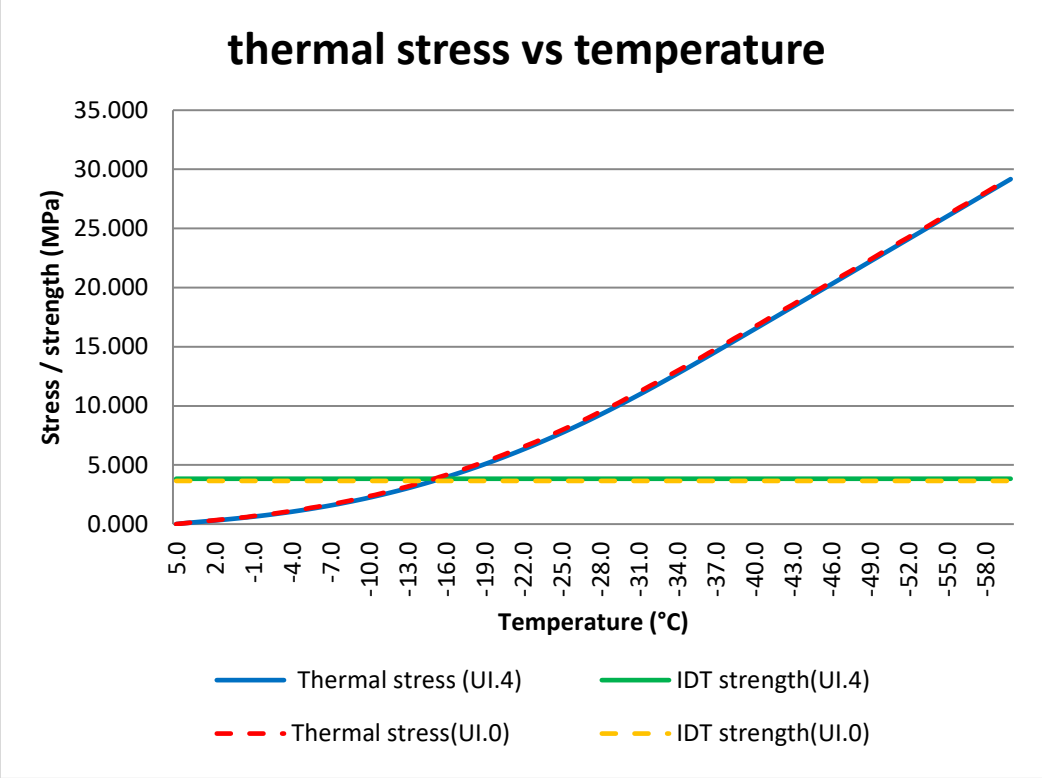

Figure 29 - Thermal stress evolution with decreasing temperature and measured IDT tensile-strength threshold for the wearing course.

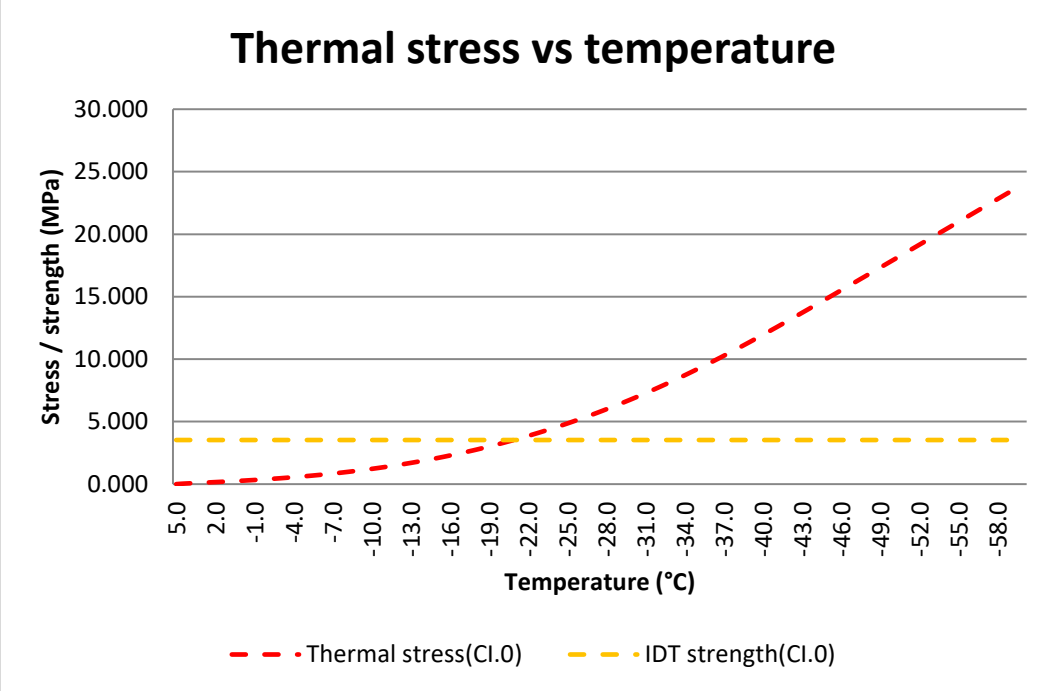

Figure 30 - Thermal stress evolution with decreasing temperature and measured IDT tensile-strength threshold for the binder course reference.

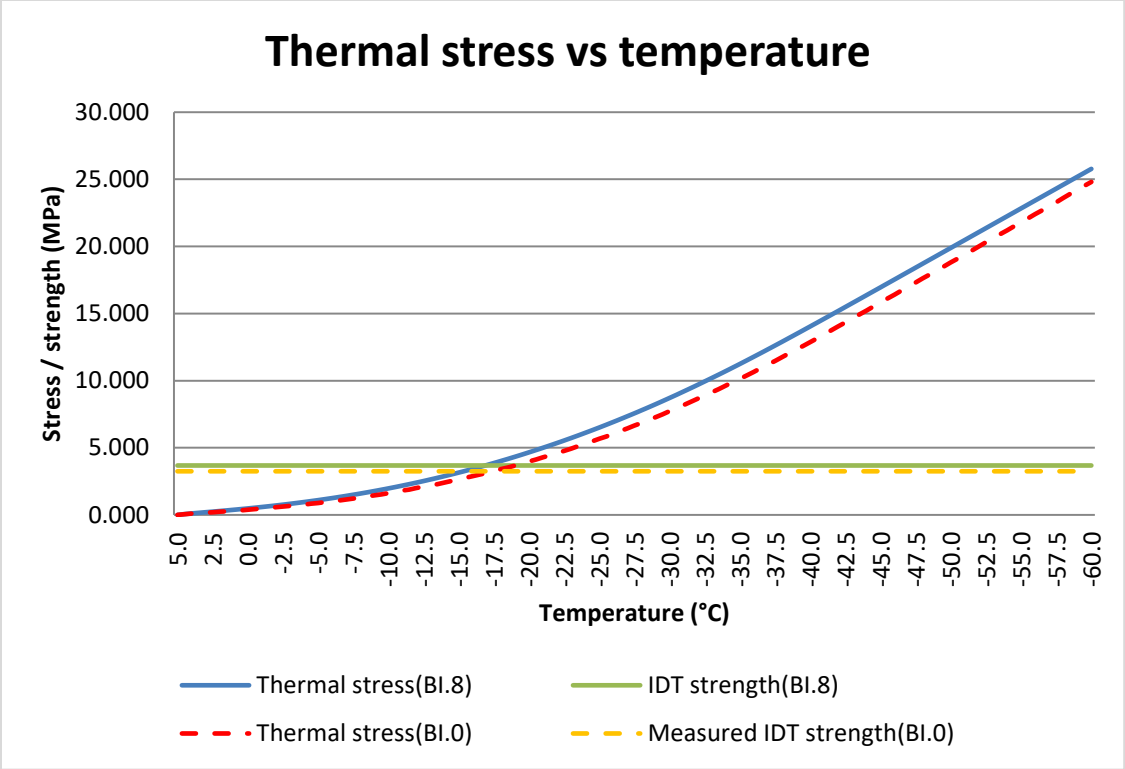

Figure 31 - Thermal stress evolution with decreasing temperature and measured IDT tensile-strength threshold for the base course.

Table 12. Summary of measured IDT tensile strength and corresponding critical cracking temperature obtained from the low-temperature cracking analysis.

MIX ID	Measured IDT strength (MPa)	Critical temperature (°C)
UI.4_4.19-1-A-1	3.84	-15.6
UI.0_4.19-1-A-1	3.66	-14.6
CI.0_3.90-1-A-1	3.47	-20.7
BI.8_2.20-0-A-1	3.68	-16.9
BI.0_2.20-0-A-1	3.25	-17.5

For the wearing course, UI.4 reached the critical condition at −15.6 °C, compared with −14.6 °C for UI.0. The modified mixture therefore showed a small improvement under the adopted analysis conditions. Given the limited difference between the two values, the results mainly indicate that the addition of waste plastic did not adversely affect the low-temperature response of the wearing mixture.

CI.0 exhibited the lowest critical temperature among the investigated mixtures, reaching −20.7 °C. It therefore provided the most favorable response within the analyzed dataset. As no modified binder-course mixture was available, this value represents only the baseline behavior of CI.0 and cannot be used to evaluate the effect of waste plastic in this layer.

The base-course mixtures showed relatively similar thermal stress responses. BI.8 reached its critical condition at −16.9 °C, whereas BI.0 reached it at −17.5 °C. The reference mixture therefore performed slightly better, although the difference was limited and both results remained within a comparable range.

Table 12 summarizes the measured IDT tensile strengths and the corresponding critical temperatures. UI.4 showed the highest tensile strength, followed by BI.8, UI.0, CI.0, and BI.0. However, this ranking did not directly correspond to the critical-temperature results because thermal cracking response also depends on viscoelastic stiffness and stress-relaxation behavior

The results show that the influence of waste plastic varied between pavement layers. A small improvement was observed for the wearing course, while a slight reduction was obtained for the base course. This confirms that the effect of plastic modification cannot be interpreted independently of mixture-specific properties.

4. Conclusions

This thesis investigated the mechanical performance of sustainable asphalt mixtures containing waste plastic within the Green Roads project. The mixtures were designed for different pavement layers and were characterized through dynamic modulus testing, master curve construction, cyclic fatigue analysis, and low-temperature cracking evaluation. Since their compositions had already been developed during earlier stages of the project, the present study did not focus on mix design optimization. Instead, the study focused on evaluating the mechanical effects associated with waste-plastic incorporation under controlled laboratory conditions.

The dynamic modulus results indicated that the addition of waste plastic generally increased mixture stiffness. This trend was observed in both the wearing and base course comparisons, with UI.4 and BI.8 showing higher modulus values than their corresponding reference mixtures over most of the investigated temperature–frequency range. However, the general shapes of the master curves remained similar within each pair. Waste-plastic incorporation therefore appeared to influence the stiffness level more than the overall linear viscoelastic response. Both the sigmoidal and 2S2P1D models described the experimental data satisfactorily within the measured reduced-frequency range.

In the wearing course comparison, UI.4 was moderately stiffer than UI.0 while maintaining a comparable master curve shape. A similar, although more pronounced, stiffening effect was found in the base course, where BI.8 showed higher modulus values than BI.0. Because the mixtures in each pair were designed for the same pavement layer and differed primarily in their waste-plastic content, the observed differences can reasonably be associated with the contribution of the plastic, together with the normal variability of asphalt mixture testing.

The fatigue results also showed differences between the reference and modified mixtures. The damage characteristic curves showed the expected reduction in the material integrity parameter, C, as accumulated damage, S, increased. These curves were used to examine the progression of fatigue damage, while the final comparison was mainly based on the fatigue indicators adopted in this thesis, particularly D_R and S_{app}. According to these indicators, UI.4 showed a more favorable fatigue-related response than UI.0, while BI.8 showed higher values than BI.0. Within the investigated conditions, waste-plastic incorporation increased mixture stiffness as well as the main fatigue indicators adopted in this thesis.

The low-temperature results provided a different perspective on the effect of waste plastic. For the wearing course, UI.4 reached a slightly lower critical cracking temperature than UI.0, indicating a modest improvement in resistance to thermally induced cracking. The two

wearing mixtures had relatively similar volumetric characteristics, including comparable VMA values. One possible interpretation is that, under these conditions, the plastic interacted sufficiently with the bituminous phase or contributed to the coating of the aggregates. This may have allowed UI.4 to gain stiffness without producing a corresponding reduction in its low-temperature performance.

The same trend was not observed in the base course. Although BI.8 was stiffer and had more favorable fatigue indicators than BI.0, its critical cracking temperature did not improve. This result indicates that the plastic may have played a different role in the base mixture. The higher plastic content may have limited complete softening or homogeneous interaction with the bituminous phase during production. Consequently, part of the plastic may have behaved as a structural inclusion within the aggregate skeleton rather than as a fully integrated binder-like component. This behavior could explain the higher stiffness and fatigue indicators, while also explaining why no improvement was observed in the critical cracking temperature. However, this mechanism was not measured directly and should therefore be regarded as a possible interpretation of the experimental results rather than a confirmed explanation.

The binder course reference mixture, CI.0, served as an intermediate-layer baseline in the overall comparison of the investigated mixtures. In relation to the wearing and base course mixtures, CI.0 showed a regular dynamic modulus master curve, a well-defined fatigue damage relationship, and the most negative critical cracking temperature. This suggests that the binder course reference mixture provided a stable mechanical response and showed favorable low-temperature cracking resistance within the tested materials. Nevertheless, because no corresponding plastic-modified binder course mixture was available, the influence of waste plastic could not be assessed directly for this layer. The CI.0 results were therefore interpreted only as a reference response for the intermediate layer and not as evidence of the effect of plastic incorporation.

Taken together, the findings show that the mechanical effect of waste plastic was dependent on the pavement layer and mixture composition. In the wearing course, plastic incorporation resulted in a relatively balanced response: stiffness and fatigue indicators increased, while low-temperature cracking resistance showed a small improvement. In the base course, the main effects were higher stiffness and more favorable fatigue indicators, without a corresponding benefit in critical cracking temperature probably due to the higher plastic dosage.

From a performance-based perspective, the investigated plastic-modified mixtures showed promising mechanical characteristics. Nevertheless, the increase in stiffness and fatigue indicators did not always result in better low-temperature performance.

Further research should include a plastic-modified binder course mixture to complete the comparison across the three pavement layers. Additional low-temperature testing, long-term

ageing evaluation, and field monitoring would also be useful for confirming the laboratory observations.

5. Bibliography

[1] A. Ben Ameur, J. Valentin, and N. Baldo, “A Review on the Use of Plastic Waste as a Modifier of Asphalt Mixtures for Road Constructions,” Jun. 01, 2025, *Multidisciplinary Digital Publishing Institute (MDPI)*. doi: 10.3390/civileng6020017.

[2] Y. Pamu, P. Svsndl, S. R. Oleti, P. Samala, and V. Nalla, “Reclaimed Asphalt Pavement in Circular Economy of Road Construction,” in *E3S Web of Conferences*, EDP Sciences, Sep. 2025. doi: 10.1051/e3sconf/202564801009.

[3] L. Yao, Z. Leng, J. Lan, R. Chen, and J. Jiang, “Environmental and economic assessment of collective recycling waste plastic and reclaimed asphalt pavement into pavement construction: A case study in Hong Kong,” *J. Clean. Prod.*, vol. 336, Feb. 2022, doi: 10.1016/j.jclepro.2022.130405.

[4] V. Antunes, J. Neves, and A. C. Freire, “Performance assessment of reclaimed asphalt pavement (RAP) in road surface mixtures,” *Recycling*, vol. 6, no. 2, Jun. 2021, doi: 10.3390/recycling6020032.

[5] J. Calderón-Ramírez, D. Sepúlveda-Valdez, L. García, M. A. Lomeli-Banda, C. Salazar-Briones, and M. Montoya-Alcaraz, “Recycled Plastics in Asphalt Mixtures: A Systematic Review of Mechanical Performance, Environmental Impact and Practical Implementation,” Sep. 01, 2025, *Multidisciplinary Digital Publishing Institute (MDPI)*. doi: 10.3390/app15189901.

[6] S. K. Shah, Y. Gao, and A. Abdelfatah, “Plastic-Waste-Modified Asphalt for Sustainable Road Infrastructure: A Comprehensive Review,” Nov. 01, 2025, *Multidisciplinary Digital Publishing Institute (MDPI)*. .

[7] Y. Richard Kim; B. Underwood; M. Sakhaei Far; N. Jackson; J. Puccinelli, “7.0035,” Sep. 2011.

[8] H. Chen, D. M. Barbieri, X. Zhang, and I. Hoff, “Reliability of Calculation of Dynamic Modulus for Asphalt Mixtures Using Different Master Curve Models and Shift Factor Equations,” *Materials*, vol. 15, no. 12, Jun. 2022.

[9] P. M. Vestena, S. L. Schuster, P. O. B. de Almeida, C. Faccin, L. P. Specht, and D. da S. Pereira, “Dynamic modulus master curve construction of asphalt mixtures: Error analysis in different models and field scenarios,” *Constr. Build. Mater.*, vol. 301, Sep. 2021.

[10] M. Pszczola, M. Jaczewski, and C. Szydlowski, “Assessment of thermal stresses in asphalt mixtures at low temperatures using the tensile creep test and the bending beam creep test,” *Applied Sciences (Switzerland)*, vol. 9, no. 5, 2019, doi: 10.3390/app9050846.

[11] S. Xu *et al.*, “Fatigue Failure Criteria of Asphalt Binders and Asphalt Mixtures: A Comprehensive Review,” Jul. 01, 2025, *Multidisciplinary Digital Publishing Institute (MDPI)*. doi: 10.3390/ma18143267.

[12] S. Spadoni, L. P. Ingrassia, P. Jaskuła, and F. Canestrari, “Advanced fatigue and rutting characterisation of Polish asphalt mixtures based on the VECD model and viscoplastic shift model,” *Road Materials and Pavement Design*, vol. 24, no. S1, pp. 145–159, 2023, doi: 10.1080/14680629.2023.2180296.

[13] S. Spadoni, L. Paolo Ingrassia, D. Mocelin, Y. Richard Kim, and F. Canestrari, “Comparison of asphalt mixtures containing polymeric compounds and polymer-modified bitumen based on the VECD theory,” *Constr. Build. Mater.*, vol. 349, Sep. 2022, doi: 10.1016/j.conbuildmat.2022.128725.

[14] S. Spadoni, L. P. Ingrassia, E. Mariani, F. Cardone, and F. Canestrari, “Long-term performance assessment of a warm recycled motorway pavement,” *Case Studies in Construction Materials*, vol. 17, Dec. 2022, doi.

[15] de L. R. C. B. H. P. A. L. R. Di Benedetto H, “FATIGUE OF BITUMINOUS MIXTURES: DIFFERENT APPROACHES AND RILEM GROUP CONTRIBUTION,” 2004.

[16] M. S. Medeiros, J. S. Daniel, M. Asce, and G. R. Chehab, “Framework for Low-Temperature Cracking Analysis of Asphalt Mixtures Using a Viscoelastic Continuum Damage Model,” 2014, doi: 10.1061/(ASCE)MT.1943-5533.

[17] Aashto TP 132-25, *Determining the Dynamic Modulus for Asphalt Mixtures Using Small Specimens in the Asphalt Mixture Performance Tester (AMPT)*. Washington, D.C.: American Association of State Highway and Transportation Officials, 2025. doi: 10.17226/14200.

[18] AASHTO R 83-22, “Preparation of Cylindrical Performance Test Specimens Using the Superpave Gyratory Compactor (SGC),” 2022.

[19] AASHTO PP 99-23, “Preparation of Small Cylindrical Performance Test Specimens Using the Superpave Gyratory Compactor (SGC) or Field Cores,” Washington, DC, 2023.

[20] FHWA / National Highway Institute, “Pavement Structural Design and Performance (FHWA / NCHRP 1-37A Baseline Designs),” *Federal Highway Administration / National Highway Institute*, 2006.

[21] G. R. Chehab, Y. R. Kim, R. A. Schapery, M. W. Witczak, and R. Bonaquist, “Characterization of Asphalt Concrete in Uniaxial Tension Using a Viscoelastoplastic Continuum Damage Model,” 2003.

[22] AASHTO T 166-16, “Standard Method of Test for Bulk Specific Gravity (G mb) of Compacted Hot Mix Asphalt (HMA) Using Saturated Surface-Dry Specimens,” 2016.

[23] BS EN 12697-6 (BSI / CEN), *Bituminous mixtures. Test methods. Part 6, Determination of bulk density of bituminous specimens*. British Standards Institution (BSI) / European Committee for Standardization (CEN), 2020.

[24] EN 12697-8 (BSI / CEN), *Bituminous mixtures — Test methods — Part 8: Determination of void characteristics of bituminous specimens*. British Standards Institution (BSI) / European Committee for Standardization (CEN), 2019.

[25] Aashto T 378-22, “Standard Method of Test for Determining the Dynamic Modulus and Flow Number for Asphalt Mixtures Using the Asphalt Mixture Performance Tester (AMPT),” Washington, DC, 2022. [Online]. Available: https://www.trb.org/Publications/Blurbs/160512.aspx

[26] AASHTO R 84-17, “Standard Practice for Developing Dynamic Modulus Master Curves for Asphalt Mixtures Using the Asphalt Mixture Performance Tester (AMPT),” Washington, DC, 2021.

[27] AASHTO T 411-24, “Standard Method of Test for Determining the Damage Characteristic Curve and Failure Criterion Using Small Specimens in the Asphalt Mixture Performance Tester (AMPT) Cyclic Fatigue Test,” 2024.

[28] AASHTO T 400-24, “Standard Method of Test for Determining the Damage Characteristic Curve and Failure Criterion Using the Asphalt Mixture Performance Tester (AMPT) Cyclic Fatigue Test,” 2024. [Online]. Available: https://www.fhwa.dot.gov/publications/research/infrastructure/pavements/21093/index.cfm

[29] FHWA / National Highway Institute, “FHWA-HRT-24-112: Development of Balanced Mixture Design Index Parameters and the Flex Suite of Performance Analysis Tools for Asphalt Pavements—Volume I.”

[30] AASHTO T 322-07 (2020), “Standard Method of Test for Determining the Creep Compliance and Strength of Hot Mix Asphalt (HMA) Using the Indirect Tensile Test Device,” 2023.

6. Appendix A

Dynamic Modulus and Master Curve:

UI.4_4.19-1-A-1

Specimen Identification	Frequency (Hz)	Dynamic Modulus (MPa)	Phase Angle (Degrees)	Average Temperature (°C)
1	*10.0*	*12137.0*	*14.86*	*20.4*
1	*1.0*	*8092.0*	*19.54*	*20.4*
1	*0.1*	*4821.0*	*24.90*	*20.5*
1	*10.0*	*5121.0*	*25.92*	*35.5*
1	*1.0*	*2559.0*	*31.42*	*35.5*
1	*0.1*	*1118.0*	*34.09*	*35.5*
1	*10.0*	*19726.0*	*8.40*	*8.4*
1	*1.0*	*15783.0*	*10.54*	*8.4*
1	*0.1*	*11831.0*	*14.65*	*8.5*
2	*10.0*	*11572.0*	*14.99*	*20.4*
2	*1.0*	*7639.0*	*20.16*	*20.4*
2	*0.1*	*4496.0*	*26.10*	*20.5*
2	*10.0*	*4704.0*	*27.08*	*35.5*
2	*1.0*	*2299.0*	*32.71*	*35.5*
2	*0.1*	*1007.0*	*34.90*	*35.5*
2	*10.0*	*19124.0*	*8.48*	*8.4*
2	*1.0*	*15146.0*	*10.91*	*8.4*
2	*0.1*	*11334.0*	*14.29*	*8.4*
3	*10.0*	*4963.0*	*25.54*	*35.5*
3	*1.0*	*2518.0*	*31.27*	*35.4*
3	*0.1*	*1117.0*	*34.31*	*35.5*
3	*10.0*	*19173.0*	*7.19*	*8.3*
3	*1.0*	*15401.0*	*9.62*	*8.4*
3	*0.1*	*11765.0*	*12.88*	*8.5*
3	*10.0*	*11509.0*	*14.29*	*20.5*
3	*1.0*	*7767.0*	*19.00*	*20.5*
3	*0.1*	*4726.0*	*24.29*	*20.4*
4	*10.0*	*12022.0*	*13.96*	*20.5*
4	*1.0*	*8081.0*	*18.78*	*20.5*
4	*0.1*	*4932.0*	*24.17*	*20.5*
4	*10.0*	*19191.0*	*7.52*	*8.4*
4	*1.0*	*15353.0*	*9.92*	*8.4*
4	*0.1*	*11701.0*	*13.10*	*8.5*
4	*10.0*	*5061.0*	*25.31*	*35.5*
4	*1.0*	*2564.0*	*30.21*	*35.5*
4	*0.1*	*1154.0*	*32.45*	*35.5*

Reduced Frequency	Reduced Angular Frequency	E' (Sigmoidal) (kPa)	E'norm	E' (2S2P1D) (kPa)	|E*| (2S2P1D) (MPa)
1.59E+07	*1.00E+08*	*2.71E+07*	*2.71E+07*	*3.16E+07*	*3.16E+04*
1.59E+06	*1.00E+07*	*2.60E+07*	*2.60E+07*	*2.92E+07*	*2.92E+04*
1.59E+05	*1.00E+06*	*2.44E+07*	*2.44E+07*	*2.63E+07*	*2.64E+04*
1.59E+04	*1.00E+05*	*2.23E+07*	*2.23E+07*	*2.31E+07*	*2.32E+04*
1.59E+03	*1.00E+04*	*1.94E+07*	*1.94E+07*	*1.96E+07*	*1.97E+04*
1.59E+02	*1.00E+03*	*1.59E+07*	*1.59E+07*	*1.58E+07*	*1.60E+04*
1.59E+01	*1.00E+02*	*1.19E+07*	*1.19E+07*	*1.18E+07*	*1.21E+04*
1.59E+00	*1.00E+01*	*7.91E+06*	*7.91E+06*	*7.95E+06*	*8.32E+03*
1.59E-01	*1.00E+00*	*4.57E+06*	*4.57E+06*	*4.59E+06*	*4.99E+03*
1.59E-02	*1.00E-01*	*2.26E+06*	*2.26E+06*	*2.25E+06*	*2.56E+03*
1.59E-03	*1.00E-02*	*9.62E+05*	*9.59E+05*	*9.61E+05*	*1.15E+03*
1.59E-04	*1.00E-03*	*3.68E+05*	*3.66E+05*	*3.81E+05*	*4.70E+02*
1.59E-05	*1.00E-04*	*1.36E+05*	*1.34E+05*	*1.45E+05*	*1.83E+02*
1.59E-06	*1.00E-05*	*5.28E+04*	*5.07E+04*	*5.54E+04*	*6.98E+01*
1.59E-07	*1.00E-06*	*2.30E+04*	*2.10E+04*	*2.17E+04*	*2.69E+01*
1.59E-08	*1.00E-07*	*1.17E+04*	*9.67E+03*	*9.24E+03*	*1.09E+01*
1.59E-09	*1.00E-08*	*6.96E+03*	*4.92E+03*	*4.67E+03*	*5.14E+00*

Maximum Limiting Modulus

Max E' (kPa)	2.94E+07

Shift Factor

Shift Factor a_1	1.24E-03
Shift Factor a_2	-1.47E-01
T_{REF} (°C)	21.1

Other Parameters

E_∞ (kPa)	2034
Start Decade of Time	-6
Sum of Error	**0.0094**
α	**3.38**

Sigmoidal Function

b	3.31E+00
d	-1.76E+00
g	-4.17E-01

2S2P1D Function

δ	2.37E+00
k	1.41E-01
h	4.38E-01
β	1.00E+12
E_{00} (MPa)	2.03E+00
E_0 (MPa)	4.00E+04
log(τ_E)	-1.30E+00
Sum of Error	9.15E-03
Average % Error	3%

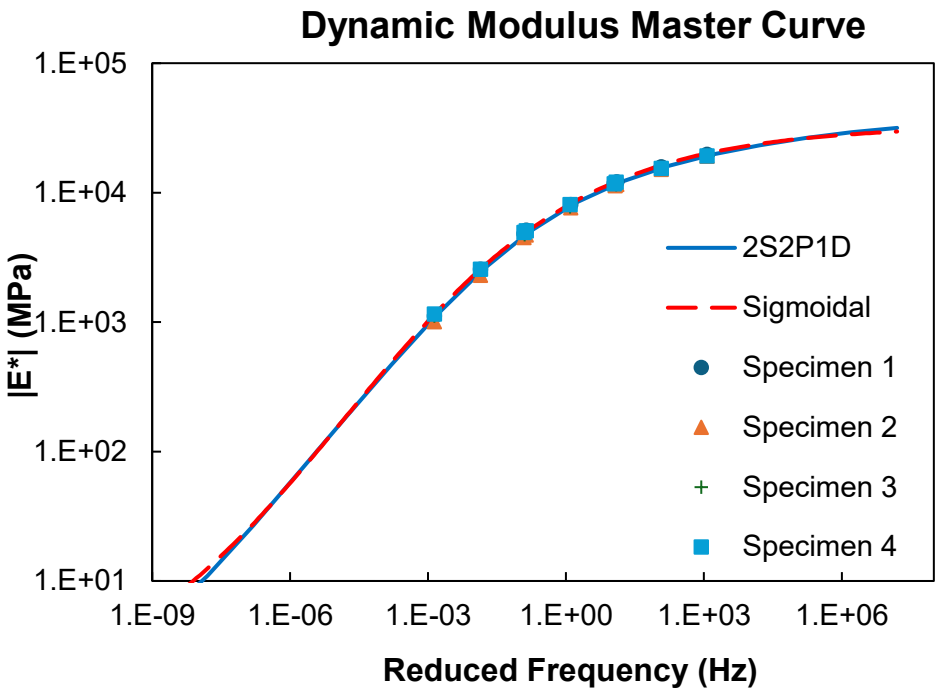
Dynamic Modulus Master Curve
1.E+05
1.E+04
1.E+03
1.E+02
1.E+01
|E*| (MPa)
1.E-09
1.E-06
1.E-03
1.E+00
1.E+03
1.E+06
Reduced Frequency (Hz)
2S2P1D
Sigmoidal
Specimen 1
Specimen 2
Specimen 3
Specimen 4

UI.0_4.19-1-A-1:

Specimen Identification	Frequency (Hz)	Dynamic Modulus (MPa)	Phase Angle (Degrees)	Average Temperature (°C)
1	10.0	17343.0	9.57	10.4
1	1.0	13294.0	12.39	10.4
1	0.1	9534.0	16.61	10.4
1	10.0	11459.0	15.48	20.5
1	1.0	7511.0	20.62	20.5
1	0.1	4387.0	26.17	20.5
1	10.0	4566.0	27.36	35.5
1	1.0	2166.0	32.56	35.5
1	0.1	918.1	33.78	35.5
2	10.0	17626.0	8.92	10.3
2	1.0	13709.0	11.55	10.3
2	0.1	10038.0	15.54	10.4
2	10.0	11912.0	14.44	20.4
2	1.0	7901.0	19.45	20.4
2	0.1	4782.0	24.77	20.5
2	10.0	4980.0	26.09	35.5
2	1.0	2430.0	31.45	35.5
2	0.1	1035.0	33.48	35.5
3	10.0	16894.0	9.42	10.4
3	1.0	13271.0	11.87	10.4
3	0.1	9872.0	16.25	10.4
3	10.0	11612.0	14.62	20.5
3	1.0	7851.0	19.23	20.5
3	0.1	4705.0	24.35	20.5
3	10.0	4810.0	25.65	35.5
3	1.0	2349.0	30.93	35.5
3	0.1	1015.0	32.70	35.5
4	10.0	18218.0	9.10	10.4
4	1.0	14225.0	11.53	10.3
4	0.1	10366.0	15.21	10.4
4	10.0	12309.0	14.38	20.5
4	1.0	8320.0	19.07	20.5
4	0.1	5053.0	24.41	20.4
4	10.0	5030.0	26.28	35.5
4	1.0	2497.0	31.32	35.5
4	0.1	1100.0	33.05	35.5
5	10.0	18373.0	9.27	10.4
5	1.0	14434.0	11.50	10.4
5	0.1	10686.0	14.96	10.4
5	10.0	11944.0	14.58	20.4
5	1.0	7967.0	19.52	20.5
5	0.1	4824.0	24.74	20.4
5	10.0	4966.0	26.48	35.5
5	1.0	2460.0	31.59	35.5
5	0.1	1082.0	33.54	35.5

Reduced Frequency	Reduced Angular Frequency	E' (Sigmoidal) (kPa)	E'norm	E' (2S2P1D) (kPa)	|E*| (2S2P1D) (MPa)
1.59E+07	*1.00E+08*	*2.57E+07*	*2.57E+07*	*3.14E+07*	*3.14E+04*
1.59E+06	*1.00E+07*	*2.48E+07*	*2.48E+07*	*2.90E+07*	*2.90E+04*
1.59E+05	*1.00E+06*	*2.35E+07*	*2.35E+07*	*2.61E+07*	*2.62E+04*
1.59E+04	*1.00E+05*	*2.16E+07*	*2.16E+07*	*2.29E+07*	*2.31E+04*
1.59E+03	*1.00E+04*	*1.91E+07*	*1.90E+07*	*1.94E+07*	*1.96E+04*
1.59E+02	*1.00E+03*	*1.57E+07*	*1.57E+07*	*1.57E+07*	*1.59E+04*
1.59E+01	*1.00E+02*	*1.19E+07*	*1.19E+07*	*1.18E+07*	*1.21E+04*
1.59E+00	*1.00E+01*	*7.95E+06*	*7.95E+06*	*7.98E+06*	*8.35E+03*
1.59E-01	*1.00E+00*	*4.58E+06*	*4.57E+06*	*4.60E+06*	*5.00E+03*
1.59E-02	*1.00E-01*	*2.23E+06*	*2.23E+06*	*2.22E+06*	*2.55E+03*
1.59E-03	*1.00E-02*	*9.38E+05*	*9.34E+05*	*9.37E+05*	*1.13E+03*
1.59E-04	*1.00E-03*	*3.59E+05*	*3.55E+05*	*3.66E+05*	*4.55E+02*
1.59E-05	*1.00E-04*	*1.37E+05*	*1.33E+05*	*1.39E+05*	*1.75E+02*
1.59E-06	*1.00E-05*	*5.68E+04*	*5.25E+04*	*5.36E+04*	*6.69E+01*
1.59E-07	*1.00E-06*	*2.72E+04*	*2.30E+04*	*2.21E+04*	*2.66E+01*
1.59E-08	*1.00E-07*	*1.54E+04*	*1.11E+04*	*1.07E+04*	*1.20E+01*
1.59E-09	*1.00E-08*	*1.01E+04*	*5.89E+03*	*6.56E+03*	*6.85E+00*

Maximum Limiting Modulus

Max E' (kPa)	2.74E+07

Shift Factor

Shift Factor a_1	8.72E-04
Shift Factor a_2	-1.44E-01
T_{REF} (°C)	21.1

Other Parameters

E_∞ (kPa)	4231
Start Decade of Time	-6
Sum of Error	**0.0170**
α	**3.37**

Sigmoidal Function

b	3.63E+00
d	-1.72E+00
g	-4.46E-01

2S2P1D Function

δ	2.39E+00
k	1.39E-01
h	4.44E-01
β	1.00E+12
E_{00} (MPa)	4.23E+00
E_0 (MPa)	4.00E+04
log(τ_ε)	-1.28E+00
Sum of Error	1.67E-02
Average % Error	4%

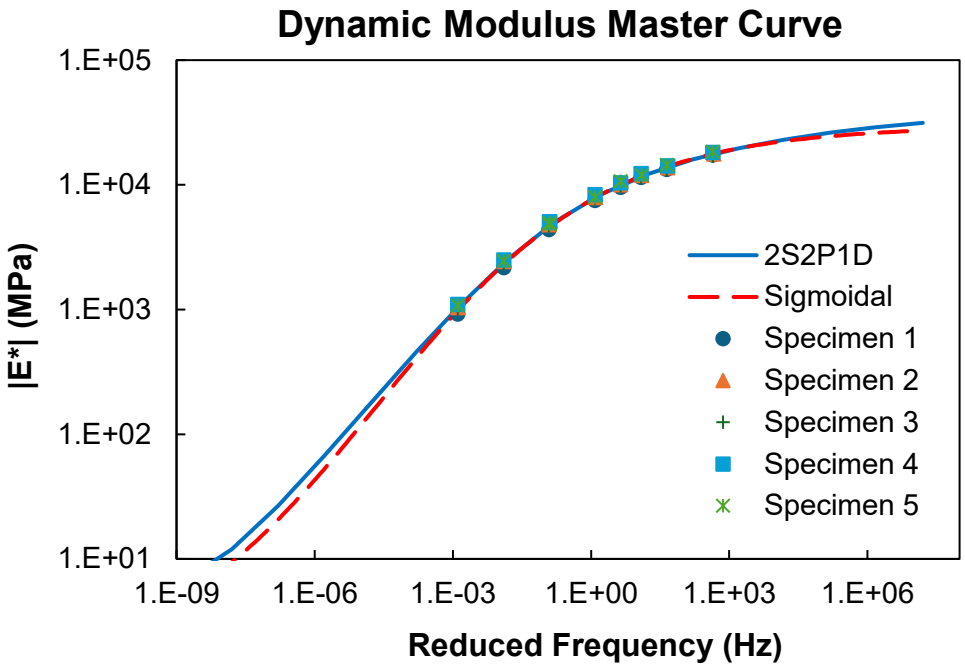
Dynamic Modulus Master Curve
1.E+05
1.E+04
1.E+03
1.E+02
1.E+01
|E*| (MPa)
1.E-09
1.E-06
1.E-03
1.E+00
1.E+03
1.E+06
Reduced Frequency (Hz)
2S2P1D
Sigmoidal
Specimen 1
Specimen 2
Specimen 3
Specimen 4
Specimen 5

Cl.0_3.90-1-A-1:

Specimen Identification	Frequency (Hz)	Dynamic Modulus (MPa)	Phase Angle (Degrees)	Average Temperature (°C)
1	*10.0*	*16163.0*	*10.61*	*10.4*
1	*1.0*	*12009.0*	*14.07*	*10.4*
1	*0.1*	*8203.0*	*18.72*	*10.4*
1	*10.0*	*9628.0*	*17.60*	*20.5*
1	*1.0*	*5943.0*	*23.24*	*20.5*
1	*0.1*	*3317.0*	*28.50*	*20.5*
1	*10.0*	*4126.0*	*27.79*	*35.5*
1	*1.0*	*1902.0*	*32.26*	*35.5*
1	*0.1*	*805.8*	*32.68*	*35.5*
2	*10.0*	*15763.0*	*11.26*	*10.3*
2	*1.0*	*11525.0*	*15.04*	*10.3*
2	*0.1*	*7830.0*	*19.42*	*10.4*
2	*10.0*	*10170.0*	*17.33*	*20.4*
2	*1.0*	*6322.0*	*22.76*	*20.4*
2	*0.1*	*3505.0*	*28.07*	*20.5*
2	*10.0*	*4222.0*	*27.87*	*35.5*
2	*1.0*	*1954.0*	*32.85*	*35.5*
2	*0.1*	*846.2*	*33.06*	*35.5*
3	*10.0*	*16116.0*	*10.48*	*10.4*
3	*1.0*	*12205.0*	*13.81*	*10.4*
3	*0.1*	*8445.0*	*18.38*	*10.4*
3	*10.0*	*9995.0*	*17.12*	*20.5*
3	*1.0*	*6246.0*	*22.86*	*20.5*
3	*0.1*	*3519.0*	*28.01*	*20.5*
3	*10.0*	*4545.0*	*28.01*	*35.5*
3	*1.0*	*2149.0*	*32.42*	*35.5*
3	*0.1*	*954.3*	*32.85*	*35.5*
4	*10.0*	*15178.0*	*11.89*	*10.4*
4	*1.0*	*11079.0*	*15.59*	*10.3*
4	*0.1*	*7426.0*	*20.42*	*10.4*
4	*10.0*	*9215.0*	*18.53*	*20.5*
4	*1.0*	*5545.0*	*24.42*	*20.5*
4	*0.1*	*3007.0*	*29.74*	*20.4*
4	*10.0*	*3893.0*	*29.06*	*35.5*
4	*1.0*	*1760.0*	*33.76*	*35.5*
4	*0.1*	*751.9*	*33.83*	*35.5*

Reduced Frequency	Reduced Angular Frequency	E' (Sigmoidal) (kPa)	E'norm	E' (2S2P1D) (kPa)	|E*| (2S2P1D) (MPa)
1.59E+07	*1.00E+08*	*2.57E+07*	*2.57E+07*	*3.12E+07*	*3.13E+04*
1.59E+06	*1.00E+07*	*2.46E+07*	*2.46E+07*	*2.85E+07*	*2.86E+04*
1.59E+05	*1.00E+06*	*2.29E+07*	*2.29E+07*	*2.54E+07*	*2.55E+04*
1.59E+04	*1.00E+05*	*2.06E+07*	*2.06E+07*	*2.18E+07*	*2.19E+04*
1.59E+03	*1.00E+04*	*1.75E+07*	*1.75E+07*	*1.78E+07*	*1.80E+04*
1.59E+02	*1.00E+03*	*1.38E+07*	*1.37E+07*	*1.37E+07*	*1.40E+04*
1.59E+01	*1.00E+02*	*9.68E+06*	*9.67E+06*	*9.64E+06*	*1.00E+04*
1.59E+00	*1.00E+01*	*5.93E+06*	*5.92E+06*	*5.94E+06*	*6.35E+03*
1.59E-01	*1.00E+00*	*3.10E+06*	*3.10E+06*	*3.11E+06*	*3.47E+03*
1.59E-02	*1.00E-01*	*1.40E+06*	*1.39E+06*	*1.40E+06*	*1.64E+03*
1.59E-03	*1.00E-02*	*5.72E+05*	*5.64E+05*	*5.70E+05*	*6.95E+02*
1.59E-04	*1.00E-03*	*2.29E+05*	*2.21E+05*	*2.22E+05*	*2.76E+02*
1.59E-05	*1.00E-04*	*9.86E+04*	*9.05E+04*	*8.74E+04*	*1.08E+02*
1.59E-06	*1.00E-05*	*4.85E+04*	*4.03E+04*	*3.70E+04*	*4.39E+01*
1.59E-07	*1.00E-06*	*2.79E+04*	*1.98E+04*	*1.86E+04*	*2.05E+01*
1.59E-08	*1.00E-07*	*1.86E+04*	*1.05E+04*	*1.19E+04*	*1.23E+01*
1.59E-09	*1.00E-08*	*1.41E+04*	*5.93E+03*	*9.49E+03*	*9.56E+00*

Maximum Limiting Modulus

Max E' (kPa)	2.78E+07

Shift Factor

Shift Factor a_1	1.83E-03
Shift Factor a_2	-1.34E-01
T_{REF} (°C)	21.1

Other Parameters

E_∞ (kPa)	8126
Start Decade of Time	-6
Sum of Error	**0.0246**
α	**3.43**

Sigmoidal Function

b	3.91E+00
d	-1.36E+00
g	-4.53E-01

2S2P1D Function

δ	2.44E+00
k	1.51E-01
h	4.43E-01
β	1.00E+12
E_{00} (MPa)	8.13E+00
E_0 (MPa)	4.00E+04
log(τ_E)	-1.81E+00
Sum of Error	2.45E-02
Average % Error	5%

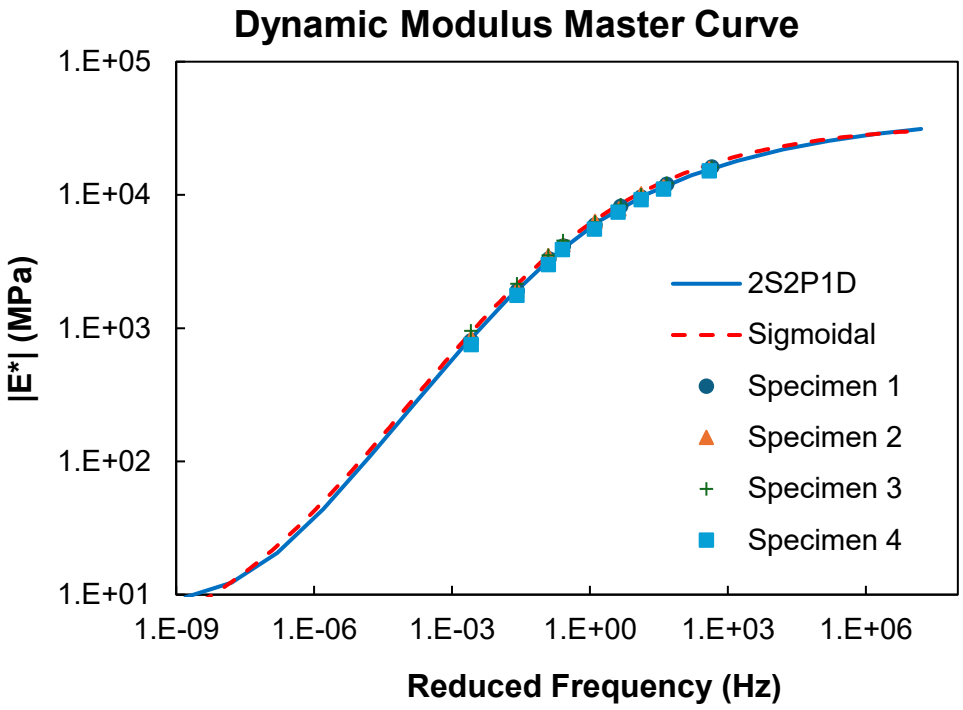
Dynamic Modulus Master Curve
1.E+05
1.E+04
1.E+03
1.E+02
1.E+01
|E*| (MPa)
1.E-09
1.E-06
1.E-03
1.E+00
1.E+03
1.E+06
Reduced Frequency (Hz)
2S2P1D
Sigmoidal
Specimen 1
Specimen 2
Specimen 3
Specimen 4

BI.8_2.20-1-A-1:

Specimen Identification	Frequency (Hz)	Dynamic Modulus (MPa)	Phase Angle (Degrees)	Average Temperature (°C)
1	*10.0*	*15860.0*	*9.59*	*10.4*
1	*1.0*	*12454.0*	*12.05*	*10.4*
1	*0.1*	*9218.0*	*15.75*	*10.3*
1	*10.0*	*11439.0*	*14.31*	*20.5*
1	*1.0*	*7695.0*	*19.00*	*20.5*
1	*0.1*	*4940.0*	*22.80*	*20.5*
1	*10.0*	*5547.0*	*22.01*	*35.5*
1	*1.0*	*3078.0*	*26.83*	*35.5*
1	*0.1*	*1526.0*	*30.03*	*35.5*
2	*10.0*	*15826.0*	*9.07*	*10.3*
2	*1.0*	*12396.0*	*11.13*	*10.4*
2	*0.1*	*9330.0*	*14.63*	*10.4*
2	*10.0*	*11439.0*	*13.59*	*20.4*
2	*1.0*	*7859.0*	*18.10*	*20.4*
2	*0.1*	*4970.0*	*23.03*	*20.5*
2	*10.0*	*5646.0*	*22.42*	*35.5*
2	*1.0*	*3055.0*	*27.82*	*35.4*
2	*0.1*	*1463.0*	*31.35*	*35.5*
3	*10.0*	*16420.0*	*9.35*	*10.4*
3	*1.0*	*12908.0*	*11.24*	*10.4*
3	*0.1*	*9703.0*	*14.26*	*10.4*
3	*10.0*	*10980.0*	*13.38*	*20.5*
3	*1.0*	*7558.0*	*17.61*	*20.4*
3	*0.1*	*4855.0*	*22.01*	*20.5*
3	*10.0*	*5585.0*	*21.95*	*35.4*
3	*1.0*	*3090.0*	*27.17*	*35.4*
3	*0.1*	*1568.0*	*30.59*	*35.5*

Reduced Frequency	Reduced Angular Frequency	E' (Sigmoidal) (kPa)	E'norm	E' (2S2P1D) (kPa)	|E*| (2S2P1D) (MPa)
1.59E+07	*1.00E+08*	*2.46E+07*	*2.46E+07*	*2.96E+07*	*2.97E+04*
1.59E+06	*1.00E+07*	*2.36E+07*	*2.36E+07*	*2.72E+07*	*2.72E+04*
1.59E+05	*1.00E+06*	*2.22E+07*	*2.22E+07*	*2.44E+07*	*2.45E+04*
1.59E+04	*1.00E+05*	*2.03E+07*	*2.03E+07*	*2.14E+07*	*2.15E+04*
1.59E+03	*1.00E+04*	*1.78E+07*	*1.78E+07*	*1.81E+07*	*1.83E+04*
1.59E+02	*1.00E+03*	*1.48E+07*	*1.48E+07*	*1.48E+07*	*1.50E+04*
1.59E+01	*1.00E+02*	*1.14E+07*	*1.14E+07*	*1.13E+07*	*1.16E+04*
1.59E+00	*1.00E+01*	*7.93E+06*	*7.93E+06*	*7.95E+06*	*8.25E+03*
1.59E-01	*1.00E+00*	*4.87E+06*	*4.87E+06*	*4.89E+06*	*5.22E+03*
1.59E-02	*1.00E-01*	*2.59E+06*	*2.59E+06*	*2.58E+06*	*2.87E+03*
1.59E-03	*1.00E-02*	*1.18E+06*	*1.18E+06*	*1.19E+06*	*1.38E+03*
1.59E-04	*1.00E-03*	*4.71E+05*	*4.70E+05*	*5.00E+05*	*6.00E+02*
1.59E-05	*1.00E-04*	*1.72E+05*	*1.71E+05*	*2.01E+05*	*2.46E+02*
1.59E-06	*1.00E-05*	*6.14E+04*	*6.08E+04*	*7.88E+04*	*9.78E+01*
1.59E-07	*1.00E-06*	*2.32E+04*	*2.25E+04*	*3.08E+04*	*3.84E+01*
1.59E-08	*1.00E-07*	*9.79E+03*	*9.16E+03*	*1.22E+04*	*1.51E+01*
1.59E-09	*1.00E-08*	*4.79E+03*	*4.16E+03*	*5.08E+03*	*6.12E+00*

Maximum Limiting Modulus

Max E' (kPa)	2.69E+07

Shift Factor

Shift Factor a_1	1.37E-03
Shift Factor a_2	-1.35E-01
T_{REF} (°C)	21.1

Other Parameters

E_∞ (kPa)	631
Start Decade of Time	-6
Sum of Error	**0.0030**
α	**3.45**

Sigmoidal Function

b	2.80E+00
d	-1.97E+00
g	-3.88E-01

2S2P1D Function

δ	2.59E+00
k	1.28E-01
h	4.18E-01
β	1.00E+12
E_{00} (MPa)	6.31E-01
E_0 (MPa)	4.00E+04
log(τ_E)	-1.21E+00
Sum of Error	2.92E-03
Average % Error	2%

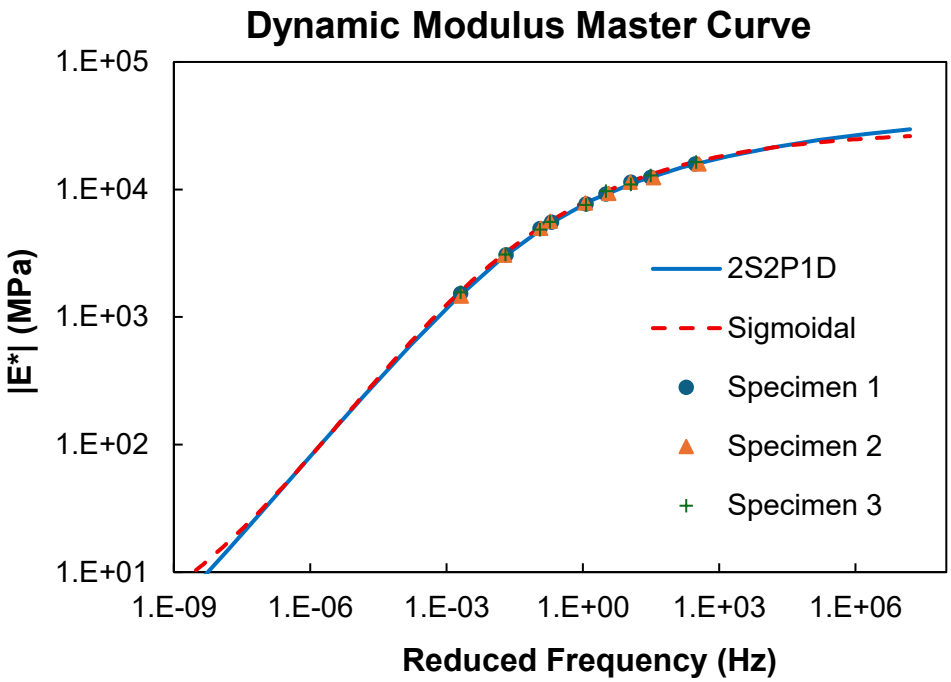
Dynamic Modulus Master Curve
1.E+05
1.E+04
1.E+03
1.E+02
1.E+01
|E*| (MPa)
1.E-09
1.E-06
1.E-03
1.E+00
1.E+03
1.E+06
Reduced Frequency (Hz)
2S2P1D
Sigmoidal
Specimen 1
Specimen 2
Specimen 3

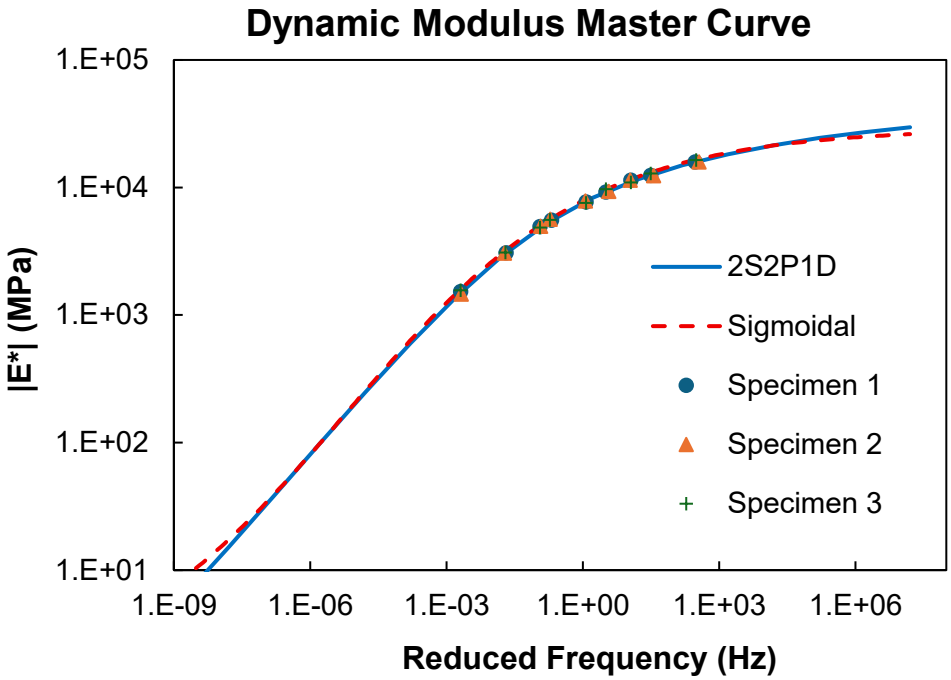
Dynamic Modulus Master Curve
1.E+05
1.E+04
1.E+03
1.E+02
1.E+01
|E*| (MPa)
1.E-09
1.E-06
1.E-03
1.E+00
1.E+03
1.E+06
Reduced Frequency (Hz)
2S2P1D
Sigmoidal
Specimen 1
Specimen 2
Specimen 3

BI.0_2.20-1-A-1:

Specimen Identification	Frequency (Hz)	Dynamic Modulus (MPa)	Phase Angle (Degrees)	Average Temperature (°C)
1	*10.0*	*15107.0*	*10.80*	*10.4*
1	*1.0*	*11021.0*	*13.65*	*10.3*
1	*0.1*	*8135.0*	*17.86*	*10.3*
1	*10.0*	*10787.0*	*15.43*	*20.4*
1	*1.0*	*7117.0*	*20.65*	*20.4*
1	*0.1*	*4311.0*	*25.91*	*20.5*
1	*10.0*	*5188.0*	*24.23*	*35.5*
1	*1.0*	*2729.0*	*28.89*	*35.5*
1	*0.1*	*1274.0*	*31.07*	*35.5*
2	*10.0*	*14707.0*	*10.50*	*10.3*
2	*1.0*	*11251.0*	*13.35*	*10.*
2	*0.1*	*8242.0*	*17.46*	*10.4*
2	*10.0*	*10039.0*	*15.82*	*20.4*
2	*1.0*	*6687.0*	*21.12*	*20.3*
2	*0.1*	*4152.0*	*26.28*	*20.5*
2	*10.0*	*5158.0*	*24.09*	*35.5*
2	*1.0*	*2682.0*	*28.53*	*35.4*
2	*0.1*	*1251.0*	*30.25*	*35.5*
3	*10.0*	*16402.0*	*9.92*	*10.3*
3	*1.0*	*12565.0*	*12.78*	*10.3*
3	*0.1*	*9092.0*	*16.87*	*10.4*
3	*10.0*	*10502.0*	*15.06*	*20.5*
3	*1.0*	*7262.0*	*20.33*	*20.5*
3	*0.1*	*4463.0*	*24.85*	*20.5*
3	*10.0*	*5247.0*	*25.27*	*35.4*
3	*1.0*	*2713.0*	*28.41*	*35.5*
3	*0.1*	*1251.0*	*31.01*	*35.5*

Reduced Frequency	Reduced Angular Frequency	E' (Sigmoidal) (kPa)	E'norm	E' (2S2P1D) (kPa)	|E*| (2S2P1D) (MPa)
1.59E+07	*1.00E+08*	*2.56E+07*	*2.56E+07*	*3.06E+07*	*3.07E+04*
1.59E+06	*1.00E+07*	*2.43E+07*	*2.43E+07*	*2.80E+07*	*2.81E+04*
1.59E+05	*1.00E+06*	*2.26E+07*	*2.26E+07*	*2.49E+07*	*2.50E+04*
1.59E+04	*1.00E+05*	*2.04E+07*	*2.04E+07*	*2.15E+07*	*2.17E+04*
1.59E+03	*1.00E+04*	*1.76E+07*	*1.76E+07*	*1.79E+07*	*1.81E+04*
1.59E+02	*1.00E+03*	*1.42E+07*	*1.42E+07*	*1.43E+07*	*1.45E+04*
1.59E+01	*1.00E+02*	*1.06E+07*	*1.06E+07*	*1.06E+07*	*1.09E+04*
1.59E+00	*1.00E+01*	*7.16E+06*	*7.16E+06*	*7.17E+06*	*7.49E+03*
1.59E-01	*1.00E+00*	*4.22E+06*	*4.22E+06*	*4.23E+06*	*4.57E+03*
1.59E-02	*1.00E-01*	*2.14E+06*	*2.14E+06*	*2.13E+06*	*2.40E+03*
1.59E-03	*1.00E-02*	*9.25E+05*	*9.25E+05*	*9.29E+05*	*1.10E+03*
1.59E-04	*1.00E-03*	*3.48E+05*	*3.48E+05*	*3.71E+05*	*4.56E+02*
1.59E-05	*1.00E-04*	*1.19E+05*	*1.19E+05*	*1.41E+05*	*1.78E+02*
1.59E-06	*1.00E-05*	*3.96E+04*	*3.94E+04*	*5.24E+04*	*6.69E+01*
1.59E-07	*1.00E-06*	*1.38E+04*	*1.36E+04*	*1.93E+04*	*2.48E+01*
1.59E-08	*1.00E-07*	*5.37E+03*	*5.15E+03*	*7.19E+03*	*9.19E+00*
1.59E-09	*1.00E-08*	*2.43E+03*	*2.20E+03*	*2.76E+03*	*3.46E+00*

Maximum Limiting Modulus

Max E' (kPa)	2.86E+07

Shift Factor

Shift Factor a_1	1.26E-03
Shift Factor a_2	-1.30E-01
T_{REF} (°C)	21.1

Other Parameters

E_∞ (kPa)	220
Start Decade of Time	-6
Sum of Error	**0.0098**
α	**3.31**

Sigmoidal Function

b	2.34E+00
d	-1.94E+00
g	-3.75E-01

2S2P1D Function

δ	2.90E+00
k	1.45E-01
h	4.40E-01
β	1.00E+12
E_{00} (MPa)	2.20E-01
E_0 (MPa)	4.00E+04
log(τ_E)	-1.27E+00
Sum of Error	9.56E-03
Average % Error	3%

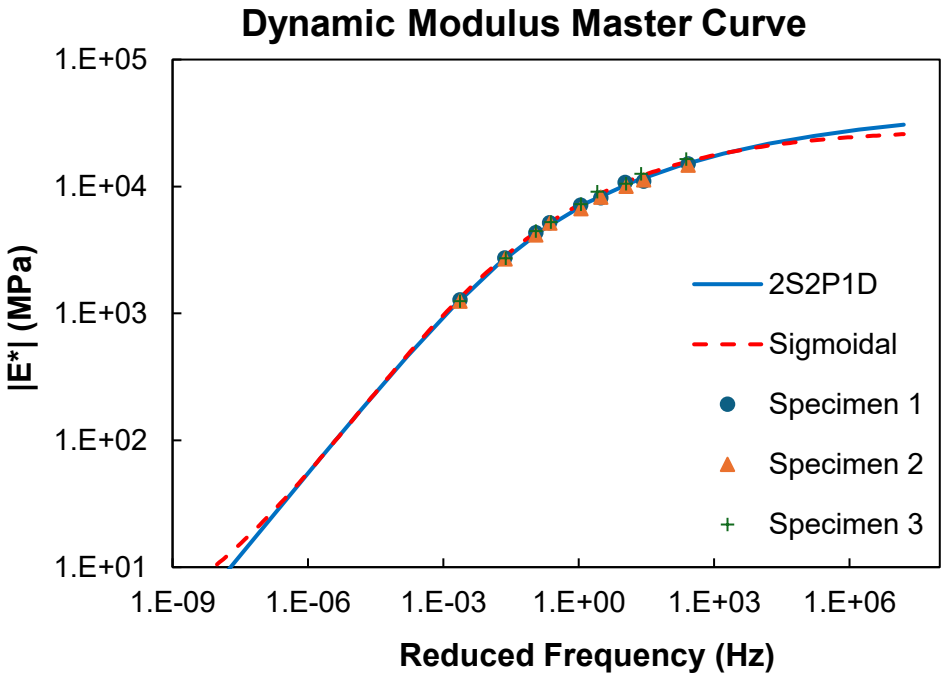
Dynamic Modulus Master Curve
1.E+05
1.E+04
1.E+03
1.E+02
1.E+01
|E*| (MPa)
1.E-09
1.E-06
1.E-03
1.E+00
1.E+03
1.E+06
Reduced Frequency (Hz)
2S2P1D
Sigmoidal
Specimen 1
Specimen 2
Specimen 3

Fatigue results:

UI.4_4.19-1-A-1

C Vs S Data for All Specimens

C Fit	S Fit	C Specimen 1	S Specimen 1	C Specimen 2	S Specimen 2	C Specimen 3	S Specimen 3	C Specimen 4	S Specimen 4
1.00E+00	0.00E+00	1.00E+00	0.00E+00	1.00E+00	0.00E+00	1.00E+00	0.00E+00	1.00E+00	0.00E+00
9.89E-01	1.00E+02	9.52E-01	1.52E+03	9.26E-01	3.01E+03	9.26E-01	3.11E+03	9.13E-01	3.31E+03
9.80E-01	3.00E+02	9.52E-01	1.52E+03	9.26E-01	3.01E+03	9.26E-01	3.11E+03	9.13E-01	3.31E+03
9.74E-01	5.00E+02	9.52E-01	1.52E+03	9.26E-01	3.01E+03	9.26E-01	3.11E+03	9.13E-01	3.31E+03
9.61E-01	1.00E+03	9.52E-01	1.52E+03	8.28E-01	1.77E+04	9.26E-01	3.11E+03	9.13E-01	3.31E+03
9.34E-01	2.61E+03	8.00E-01	2.37E+04	7.96E-01	2.40E+04	9.26E-01	3.11E+03	9.13E-01	3.31E+03
8.40E-01	1.31E+04	8.00E-01	2.37E+04	7.96E-01	2.40E+04	9.26E-01	3.11E+03	7.68E-01	2.69E+04
7.65E-01	2.61E+04	8.00E-01	2.37E+04	7.64E-01	3.13E+04	7.48E-01	3.34E+04	7.68E-01	2.69E+04
7.06E-01	3.92E+04	7.29E-01	3.98E+04	7.34E-01	3.82E+04	7.48E-01	3.34E+04	7.68E-01	2.69E+04
6.55E-01	5.22E+04	7.29E-01	3.98E+04	7.08E-01	4.45E+04	7.48E-01	3.34E+04	7.68E-01	2.69E+04
6.10E-01	6.53E+04	6.89E-01	4.97E+04	6.89E-01	4.94E+04	7.48E-01	3.34E+04	6.67E-01	4.92E+04
5.30E-01	9.14E+04	6.89E-01	4.97E+04	6.73E-01	5.37E+04	6.61E-01	5.30E+04	6.67E-01	4.92E+04
4.94E-01	1.04E+05	6.65E-01	5.60E+04	6.59E-01	5.76E+04	6.61E-01	5.30E+04	6.67E-01	4.92E+04
4.60E-01	1.17E+05	6.37E-01	6.37E+04	6.37E-01	6.40E+04	6.26E-01	6.23E+04	6.16E-01	6.13E+04
4.27E-01	1.31E+05	6.19E-01	6.86E+04	6.20E-01	6.88E+04	6.06E-01	6.78E+04	5.90E-01	6.81E+04
3.96E-01	1.44E+05	6.01E-01	7.38E+04	6.02E-01	7.43E+04	5.82E-01	7.49E+04	5.72E-01	7.30E+04
3.66E-01	1.57E+05	5.81E-01	8.00E+04	5.84E-01	7.96E+04	5.67E-01	7.98E+04	5.58E-01	7.70E+04
3.38E-01	1.70E+05	5.66E-01	8.44E+04	5.67E-01	8.47E+04	5.55E-01	8.38E+04	5.38E-01	8.30E+04
3.10E-01	1.83E+05	5.49E-01	8.97E+04	5.52E-01	8.96E+04	5.37E-01	8.99E+04	5.16E-01	8.96E+04
2.83E-01	1.96E+05	5.33E-01	9.50E+04	5.35E-01	9.49E+04	5.23E-01	9.48E+04	5.00E-01	9.47E+04
2.57E-01	2.09E+05	5.19E-01	9.98E+04	5.20E-01	9.99E+04	5.10E-01	9.97E+04	4.84E-01	1.00E+05
2.32E-01	2.22E+05	5.05E-01	1.05E+05	5.05E-01	1.05E+05	4.97E-01	1.05E+05	4.71E-01	1.04E+05
2.07E-01	2.35E+05	4.92E-01	1.10E+05	4.90E-01	1.10E+05	4.84E-01	1.10E+05	4.56E-01	1.10E+05
1.83E-01	2.48E+05	4.79E-01	1.15E+05	4.75E-01	1.15E+05	4.71E-01	1.15E+05	4.44E-01	1.14E+05
1.59E-01	2.61E+05	4.66E-01	1.20E+05	4.60E-01	1.20E+05	4.60E-01	1.20E+05	4.30E-01	1.20E+05
-	-	4.56E-01	1.24E+05	4.46E-01	1.25E+05	4.51E-01	1.23E+05	4.18E-01	1.24E+05
-	-	4.44E-01	1.30E+05	4.31E-01	1.30E+05	4.37E-01	1.30E+05	4.08E-01	1.28E+05
-	-	4.32E-01	1.35E+05	4.16E-01	1.35E+05	4.27E-01	1.34E+05	3.95E-01	1.34E+05
-	-	4.22E-01	1.40E+05	4.10E-01	1.37E+05	4.16E-01	1.40E+05	3.83E-01	1.39E+05
-	-	4.11E-01	1.45E+05	3.91E-01	1.43E+05	4.06E-01	1.44E+05	3.69E-01	1.45E+05

-	-	4.01E-01	1.50E+05	3.72E-01	1.50E+05	3.96E-01	1.49E+05	3.59E-01	1.49E+05
-	-	3.91E-01	1.55E+05	3.62E-01	1.53E+05	3.84E-01	1.55E+05	3.48E-01	1.54E+05
-	-	3.81E-01	1.60E+05	3.47E-01	1.58E+05	3.75E-01	1.59E+05	3.36E-01	1.58E+05
-	-	3.71E-01	1.65E+05	3.27E-01	1.65E+05	3.64E-01	1.64E+05	3.23E-01	1.64E+05
-	-	3.61E-01	1.70E+05	3.15E-01	1.69E+05	3.55E-01	1.69E+05	3.10E-01	1.69E+05
-	-	3.51E-01	1.75E+05	3.00E-01	1.75E+05	3.41E-01	1.75E+05	2.96E-01	1.74E+05
-	-	3.42E-01	1.80E+05	2.90E-01	1.78E+05	3.33E-01	1.79E+05	2.84E-01	1.79E+05
-	-	3.31E-01	1.85E+05	2.77E-01	1.83E+05	3.21E-01	1.84E+05	2.70E-01	1.84E+05
-	-	3.21E-01	1.90E+05	2.62E-01	1.89E+05	3.10E-01	1.89E+05	2.56E-01	1.90E+05
-	-	3.11E-01	1.95E+05	2.49E-01	1.95E+05	2.98E-01	1.95E+05	2.45E-01	1.95E+05
-	-	2.98E-01	2.00E+05	2.38E-01	1.99E+05	2.88E-01	2.00E+05	2.33E-01	2.00E+05
-	-	2.94E-01	2.02E+05	2.24E-01	2.05E+05	2.78E-01	2.05E+05	2.23E-01	2.04E+05
-	-	-	-	2.12E-01	2.10E+05	2.69E-01	2.10E+05	2.10E-01	2.10E+05
-	-	-	-	2.00E-01	2.15E+05	2.59E-01	2.15E+05	1.99E-01	2.14E+05
-	-	-	-	1.90E-01	2.19E+05	2.50E-01	2.20E+05	1.87E-01	2.20E+05
-	-	-	-	1.77E-01	2.25E+05	2.40E-01	2.24E+05	1.75E-01	2.25E+05
-	-	-	-	1.66E-01	2.29E+05	2.31E-01	2.29E+05	1.65E-01	2.30E+05
-	-	-	-	1.54E-01	2.34E+05	2.19E-01	2.35E+05	1.59E-01	2.32E+05
-	-	-	-	1.44E-01	2.39E+05	2.17E-01	2.36E+05	-	-
-	-	-	-	1.33E-01	2.45E+05	-	-	-	-
-	-	-	-	1.22E-01	2.50E+05	-	-	-	-
-	-	-	-	1.12E-01	2.55E+05	-	-	-	-
-	-	-	-	1.02E-01	2.60E+05	-	-	-	-
-	-	-	-	9.92E-02	2.61E+05	-	-	-	-

Fatigue Analysis Output Summary

Specimen No & ID	Fingerprint |E*| (MPa)	DMR, 0.85<DMR<1.15	Nf	log (Nf)	Cum. (1-C)	DR	Input Strain (μ)	Sapp (DR = f(|E*|))
1	**10969**	**0.992**	**46780**	**4.670**	**28418**	**0.607**	**340**	**23.7**
2	**11061**	**1.003**	**14420**	**4.159**	**11247**	**0.780**	**410**	**21.5**
3	**9959**	**0.902**	**25970**	**4.414**	**17215**	**0.663**	**410**	**22.7**
4	**9504**	**0.857**	**21710**	**4.337**	**15525**	**0.715**	**410**	**20.4**
Average	**-**	**-**	**-**	**-**	**-**	**0.691**	**-**	**22.2**

UI.4_4.19-1-A-1:

C Vs S Data for All Specimens

C Fit	S Fit	C Specimen 1	S Specimen 1	C Specimen 2	S Specimen 2	C Specimen 3	S Specimen 3	C Specimen 4	S Specimen 4	C Specimen 5	S Specimen 5
1.00E+00	0.00E+00	1.00E+00	0.00E+00	1.00E+00	0.00E+00	1.00E+00	0.00E+00	1.00E+00	0.00E+00	1.00E+00	0.00E+00
9.92E-01	1.00E+02	9.48E-01	1.47E+03	9.54E-01	1.97E+03	9.43E-01	2.15E+03	9.71E-01	1.06E+03	9.52E-01	2.28E+03
9.84E-01	3.00E+02	9.48E-01	1.47E+03	9.54E-01	1.97E+03	9.43E-01	2.15E+03	9.71E-01	1.06E+03	9.52E-01	2.28E+03
9.79E-01	5.00E+02	9.48E-01	1.47E+03	9.54E-01	1.97E+03	9.43E-01	2.15E+03	9.71E-01	1.06E+03	9.52E-01	2.28E+03
9.68E-01	1.00E+03	8.14E-01	1.92E+04	9.54E-01	1.97E+03	9.43E-01	2.15E+03	9.71E-01	1.06E+03	9.52E-01	2.28E+03
9.48E-01	2.32E+03	7.96E-01	2.24E+04	9.54E-01	1.97E+03	9.43E-01	2.15E+03	9.71E-01	1.06E+03	9.52E-01	2.28E+03
8.66E-01	1.16E+04	7.61E-01	2.94E+04	7.94E-01	2.75E+04	9.43E-01	2.15E+03	8.08E-01	2.57E+04	9.52E-01	2.28E+03
7.99E-01	2.32E+04	7.45E-01	3.27E+04	7.94E-01	2.75E+04	7.62E-01	3.08E+04	8.08E-01	2.57E+04	9.52E-01	2.28E+03
7.45E-01	3.48E+04	7.20E-01	3.84E+04	7.94E-01	2.75E+04	7.62E-01	3.08E+04	8.08E-01	2.57E+04	7.57E-01	3.65E+04
6.99E-01	4.63E+04	6.95E-01	4.43E+04	7.94E-01	2.75E+04	7.62E-01	3.08E+04	8.08E-01	2.57E+04	7.57E-01	3.65E+04
6.57E-01	5.79E+04	6.77E-01	4.88E+04	7.15E-01	4.53E+04	7.62E-01	3.08E+04	8.08E-01	2.57E+04	7.57E-01	3.65E+04
5.82E-01	8.11E+04	6.55E-01	5.44E+04	6.74E-01	5.49E+04	6.73E-01	5.09E+04	6.96E-01	5.05E+04	7.57E-01	3.65E+04
5.48E-01	9.27E+04	6.34E-01	5.99E+04	6.74E-01	5.49E+04	6.73E-01	5.09E+04	6.96E-01	5.05E+04	7.57E-01	3.65E+04
5.15E-01	1.04E+05	6.16E-01	6.49E+04	6.41E-01	6.38E+04	6.33E-01	6.09E+04	6.42E-01	6.38E+04	6.55E-01	6.09E+04
4.85E-01	1.16E+05	6.00E-01	6.90E+04	6.22E-01	6.91E+04	6.12E-01	6.66E+04	6.42E-01	6.38E+04	6.55E-01	6.09E+04
4.55E-01	1.27E+05	5.79E-01	7.49E+04	6.03E-01	7.47E+04	5.87E-01	7.38E+04	6.02E-01	7.49E+04	6.14E-01	7.19E+04
4.27E-01	1.39E+05	5.65E-01	7.90E+04	5.89E-01	7.90E+04	5.71E-01	7.88E+04	5.90E-01	7.83E+04	5.92E-01	7.81E+04
3.99E-01	1.51E+05	5.48E-01	8.39E+04	5.72E-01	8.45E+04	5.53E-01	8.44E+04	5.72E-01	8.36E+04	5.78E-01	8.25E+04
3.72E-01	1.62E+05	5.33E-01	8.86E+04	5.57E-01	8.94E+04	5.40E-01	8.88E+04	5.54E-01	8.95E+04	5.57E-01	8.90E+04
3.47E-01	1.74E+05	5.16E-01	9.41E+04	5.42E-01	9.47E+04	5.23E-01	9.47E+04	5.39E-01	9.42E+04	5.42E-01	9.38E+04
3.21E-01	1.85E+05	4.98E-01	9.99E+04	5.28E-01	9.99E+04	5.10E-01	9.94E+04	5.25E-01	9.92E+04	5.25E-01	9.95E+04
2.97E-01	1.97E+05	4.85E-01	1.04E+05	5.15E-01	1.05E+05	4.96E-01	1.05E+05	5.11E-01	1.04E+05	5.12E-01	1.04E+05
2.73E-01	2.09E+05	4.68E-01	1.10E+05	5.02E-01	1.10E+05	4.83E-01	1.10E+05	4.97E-01	1.09E+05	4.95E-01	1.10E+05
2.49E-01	2.20E+05	4.55E-01	1.14E+05	4.91E-01	1.14E+05	4.71E-01	1.15E+05	4.85E-01	1.14E+05	4.84E-01	1.14E+05
2.27E-01	2.32E+05	4.40E-01	1.19E+05	4.78E-01	1.20E+05	4.61E-01	1.19E+05	4.72E-01	1.20E+05	4.70E-01	1.19E+05
-	-	4.24E-01	1.25E+05	4.68E-01	1.24E+05	4.51E-01	1.24E+05	4.60E-01	1.25E+05	4.57E-01	1.24E+05
-	-	4.10E-01	1.30E+05	4.57E-01	1.29E+05	4.39E-01	1.29E+05	4.49E-01	1.30E+05	4.49E-01	1.28E+05
-	-	3.96E-01	1.35E+05	4.45E-01	1.35E+05	4.29E-01	1.34E+05	4.40E-01	1.34E+05	4.33E-01	1.35E+05
-	-	3.81E-01	1.40E+05	4.34E-01	1.40E+05	4.19E-01	1.39E+05	4.29E-01	1.39E+05	4.24E-01	1.38E+05
-	-	3.66E-01	1.44E+05	4.23E-01	1.45E+05	4.08E-01	1.45E+05	4.18E-01	1.45E+05	4.12E-01	1.44E+05
-	-	3.49E-01	1.49E+05	4.13E-01	1.49E+05	4.00E-01	1.49E+05	4.09E-01	1.50E+05	4.01E-01	1.49E+05
-	-	3.32E-01	1.54E+05	4.01E-01	1.54E+05	3.90E-01	1.55E+05	3.99E-01	1.55E+05	3.88E-01	1.55E+05
-	-	-	-	3.89E-01	1.60E+05	3.80E-01	1.60E+05	3.91E-01	1.59E+05	3.77E-01	1.60E+05
-	-	-	-	3.78E-01	1.65E+05	3.72E-01	1.64E+05	3.81E-01	1.65E+05	3.66E-01	1.65E+05
-	-	-	-	3.67E-01	1.70E+05	3.63E-01	1.70E+05	3.73E-01	1.70E+05	3.57E-01	1.69E+05

-	-	-	-	3.56E-01	1.75E+05	3.54E-01	1.74E+05	3.65E-01	1.75E+05	3.46E-01	1.75E+05
-	-	-	-	3.45E-01	1.80E+05	3.45E-01	1.79E+05	3.56E-01	1.80E+05	3.36E-01	1.80E+05
-	-	-	-	3.34E-01	1.85E+05	3.35E-01	1.85E+05	3.48E-01	1.85E+05	3.26E-01	1.85E+05
-	-	-	-	3.22E-01	1.90E+05	3.25E-01	1.90E+05	3.40E-01	1.90E+05	3.16E-01	1.90E+05
-	-	-	-	3.11E-01	1.94E+05	3.15E-01	1.95E+05	3.31E-01	1.95E+05	3.06E-01	1.95E+05
-	-	-	-	2.97E-01	2.00E+05	3.05E-01	2.00E+05	3.23E-01	1.99E+05	2.97E-01	1.99E+05
-	-	-	-	2.87E-01	2.04E+05	2.96E-01	2.04E+05	3.15E-01	2.04E+05	2.85E-01	2.05E+05
-	-	-	-	2.73E-01	2.10E+05	2.85E-01	2.10E+05	3.06E-01	2.10E+05	2.75E-01	2.10E+05
-	-	-	-	2.72E-01	2.10E+05	2.79E-01	2.13E+05	2.97E-01	2.14E+05	2.63E-01	2.15E+05
-	-	-	-	-	-	-	-	2.93E-01	2.16E+05	2.53E-01	2.20E+05
-	-	-	-	-	-	-	-	-	-	2.43E-01	2.25E+05
-	-	-	-	-	-	-	-	-	-	2.32E-01	2.29E+05
-	-	-	-	-	-	-	-	-	-	2.27E-01	2.32E+05

Fatigue Analysis Output Summary

Specimen No & ID	Fingerprint |E*| (MPa)	DMR, 0.85<DMR<1.15	Nf	log (Nf)	Cum. (1-C)	DR	Input Strain (μ)	Sapp (DR = f(|E*|))
1	**10287**	**0.924**	**8330**	**3.921**	**4529**	**0.544**	**360**	**16.2**
2	**10698**	**0.959**	**29900**	**4.476**	**17907**	**0.599**	**360**	**18.2**
3	**9934**	**0.898**	**25250**	**4.402**	**15635**	**0.619**	**410**	**17.3**
4	**10431**	**0.942**	**27690**	**4.442**	**17227**	**0.622**	**410**	**18.5**
5	**10359**	**0.929**	**20010**	**4.301**	**13177**	**0.659**	**410**	**18.0**
Average	**-**	**-**	**-**	**-**	**-**	**0.609**	**-**	**17.7**

Cl.0_3.90-1-A-1:

C Vs S Data for All Specimens

C Fit	S Fit	C Specimen 1	S Specimen 1	C Specimen 2	S Specimen 2	C Specimen 3	S Specimen 3
1.00E+00	0.00E+00	1.00E+00	0.00E+00	1.00E+00	0.00E+00	1.00E+00	0.00E+00
9.84E-01	1.00E+02	8.88E-01	3.49E+03	9.18E-01	2.53E+03	9.26E-01	1.72E+03
9.71E-01	3.00E+02	8.88E-01	3.49E+03	9.18E-01	2.53E+03	9.26E-01	1.72E+03
9.62E-01	5.00E+02	8.88E-01	3.49E+03	9.18E-01	2.53E+03	9.26E-01	1.72E+03
9.46E-01	1.00E+03	8.88E-01	3.49E+03	7.66E-01	1.72E+04	7.55E-01	1.82E+04
9.21E-01	2.02E+03	8.88E-01	3.49E+03	7.35E-01	2.15E+04	7.25E-01	2.20E+04
8.16E-01	1.01E+04	8.88E-01	3.49E+03	7.01E-01	2.68E+04	6.97E-01	2.62E+04
7.35E-01	2.02E+04	6.63E-01	3.45E+04	6.69E-01	3.22E+04	6.68E-01	3.10E+04
6.72E-01	3.04E+04	6.63E-01	3.45E+04	6.43E-01	3.69E+04	6.40E-01	3.63E+04
6.18E-01	4.05E+04	6.63E-01	3.45E+04	6.06E-01	4.40E+04	5.99E-01	4.48E+04
5.70E-01	5.06E+04	6.63E-01	3.45E+04	5.78E-01	4.99E+04	5.84E-01	4.80E+04
4.87E-01	7.09E+04	5.75E-01	5.20E+04	5.58E-01	5.43E+04	5.60E-01	5.36E+04
4.50E-01	8.10E+04	5.75E-01	5.20E+04	5.36E-01	5.93E+04	5.34E-01	5.99E+04
4.15E-01	9.11E+04	5.36E-01	6.10E+04	5.15E-01	6.42E+04	5.15E-01	6.46E+04
3.81E-01	1.01E+05	5.12E-01	6.66E+04	4.93E-01	6.95E+04	4.97E-01	6.94E+04
3.49E-01	1.11E+05	4.82E-01	7.42E+04	4.71E-01	7.50E+04	4.76E-01	7.48E+04
3.19E-01	1.21E+05	4.62E-01	7.97E+04	4.52E-01	7.99E+04	4.58E-01	7.98E+04
2.90E-01	1.32E+05	4.46E-01	8.42E+04	4.33E-01	8.49E+04	4.40E-01	8.49E+04
2.61E-01	1.42E+05	4.26E-01	8.97E+04	4.14E-01	9.00E+04	4.22E-01	8.99E+04
2.34E-01	1.52E+05	4.10E-01	9.44E+04	3.96E-01	9.48E+04	4.05E-01	9.50E+04
2.08E-01	1.62E+05	3.91E-01	9.99E+04	3.78E-01	9.98E+04	3.88E-01	9.99E+04
1.82E-01	1.72E+05	3.73E-01	1.05E+05	3.59E-01	1.05E+05	3.71E-01	1.05E+05
1.57E-01	1.82E+05	3.58E-01	1.10E+05	3.41E-01	1.10E+05	3.55E-01	1.10E+05
1.33E-01	1.92E+05	3.41E-01	1.15E+05	3.23E-01	1.15E+05	3.39E-01	1.15E+05
1.09E-01	2.02E+05	3.24E-01	1.20E+05	3.06E-01	1.19E+05	3.23E-01	1.19E+05
-	-	3.11E-01	1.24E+05	2.92E-01	1.23E+05	3.08E-01	1.24E+05
-	-	2.95E-01	1.29E+05	2.74E-01	1.29E+05	2.94E-01	1.29E+05
-	-	2.82E-01	1.34E+05	2.55E-01	1.34E+05	2.80E-01	1.33E+05
-	-	2.66E-01	1.40E+05	2.40E-01	1.39E+05	2.66E-01	1.38E+05
-	-	2.53E-01	1.45E+05	2.24E-01	1.45E+05	2.45E-01	1.45E+05
-	-	2.41E-01	1.50E+05	2.11E-01	1.50E+05	2.33E-01	1.49E+05
-	-	2.32E-01	1.54E+05	1.98E-01	1.55E+05	2.17E-01	1.55E+05

-	-	2.19E-01	1.60E+05	1.88E-01	1.60E+05	2.05E-01	1.59E+05
-	-	2.08E-01	1.65E+05	1.76E-01	1.65E+05	1.93E-01	1.64E+05
-	-	1.98E-01	1.70E+05	1.65E-01	1.70E+05	1.82E-01	1.69E+05
-	-	1.89E-01	1.75E+05	1.56E-01	1.75E+05	1.71E-01	1.74E+05
-	-	1.79E-01	1.80E+05	1.45E-01	1.80E+05	1.59E-01	1.80E+05
-	-	1.71E-01	1.85E+05	1.35E-01	1.85E+05	1.49E-01	1.85E+05
-	-	1.61E-01	1.90E+05	1.27E-01	1.88E+05	1.39E-01	1.90E+05
-	-	1.52E-01	1.95E+05	-	-	1.29E-01	1.95E+05
-	-	1.44E-01	2.00E+05	-	-	1.19E-01	2.00E+05
-	-	1.43E-01	2.01E+05	-	-	1.13E-01	2.02E+05

Fatigue Analysis Output Summary

Specimen No & ID	Fingerprint |E*| (MPa)	DMR, 0.85<DMR<1.15	Nf	log (Nf)	Cum. (1-C)	DR	Input Strain (μ)	Sapp (DR = f(|E*|))
1	**9018**	**1.019**	**20630**	**4.314**	**16253**	**0.788**	**440**	**22.3**
2	**8756**	**0.988**	**11510**	**4.061**	**8988**	**0.781**	**440**	**20.9**
3	**8668**	**0.977**	**12150**	**4.085**	**9764**	**0.804**	**460**	**21.6**
Average	**-**	**-**	**-**	**-**	**-**	**0.791**	**-**	**21.6**

BI.8_2.20-1-A-1:

C Fit	S Fit	C Specimen 1	S Specimen 1	C Specimen 2	S Specimen 2	C Specimen 3	S Specimen 3
1.00E+00	0.00E+00	1.00E+00	0.00E+00	1.00E+00	0.00E+00	1.00E+00	0.00E+00
9.92E-01	1.00E+02	9.69E-01	9.25E+02	9.62E-01	1.14E+03	9.53E-01	1.63E+03
9.84E-01	3.00E+02	9.69E-01	9.25E+02	9.62E-01	1.14E+03	9.53E-01	1.63E+03
9.78E-01	5.00E+02	9.69E-01	9.25E+02	9.62E-01	1.14E+03	9.53E-01	1.63E+03
9.66E-01	1.00E+03	9.69E-01	9.25E+02	9.62E-01	1.14E+03	9.53E-01	1.63E+03
9.44E-01	2.29E+03	9.69E-01	9.25E+02	9.62E-01	1.14E+03	9.53E-01	1.63E+03
8.51E-01	1.15E+04	7.85E-01	2.56E+04	9.62E-01	1.14E+03	9.53E-01	1.63E+03
7.74E-01	2.29E+04	7.53E-01	3.08E+04	7.26E-01	3.37E+04	7.59E-01	3.28E+04
7.10E-01	3.44E+04	7.22E-01	3.59E+04	7.26E-01	3.37E+04	7.59E-01	3.28E+04
6.55E-01	4.58E+04	6.91E-01	4.11E+04	6.77E-01	4.16E+04	7.22E-01	4.03E+04
6.05E-01	5.73E+04	6.59E-01	4.67E+04	6.48E-01	4.66E+04	6.91E-01	4.68E+04
5.16E-01	8.02E+04	6.28E-01	5.21E+04	6.11E-01	5.28E+04	6.62E-01	5.30E+04
4.75E-01	9.16E+04	5.97E-01	5.79E+04	5.73E-01	5.95E+04	6.34E-01	5.93E+04
4.36E-01	1.03E+05	5.68E-01	6.38E+04	5.73E-01	5.95E+04	6.34E-01	5.93E+04
3.99E-01	1.15E+05	5.43E-01	6.94E+04	5.33E-01	6.64E+04	6.08E-01	6.53E+04
3.63E-01	1.26E+05	5.22E-01	7.43E+04	4.93E-01	7.36E+04	5.84E-01	7.13E+04
3.28E-01	1.37E+05	5.05E-01	7.86E+04	4.93E-01	7.36E+04	5.61E-01	7.72E+04
2.95E-01	1.49E+05	4.89E-01	8.25E+04	4.58E-01	8.05E+04	5.40E-01	8.30E+04
2.62E-01	1.60E+05	4.63E-01	8.94E+04	4.30E-01	8.63E+04	5.21E-01	8.86E+04
2.31E-01	1.72E+05	4.44E-01	9.46E+04	3.95E-01	9.43E+04	5.02E-01	9.39E+04
2.00E-01	1.83E+05	4.28E-01	9.91E+04	3.83E-01	9.73E+04	4.86E-01	9.88E+04
1.70E-01	1.95E+05	4.09E-01	1.04E+05	3.56E-01	1.04E+05	4.69E-01	1.04E+05
1.41E-01	2.06E+05	3.94E-01	1.09E+05	3.38E-01	1.09E+05	4.54E-01	1.08E+05
1.12E-01	2.18E+05	3.73E-01	1.15E+05	3.18E-01	1.14E+05	4.42E-01	1.12E+05
8.40E-02	2.29E+05	3.59E-01	1.19E+05	2.99E-01	1.20E+05	4.22E-01	1.18E+05
-	-	3.43E-01	1.24E+05	2.83E-01	1.25E+05	4.06E-01	1.23E+05
-	-	3.27E-01	1.30E+05	2.66E-01	1.30E+05	3.88E-01	1.29E+05
-	-	3.12E-01	1.35E+05	2.51E-01	1.35E+05	3.74E-01	1.34E+05
-	-	2.99E-01	1.40E+05	2.38E-01	1.40E+05	3.60E-01	1.39E+05
-	-	2.85E-01	1.45E+05	2.24E-01	1.45E+05	3.46E-01	1.44E+05
-	-	2.75E-01	1.49E+05	2.13E-01	1.50E+05	3.31E-01	1.50E+05
-	-	2.61E-01	1.55E+05	2.03E-01	1.54E+05	3.17E-01	1.55E+05
-	-	2.49E-01	1.60E+05	1.92E-01	1.60E+05	3.05E-01	1.60E+05
-	-	2.37E-01	1.65E+05	1.83E-01	1.65E+05	2.93E-01	1.65E+05
-	-	2.27E-01	1.70E+05	1.75E-01	1.70E+05	2.81E-01	1.70E+05

-	-	2.16E-01	1.75E+05	1.66E-01	1.75E+05	2.68E-01	1.75E+05
-	-	2.07E-01	1.80E+05	1.59E-01	1.80E+05	2.60E-01	1.79E+05
-	-	1.95E-01	1.85E+05	1.58E-01	1.80E+05	2.48E-01	1.84E+05
-	-	1.85E-01	1.89E+05	-	-	2.37E-01	1.90E+05
-	-	-	-	-	-	2.27E-01	1.95E+05
-	-	-	-	-	-	2.19E-01	1.99E+05
-	-	-	-	-	-	2.09E-01	2.05E+05
-	-	-	-	-	-	2.00E-01	2.10E+05
-	-	-	-	-	-	1.91E-01	2.15E+05
-	-	-	-	-	-	1.82E-01	2.20E+05
-	-	-	-	-	-	1.74E-01	2.25E+05
-	-	-	-	-	-	1.66E-01	2.29E+05

Fatigue Analysis Output Summary

Specimen No & ID	Fingerprint |E*| (MPa)	DMR, 0.85<DMR<1.15	Nf	log (Nf)	Cum. (1-C)	DR	Input Strain (μ)	Sapp (DR = f(|E*|))
1	**11115**	**1.053**	**12590**	**4.100**	**9723**	**0.772**	**320**	**23.7**
2	**10560**	**1.002**	**10110**	**4.005**	**8161**	**0.807**	**340**	**21.1**
3	**10678**	**1.014**	**12660**	**4.102**	**10010**	**0.791**	**380**	**28.0**
Average	**-**	**-**	**-**	**-**	**-**	**0.790**	**-**	**24.5**

BI.0_2.20-1-A-1:

C Fit	S Fit	C Specimen 1	S Specimen 1	C Specimen 2	S Specimen 2	C Specimen 3	S Specimen 3
1.00E+00	0.00E+00	1.00E+00	0.00E+00	1.00E+00	0.00E+00	1.00E+00	0.00E+00
9.86E-01	1.00E+02	9.20E-01	9.21E+03	9.23E-01	1.46E+03	9.45E-01	1.18E+03
9.74E-01	3.00E+02	9.20E-01	9.21E+03	9.23E-01	1.46E+03	9.45E-01	1.18E+03
9.65E-01	5.00E+02	9.20E-01	9.21E+03	9.23E-01	1.46E+03	9.45E-01	1.18E+03
9.49E-01	1.00E+03	8.48E-01	1.86E+04	9.23E-01	1.46E+03	9.45E-01	1.18E+03
9.38E-01	1.47E+03	8.48E-01	1.86E+04	9.23E-01	1.46E+03	7.41E-01	2.25E+04
8.50E-01	7.33E+03	7.99E-01	2.60E+04	9.23E-01	1.46E+03	7.41E-01	2.25E+04
7.81E-01	1.47E+04	7.63E-01	3.22E+04	9.23E-01	1.46E+03	7.41E-01	2.25E+04
7.27E-01	2.20E+04	7.36E-01	3.69E+04	9.23E-01	1.46E+03	7.41E-01	2.25E+04
6.81E-01	2.93E+04	7.01E-01	4.34E+04	9.23E-01	1.46E+03	6.32E-01	4.01E+04
6.39E-01	3.67E+04	6.66E-01	4.99E+04	9.23E-01	1.46E+03	6.32E-01	4.01E+04
5.66E-01	5.13E+04	6.42E-01	5.46E+04	4.43E-01	5.41E+04	5.68E-01	5.15E+04
5.34E-01	5.87E+04	6.18E-01	5.93E+04	4.02E-01	5.99E+04	5.33E-01	5.82E+04
5.03E-01	6.60E+04	5.91E-01	6.45E+04	3.76E-01	6.40E+04	5.09E-01	6.29E+04
4.73E-01	7.33E+04	5.64E-01	6.97E+04	3.40E-01	7.00E+04	4.79E-01	6.91E+04
4.45E-01	8.07E+04	5.41E-01	7.42E+04	3.17E-01	7.41E+04	4.60E-01	7.33E+04
4.18E-01	8.80E+04	5.14E-01	7.96E+04	2.92E-01	7.92E+04	4.36E-01	7.91E+04
3.92E-01	9.53E+04	4.92E-01	8.41E+04	2.65E-01	8.50E+04	4.13E-01	8.46E+04
3.67E-01	1.03E+05	4.65E-01	8.96E+04	2.44E-01	8.98E+04	3.94E-01	8.96E+04
3.43E-01	1.10E+05	4.42E-01	9.43E+04	2.23E-01	9.49E+04	3.76E-01	9.47E+04
3.19E-01	1.17E+05	4.15E-01	1.00E+05	2.05E-01	1.00E+05	3.58E-01	9.98E+04
2.97E-01	1.25E+05	3.95E-01	1.04E+05	1.88E-01	1.05E+05	3.42E-01	1.05E+05
2.74E-01	1.32E+05	3.70E-01	1.10E+05	1.74E-01	1.10E+05	3.28E-01	1.10E+05
2.53E-01	1.39E+05	3.47E-01	1.15E+05	1.61E-01	1.15E+05	3.12E-01	1.15E+05
2.31E-01	1.47E+05	3.25E-01	1.20E+05	1.50E-01	1.20E+05	2.97E-01	1.20E+05
-	-	3.02E-01	1.25E+05	1.39E-01	1.25E+05	2.84E-01	1.25E+05
-	-	2.82E-01	1.29E+05	1.27E-01	1.30E+05	2.70E-01	1.30E+05
-	-	2.78E-01	1.30E+05	1.16E-01	1.34E+05	2.57E-01	1.35E+05
-	-	-	-	1.11E-01	1.36E+05	2.44E-01	1.40E+05
-	-	-	-	-	-	2.32E-01	1.45E+05
-	-	-	-	-	-	2.27E-01	1.47E+05

Fatigue Analysis Output Summary

Specimen No & ID	Fingerprint |E*| (MPa)	DMR, 0.85<DMR<1.15	Nf	log (Nf)	Cum. (1-C)	DR	Input Strain (μ)	Sapp (DR = f(|E*|))
1	**10514**	**1.070**	**20010**	**4.301**	**11994**	**0.599**	**260**	**19.6**
2	**9784**	**0.993**	**9160**	**3.962**	**7726**	**0.843**	**340**	**11.9**
3	**9331**	**0.947**	**37160**	**4.570**	**26719**	**0.719**	**340**	**17.8**
Average	**-**	**-**	**-**	**-**	**-**	**0.721**	**-**	**18.1**

Low – temperature Cracking

Result of IDT Test:

MIX ID	Specimen ID	P (KN)	D (mm)	t (mm)	σ (MPa)	Average (σ)
UI.0_4.19-1-A-1	1	29.24	150	38.5	3.22	3.66
	2	39.16	150	38.5	4.32	
	3	30.39	150	42.5	3.04	
	4	42.61	150	44.5	4.06	

MIX ID	Specimen ID	P (KN)	D (mm)	t (mm)	σ (MPa)	Average (σ)
UI.4_4.19-1-A-1	1	31.67	150	40	3.36	3.84
	2	36.95	150	40	3.92	
	3	39.83	150	40	4.23	

MIX ID	Specimen ID	P (KN)	D (mm)	t (mm)	σ (MPa)	Average (σ)
CI.0_3.90-1-A-1	1	36.72	150	42.6	3.65	3.47
	2	34.55	150	43	3.41	
	3	35.65	150	45	3.36	

MIX ID	Specimen ID	P (KN)	D (mm)	t (mm)	σ (MPa)	Average (σ)
BI.8_2.20-0-A-1	1	37.99	150	42	3.84	3.68
	2	41.19	150	43	4.07	
	3	31.79	150	43	3.14	

MIX ID	Specimen ID	P (KN)	D (mm)	t (mm)	σ (MPa)	Average (σ)
BI.0_2.20-0-A-1	1	38.58	150	42.75	3.83	3.25
	2	30.35	150	42.75	3.01	
	3	27.23	150	39.75	2.91	

Thermal Stress:

UI.4_4.19-1-A-1:

Thermal stress, MPa	Stress – IDT, MPa	Measured IDT strength, MPa	Crossing flag
0.00	-3.84	3.84	
0.06	-3.77	3.84	
0.11	-3.72	3.84	
0.16	-3.67	3.84	
0.21	-3.63	3.84	
0.25	-3.58	3.84	
0.30	-3.53	3.84	
0.35	-3.48	3.84	
0.40	-3.43	3.84	
0.46	-3.38	3.84	
0.51	-3.32	3.84	
0.57	-3.27	3.84	
0.63	-3.21	3.84	
0.69	-3.14	3.84	
0.76	-3.08	3.84	
0.82	-3.01	3.84	
0.89	-2.94	3.84	
0.97	-2.87	3.84	
1.04	-2.79	3.84	
1.12	-2.71	3.84	
1.21	-2.63	3.84	
1.29	-2.54	3.84	
1.38	-2.45	3.84	
1.48	-2.36	3.84	
1.57	-2.26	3.84	
1.67	-2.16	3.84	
1.78	-2.06	3.84	
1.88	-1.95	3.84	
2.00	-1.84	3.84	
2.11	-1.72	3.84	
2.23	-1.61	3.84	
2.35	-1.48	3.84	
2.48	-1.36	3.84	
2.61	-1.23	3.84	
2.74	-1.09	3.84	
2.88	-0.95	3.84	
3.02	-0.81	3.84	
3.17	-0.66	3.84	
3.32	-0.51	3.84	
3.48	-0.36	3.84	
3.63	-0.20	3.84	
3.80	-0.04	3.84	
3.96	0.13	3.84	Tcrit interval
4.14	0.30	3.84	
4.31	0.48	3.84	

UI.0_4.19-1-A-1:

Thermal stress, MPa	Stress – IDT, MPa	Measured IDT strength, MPa	Crossing flag
0.000	-3.660	3.660	
0.066	-3.594	3.660	
0.120	-3.540	3.660	
0.171	-3.489	3.660	
0.221	-3.439	3.660	
0.271	-3.389	3.660	
0.322	-3.338	3.660	
0.375	-3.285	3.660	
0.429	-3.231	3.660	
0.486	-3.174	3.660	
0.544	-3.116	3.660	
0.605	-3.055	3.660	
0.668	-2.992	3.660	
0.735	-2.925	3.660	
0.804	-2.856	3.660	
0.875	-2.785	3.660	
0.950	-2.710	3.660	
1.028	-2.632	3.660	
1.109	-2.551	3.660	
1.193	-2.467	3.660	
1.281	-2.379	3.660	
1.372	-2.288	3.660	
1.465	-2.195	3.660	
1.563	-2.097	3.660	
1.664	-1.996	3.660	
1.769	-1.891	3.660	
1.878	-1.782	3.660	
1.990	-1.670	3.660	
2.105	-1.555	3.660	
2.225	-1.435	3.660	
2.349	-1.311	3.660	
2.476	-1.184	3.660	
2.608	-1.052	3.660	
2.743	-0.917	3.660	
2.882	-0.778	3.660	
3.025	-0.635	3.660	
3.172	-0.488	3.660	
3.323	-0.337	3.660	
3.478	-0.182	3.660	
3.637	-0.023	3.660	
3.800	0.140	3.660	Tcrit interval
3.968	0.308	3.660	
4.139	0.479	3.660	

Cl.0_3.90-1-A-1:

Thermal stress(Cl.0)	Stress – IDT, MPa	IDT strength(Cl.0)	**Crossing flag**
0.000	-3.470	3.470	
0.035	-3.435	3.470	
0.063	-3.407	3.470	
0.088	-3.382	3.470	
0.112	-3.358	3.470	
0.137	-3.333	3.470	
0.162	-3.308	3.470	
0.187	-3.283	3.470	
0.214	-3.256	3.470	
0.241	-3.229	3.470	
0.270	-3.200	3.470	
0.300	-3.170	3.470	
0.332	-3.138	3.470	
0.365	-3.105	3.470	
0.399	-3.071	3.470	
0.435	-3.035	3.470	
0.473	-2.997	3.470	
0.512	-2.958	3.470	
0.553	-2.917	3.470	
0.596	-2.874	3.470	
0.642	-2.828	3.470	
0.689	-2.781	3.470	
0.739	-2.731	3.470	
0.790	-2.680	3.470	
0.845	-2.625	3.470	
0.901	-2.569	3.470	
0.960	-2.510	3.470	
1.022	-2.448	3.470	
1.086	-2.384	3.470	
1.152	-2.318	3.470	
1.221	-2.249	3.470	
1.293	-2.177	3.470	
1.368	-2.102	3.470	
1.446	-2.024	3.470	
1.528	-1.942	3.470	
1.612	-1.858	3.470	
1.699	-1.771	3.470	
1.789	-1.681	3.470	
1.883	-1.587	3.470	
1.979	-1.491	3.470	
2.080	-1.390	3.470	
2.184	-1.286	3.470	
2.291	-1.179	3.470	
2.401	-1.069	3.470	
2.514	-0.956	3.470	
2.632	-0.838	3.470	
2.753	-0.717	3.470	
2.878	-0.592	3.470	
3.007	-0.463	3.470	
3.140	-0.330	3.470	
3.276	-0.194	3.470	
3.416	-0.054	3.470	
3.560	0.090	3.470	Tcrit interval
3.707	0.237	3.470	
3.859	0.389	3.470	

BI.8_2.20-1-A-1:

Thermal stress, MPa	Stress – IDT, MPa	Measured IDT strength, MPa	Crossing flag
0.00	-3.68	3.68	
0.06	-3.62	3.68	
0.11	-3.57	3.68	
0.15	-3.53	3.68	
0.20	-3.48	3.68	
0.24	-3.44	3.68	
0.29	-3.39	3.68	
0.33	-3.35	3.68	
0.38	-3.30	3.68	
0.43	-3.25	3.68	
0.48	-3.20	3.68	
0.53	-3.15	3.68	
0.59	-3.09	3.68	
0.64	-3.04	3.68	
0.70	-2.98	3.68	
0.76	-2.92	3.68	
0.82	-2.86	3.68	
0.89	-2.79	3.68	
0.96	-2.72	3.68	
1.03	-2.65	3.68	
1.10	-2.58	3.68	
1.17	-2.51	3.68	
1.25	-2.43	3.68	
1.33	-2.35	3.68	
1.41	-2.27	3.68	
1.50	-2.18	3.68	
1.59	-2.09	3.68	
1.68	-2.00	3.68	
1.77	-1.91	3.68	
1.87	-1.81	3.68	
1.97	-1.71	3.68	
2.08	-1.60	3.68	
2.18	-1.50	3.68	
2.29	-1.39	3.68	
2.41	-1.27	3.68	
2.52	-1.16	3.68	
2.64	-1.04	3.68	
2.76	-0.92	3.68	
2.89	-0.79	3.68	
3.02	-0.66	3.68	
3.15	-0.53	3.68	
3.29	-0.39	3.68	
3.42	-0.26	3.68	
3.57	-0.11	3.68	
3.71	0.03	3.68	Tcrit interval
3.86	0.18	3.68	
4.01	0.33	3.68	

BI.0_2.20-1-A-1:

Thermal stress, MPa	Stress – IDT, MPa	Measured IDT strength, MPa	Crossing flag
0.00	-3.25	3.25	
0.05	-3.20	3.25	
0.09	-3.16	3.25	
0.12	-3.13	3.25	
0.16	-3.09	3.25	
0.20	-3.05	3.25	
0.23	-3.02	3.25	
0.27	-2.98	3.25	
0.31	-2.94	3.25	
0.35	-2.90	3.25	
0.39	-2.86	3.25	
0.43	-2.82	3.25	
0.47	-2.78	3.25	
0.52	-2.73	3.25	
0.57	-2.68	3.25	
0.62	-2.63	3.25	
0.67	-2.58	3.25	
0.72	-2.53	3.25	
0.77	-2.48	3.25	
0.83	-2.42	3.25	
0.89	-2.36	3.25	
0.95	-2.30	3.25	
1.02	-2.23	3.25	
1.08	-2.17	3.25	
1.15	-2.10	3.25	
1.23	-2.02	3.25	
1.30	-1.95	3.25	
1.38	-1.87	3.25	
1.46	-1.79	3.25	
1.54	-1.71	3.25	
1.62	-1.63	3.25	
1.71	-1.54	3.25	
1.80	-1.45	3.25	
1.90	-1.35	3.25	
1.99	-1.26	3.25	
2.09	-1.16	3.25	
2.20	-1.05	3.25	
2.30	-0.95	3.25	
2.41	-0.84	3.25	
2.52	-0.73	3.25	
2.64	-0.61	3.25	
2.76	-0.49	3.25	
2.88	-0.37	3.25	
3.00	-0.25	3.25	
3.13	-0.12	3.25	
3.27	0.02	3.25	Tcrit interval
3.40	0.15	3.25	
3.54	0.29	3.25	